Functional analysis of the Retinitis pigmentosa GTPase regulator(RPGR) gene

Abstract

The retinitis pigmentosa GTPase regulator (RPGR) gene is mutated in several forms of photoreceptor degeneration resulting in severe visual impairment and probably blindness. Most patients develop Retinitis pigmentosa(RP), which is a clinically and genetically heterogeneous disease characterized by degeneration initially of rod and later in disease also of cone photoreceptors. Mutations in RPGR were also described in patients with cone-rod dystrophy, cone dystrophy, Coats' like exsudative vitreoretinopathy and atrophic macular degeneration. Additionally, the spectrum of diseases due to RPGR mutations was further expanded by describing patients with a syndromic phenotype including RP, sinorespiratory infections and hearing problems and in patients manifesting with primary ciliary dyskinesia (PCD). To date, no phenotype-genotype correlation could be established. Evidence exist that genetic modifiers might act on disease expressivity as one mutation can lead to different phenotypes even within one family. In order to gain a better understand the function of RPGR, two mouse models for RPGR-related diseases have been characterized in this study. The transgenic mouse line with Rpgr-overexpression of the wild type protein exhibits infertility. In contrast,the knock-in mouse model, harbouring a deletion of exon 4, develops either rod disease or cone-rod disease depending on the genetic background (BL/6 or BALB/c, respectively). The difference in retinal manifestations in the mouse resembles the clinical heterogeneity in humans. In addition, mislocalization of visual pigments was found to be an early pathologic event further mounting evidence that RPGR might be involved in the transport of proteins. Overall, the two mouse models further support the assumed function of RPGR in cilia and flagella. RPGR was for the first time shown to be involved in mouse flagellar biogenesis and can therefore be regarded as a novel candidate gene for male infertility. In addition, the knock-in mouse on the BALB/c background serves as a model for cone-dominated phenotypes including cone dystrophy, cone-rod dystrophy and even macular degeneration. The two knock-in lines provide a powerful tool to study the influence of modifier genes.

Functional analysis of the Retinitis pigmentosa GTPase regulator (*RPGR*) gene

---

Dissertation

zur

Erlangung der naturwissenschaftlichen Doktorwürde

(Dr. sc. nat.)

vorgelegt der

Mathematisch-naturwissenschaftlichen Fakultät

der

Universität Zürich

von

Sandra Brunner

aus

Deutschland

Promotionskomitee

Prof. Dr. Eric Berger (Vorsitz)

Prof. Dr. Wolfgang Berger (Leitung der Dissertation)

Prof. Dr. Stephan Neuhauss

Zürich, 2008

Declaration

I declare that the present thesis was composed by myself and
the enclosed experimental work was performed on my own
as indicated in the respective chapters.
This dissertation has not been submitted for any other degree
or professional qualification except as specified.

Sandra Brunner, Zürich 2008

Für Heidi

Für Josef

Abbreviations

A	adenine
aa	amino acid
AC	amacrine cell
AD	autosomal dominant
ALMS	Alstrom syndrome
ANOVA	analysis of variance
AR	autosomal recessive
ARF4	ADP-ribosylation factor 4
BS	Biemond syndrome
BBS	Bardet-Biedl sydrome
BC	bipolar cell
BOR	Biology of Reproduction
bp	base pair
C	cytosine
Ca	calcium
cDNA	complementary DNA
CEP290	centrosomal protein 290
cGMP	cyclic guanosine monophosphate
CNG	cGMP-nucleotide gated channels
CIS	cone inner segment
CO_2	carbon dioxide
COD	cone dystrophy
CORD	cone-rod dystrophy
COS	cone outer segments
DIC	dynein intermediate chain
DNA	deoxyribonucleic acid
DNAI	dynein axonemal intermediate chain
DNAH	dynein axonemal heavy chain
EDTA	ethylenediaminetetraacetic acid
ER	endoplasmatic reticulum
ERG	electroretinography
ES	embryonic stem cell
FS	fibrous sheath
G	guanine
GC	ganglion cell
GCL	ganglion cell layer
GDP	guanosine diphosphate
GCAP	guanylate cyclase activation protein
GEF	guanine nucleotide exchange factor
GTP	guanosine triphosphate
HC	horizontal cell
hCG	human chorionic gonadotropin
IFT	Intraflagellar transport
IgG	immunoglobulin G
IHC	immunohistochemistry
INL	inner nuclear layer
IOVS	Investigative Ophthalmology and Vision Research
IPL	inner plexiform layer

IS	inner segment
IVF	*in-vitro* fertilization
JBTS	Joubert syndrome
KAP	kinesin-associated protein
kDa	kilo Dalton
K.I.	knock-in
KIF3A/B	kinesin family member 3A/B
K.O.	knock-out
LCA	Leber congenital amaurosis
Leu	leucine
LMS	Laurence-Moon syndrome
M	molar
MC	Mueller cell
mcds	milli candelar seconds
Met	methionine
MKS	Meckel-Gruber syndrome
MKKS	McKusick-Kaufmann syndrome
mRNA	messenger RNA
MS	mitochondrial sheath
mut	mutant
mV	millivolt
NaCl	sodium chloride
NaOH	sodium hydroxide
NCBI	National Center for Biotechnology Information
NGS	normal goat serum
NPHP	nephronophthisis
OCT	optimal cutting temperature
ODF	outer dense fibers
OFD1	orofacialdigital syndrome I
OMIM	Online Mendelian Inheritance in Man
o/n	over night
ONL	outer nuclear layer
OPL	outer plexiform layer
ORF	open reading frame
OS	outer segment
PAC	P1 artificial chromosome
PBS	phosphate buffered salt
PC	polycystin
PCD	Primary ciliary dyskinesia
PCM	pericentriolar matrix
PCR	polymerase chain reaction
PDE	phosphodiesterase
PFA	paraformaldehyde
P.I.	Principal investigator
PKD	Polycystic kidney disease
PrBP	prenyl-binding protein
PVDF	polyvinylidene fluoride
RCC1	regulator of chromatin condensation 1

RetNet	Retinal Information Network
RHO	rhodopsin
RIS	rod inner segment
RNA	ribonucleic acid
ROS	rod outer segment
RP	retinitis pigmentosa
RPGR	retinitis pigmentosa GTPase regulator
RPGRIP1	retinitis pigmentosa GTPase regulator interacting protein 1
RLD	RCC1-like domain
RPE	retinal pigment epithelium
RPE65	retinal pigment epithelium-specific protein 65
rpm	revolution per minute
RT	room temperature
RT-PCR	reverse transcriptase polymerase chain reaction
SANS	scaffold protein containing ankyrin repeats and sam domain
SDS-PAGE	sodium dodecylsulfate polyacrylamide gel electrophoresis
SLS	Senior-Loken syndrome
SMC	structural maintenance of chromosome condensation protein
T	thymine
Taq	*Thermus aquaticus* polymerase
TE	Tris-EDTA buffer
Tg	transgene
TGN	trans-Golgi network
TMEM67	transmembrane protein 67
Tris	2-Amino-2-hydroxymethyl-propane-1,3-diol
TXNDC3	thioredoxin domain-containing protein 3
USH	Usher syndrome
VLRG	very large G-protein coupled receptor
WB	Western blot
wt	wild type
XlPRA	X-linked progressive retinal atrophy
XlRP	X-linked Retinitis pigmentosa

Summary

The retinitis pigmentosa GTPase regulator (RPGR) gene is mutated in several forms of photoreceptor degeneration resulting in severe visual impairment and probably blindness. Most patients develop Retinitis pigmentosa (RP), which is a clinically and genetically heterogeneous disease characterized by degeneration initially of rod and later in disease also of cone photoreceptors. Mutations in *RPGR* were also described in patients with cone-rod dystrophy, cone dystrophy, Coats' like exsudative vitreoretinopathy and atrophic macular degeneration. Additionally, the spectrum of diseases due to *RPGR* mutations was further expanded by describing patients with a syndromic phenotype including RP, sinorespiratory infections and hearing problems and in patients manifesting with primary ciliary dyskinesia (PCD). To date, no phenotype-genotype correlation could be established. Evidence exist that genetic modifiers might act on disease expressivity as one mutation can lead to different phenotypes even within one family.

In order to gain a better understand the function of *RPGR*, two mouse models for *RPGR*-related diseases have been characterized in this study. The transgenic mouse line with *Rpgr*-overexpression of the wild type protein exhibits infertility. In contrast, the knock-in mouse model, harbouring a deletion of exon 4, develops either rod disease or cone-rod disease depending on the genetic background (BL/6 or BALB/c, respectively). The difference in retinal manifestations in the mouse resembles the clinical heterogeneity in humans. In addition, mislocalization of visual pigments was found to be an early pathologic event further mounting evidence that *RPGR* might be involved in the transport of proteins.

Overall, the two mouse models further support the assumed function of *RPGR* in cilia and flagella. *RPGR* was for the first time shown to be involved in mouse flagellar biogenesis and can therefore be regarded as a novel candidate gene for male infertility. In addition, the knock-in mouse on the BALB/c background serves as a model for cone-dominated phenotypes including cone dystrophy, cone-rod dystrophy and even macular degeneration. The two knock-in lines provide a powerful tool to study the influence of modifier genes.

Zusammenfassung

Mutationen im Retinitis pigmentosa GTPase Regulator (*RPGR*) Gen führen zu schweren Netzhautdystrophien. Die klinische Variabilität der Phänotypen ist sehr ausgeprägt. In den meisten Fällen führen Mutationen zu Retinitis pigmentosa (RP), einer erblichen Form der Netzhautsdystrophie, bei der hauptsächlich die Stäbchen degenerieren. Im weiteren Krankheitsverlauf können auch die Zapfen betroffen sein und absterben. Somit sind Patienten in ihrem Sehvermögen stark eingeschränkt und erblinden in manchen Fällen vollkommen. Inzwischen ist bekannt, dass Mutationen in *RPGR* nicht nur zu RP sondern auch anderen Formen der Netzhautdegeneration wie Zapfen-Stäbchen Degeneration, Zapfen Degeneration, Coats-like exsudative Vitreoretinopathie und atropher Makuladegeneration führen können. Desweiteren wurden Patienten beschrieben, die unter einer syndromalen Form von RP mit sinorespiratorischen Infektionen und Hörproblemen leiden. Interessanterweise wurden Mutationen in *RPGR* auch bei Patienten mit Primärer Ziliärer Dyskinesie beschreiben. Die klinische Heterogenität konnte bisher keiner Genotyp-Phänotyp Korrelation zugeordnet werden. Daher wird angenommen, dass weitere Gene einen modifizierenden Einfluss auf den Krankheitsverlauf und die Krankheitsausprägung ausüben. Diese Vermutung wurde durch Berichte über Familien verstärkt, die unterschiedliche Phänotypen aufgrund der gleichen *RPGR* Mutation interfamiliär aber auch intrafamiliär aufweisen.

Um die Funktion des RPGR-Gens besser zu verstehen wurden in dieser Studie zwei *RPGR*-Mausmodelle charakterisiert. Die Generierung erfolgte im Rahmen dieser Studie vorangegangener Arbeiten. Die eine Mausline ist eine transgene *Rpgr* überexprimierende Linie, welche Infertilität der Männchen aufgrund von fehlendem Spermienflagellum entwickelt. Die zweite Mauslinie ist ein knock-in Modell, bei dem Exon 4 des *Rpgr* Gens deletiert wurde. Da Exon 4 im Leserahmen liegt, kommt es zu Veränderungen im Protein, welches aber weiterhin exprimiert wird. Diese spezifische Mutation in der Maus soll Spleissmutationen nachahmen, die bei Patienten im *RPGR*-Gen gefunden wurden und zum Verlust von Exon 4 im Transkript führen.

Im Rahmen der vorliegenden Arbeit wurden beide Mausmodelle weiter charakterisiert. Die Infertilität der *Rpgr* überexprimierenden Maus wurde dazu auf elektronenmikroskopischer und molekularer Ebene untersucht. Dabei konnte festgestellt werden, dass der identifizierte Phänotyp mit der Proteinmenge korreliert.

In trangenen Mäusen mit moderater Kopienanzahl (4-5 Kopien) wurde ein Defekt in der Organisation der akzessorischen Strukturen des Flagellums festgestellt. In Tieren mit hoher Kopienanzahl (> 8 Kopien) fehlte das Flagellum gänzlich, wobei jedoch die initiale Biogenese stattfand. Die Charakterisierung von Mäusen mit der knock-in Mutation zeigte Unterschiede in der phänotypischen Ausprägung der Netzhautdegeneration. In der BL/6 Linie konnte ein milder Stäbchen-Phänotyp identifiziert werden. Um den Effekt von modifizierenden genetischen Einflüssen zu testen wurde die knock-in Mutation zusätzlich in die BALB/c Mauslinie gekreuzt. Funktionelle und histologische Untersuchungen zeigten unerwarteterweise einen Zapfen-dominierenden Phänotypen. In beiden Mauslinien wurde ausserdem ein Defekt in der Lokalisierung der Photopigmente gefunden.

In dieser Arbeit konnte zum ersten Mal gezeigt werden, dass *Rpgr* eine wichtige Rolle in der Entwicklung des Spermienflagellums spielt. *RPGR* kann damit als neues mögliches Kandidatengen für männliche Infertilität betrachtet werden und im Rahmen von genetischen Screenings für Ursachen von vererbter Infertilität untersucht werden. Desweiteren konnte gezeigt werden, dass sich die Ausprägung der Netzhautdegeneration durch ein und dieselbe Mutation auch in Mäusen spezifisch auf einen Photorezeptorzelltyp auswirken kann. Somit dient die knock-in Mauslinie als wertvolles Modell um den Effekt von modifizierenden genetischen Einflüssen zu untersuchen. Solche photorezeptorspezifischen Gene können wichtige Einsichten in die molekularen Unterschiede von Stäbchen und Zapfen liefern.

Table of Contents

1. General Introduction

The aim of this general introduction is to give a comprehensive review of the structure and function of the retina as well as cilia and flagella in general to provide a basis for understanding the rational and the results of this thesis.

1.1 The retina and photoreceptors in health

The ability of vision is an amazing and highly complex process. The structural and biochemical features of the retina and the photoreceptors are as elaborated and complex as the process of vision itself.

1.1.1 The mammalian retina

The mammalian retina is a very organized and highly specialized tissue which enables us to perceive light in all its intensities and colors. The retina is located at the back of the eyeball where it is connected via the optic nerve with information-processing centers of the brain (Figure 1).

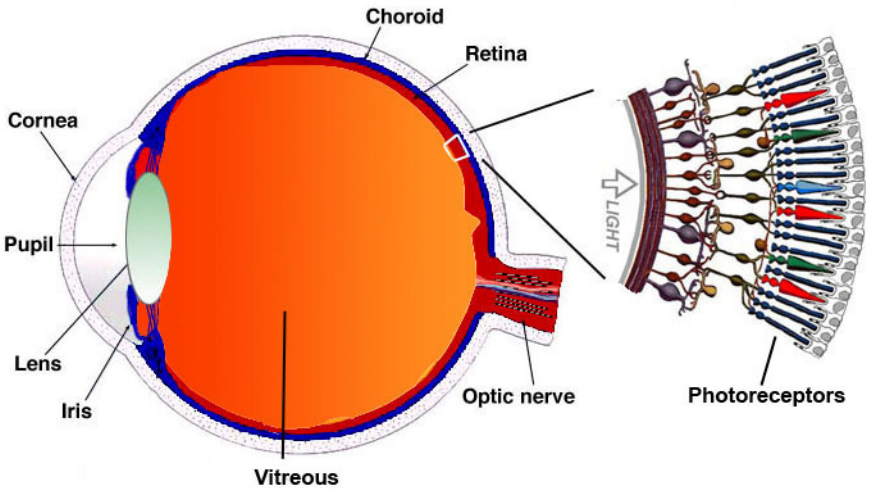

Figure 1: Scheme of the structures of the human eye and the retina

The human eye is composed of several structures important for the process of vision. In the anterior part of the eye the crucial structures are cornea, iris, the pupil and the lens. The cornea and the lens are the two major refractive structures of light entering the eye. The pupil is a hole in the center of the iris controlling the amount of light entering the eye. In the posterior part includes the vitreous, the choroid, the optic nerve and the retina. Light has to pass the vitreous that fills the space between the lens and the retina. Perception of light is accomplished by the retina, where the photons are converted into electrical signals which in turn are propagated to the image processing centers in the brain via the

optic nerve. The choroid lies behind the retina and is responsible for nutrition of the photoreceptors. (modified after www.webvision.med.utah.edu/imageswv/Sagschem.jpeg)

In histological sections the retina can be structurally divided into five layers – three layers of the cell bodies of the light-perceiving and signal-transmitting neurons and two layers of synaptic connections between those (Figure 2).

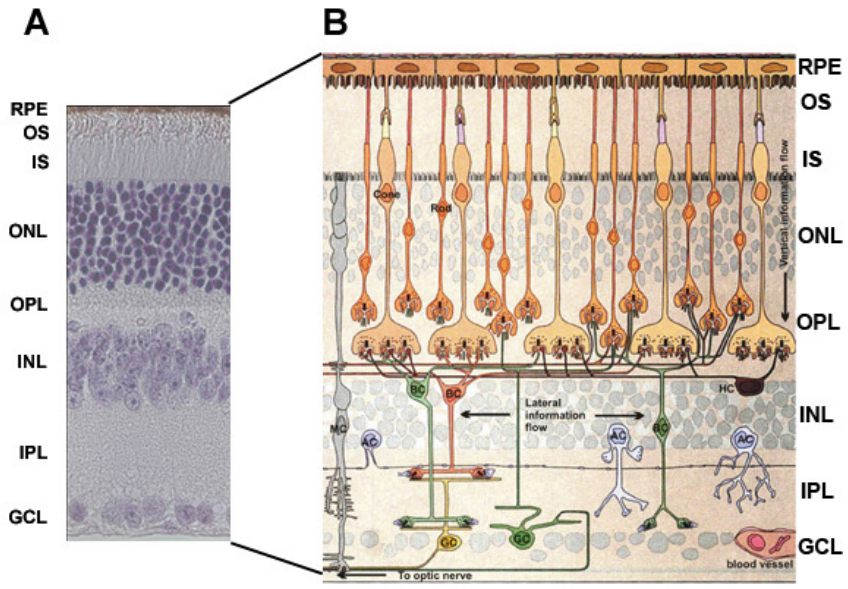

Figure 2: Architecture of the layers in a vertebrate retina

The vertebrate retina is a highly organized structure. (A) In histological sections five major layers can be observed. (B) Illustration of the layered organization and the cell types they are composed off. The most apical layer is the retinal pigment epithelium (RPE). The outer segments (OS) of the rod and cone photoreceptors are in close contact to the RPE. The photoreceptor cells further consist of the inner segments (IS) and the cell soma. The nuclei are arranged in the outer nuclear layer (ONL). The synapses of the photoreceptors contact in the outer plexiform layer (OPL) to the second order neurons which are the (rod and cone) bipolar cells (BC). Additionally, amacrine cells (AC) and horizontal cells (HC) are involved in signal implementation. The cell bodies and nuclei of these cells built the inner nuclear layer (INL). Second order neurons form synaptic connections to the ganglion cells (GC) in the inner plexiform layer (IPL). The ganglion cells are located in the ganglion cell layer (GCL) which is the outermost distal layer of the retina. Mueller cells (MC) are glial cells spanning through the entire retina. (modified after www.anatomy.unimelb.edu.au/researchlabs/rees/images/retina.jpg)

The light-perceiving cells are the photoreceptor cells (Figure 2B) [1,2]. The photoreceptor nuclei are arranged in the outer nuclear layer (ONL). Their slender and specialized cell bodies form the inner and outer segments (IS and OS) which project towards the retinal pigment epithelium (RPE). The RPE is a pigmented cell layer that reduces scattering of light. It closely interacts with the photoreceptors and is essential

for maintenance by nutrition most importantly with Vitamin A (Retinal) and metabolic turnover. In addition, it is involved in phagocytosis of outer segment disk membranes. In the adjacent distal outer plexiform layer (OPL) photoreceptors are connected to the signal-transmitting and modulating neurons (vertical information flow via chemical synapses). These are the bipolar-, amacrine- and horizontal cells (BC, AC and HC) grouped in the second cell layer (inner nuclear layer, INL). Within this layer an initial intricately processing of visual information is implemented (lateral information flow). The bipolar and amacrine cells in turn are connected to the ganglion cells (GC) in the second synaptic layer (inner plexiform layer, IPL). Ganglion cell nuclei are packed in the third cell layer (ganglion cell layer, GCL) and finally relay an electrical action potential via the optic nerve (ON) to the brain. The glial cells of the retina are the Mueller cells (MC) radially passing through the entire retina.

1.1.2 Photoreceptors

The vertebrate photoreceptors are highly polarized neurons and responsible for the ability to detect light in a broad range of illumination. They are morphologically and functionally subdivided into two compartments (Figure 3). The outer segment is the light-sensing part of the photoreceptor. It is packed with membranous disks containing the visual pigment molecules in high density. The outer segment is connected via the connecting cilium to the inner segment which contains all typical eukaryotic organelles involved in protein synthesis and metabolism. The connecting cilium is a narrow link between the two photoreceptor segments. The inner segment ends at the distal side with the synaptic ending where the electrical signals generated during phototransduction are transformed into chemical signals (glutamate) and are propagated to the bipolar cells.

Two types of photoreceptors exist: the very light sensitive rod photoreceptors working at dim light conditions (scotopic) and the less light sensitive but therefore color discriminating and visual-acuity determining cone photoreceptors responsible for daylight vision (photopic). Structurally rods and cones share a similar architecture. However, their outer segment disks are built in two different ways. The disks in rods are membrane stacks evaginating from the plasma membrane while the disks in cones are invaginations of the cell membrane. The disk membranes have a high turn-over rate and are renewed constantly by adding new membrane at the base and shedding of disks at the tip by the RPE. Regarding their protein content rods and

cones are very similar as well; nonetheless each has cell type-specific isoforms of distinct proteins.

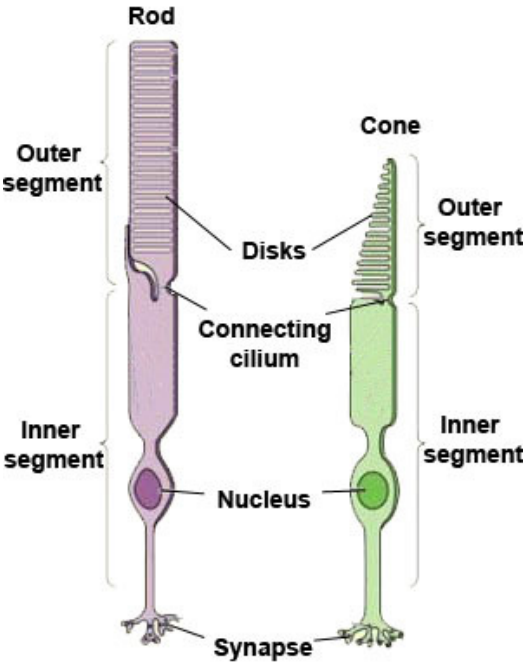

Figure 3: Schematic representation of rod and cone photoreceptor cells

Two photoreceptor cell types are known to exist within the retina. The rod and cone photoreceptor cells share the basic organization. They are divided into an outer segment consisting of membrane disks that contain the visual pigment and an inner segment harbouring the nucleus. Of note, rod disks are evaginations while cone disks are invaginations from the plasma membrane. The inner and the outer segments are connected via the connecting cilium. The synapse is at the most distal side. (modified after www.thebrain.mcgill.ca/flash/d/d_02/d_02_m/d_02_m_vis/d_02_m_vis_1a.jpg)

The visual pigment in both rods and cones consists of an opsin protein backbone and a covalently bound chromophore [3]. Rods and cones both use 11-cis retinal as chromophore albeit it is incorporated into different opsin backbones resulting in spectral fine tuning. Rods are able to operate at night under very dim light conditions using only one type of opsin. In contrast, several different opsin proteins are present in cones in different species allowing them to detect different colors. In humans, three different types of cones exist which are short wave cones (S cones) detecting blue light and middle- and long wave cones (M-and L cones) detecting green and red light, respectively [4]. Mice posses only two types of cones (S- and M cones). S-cones have their spectral sensitivity maxima at the near-ultraviolet to blue light range while M-cones sense green light [5]. Interestingly, in some cones co-expression of both opsins was detected [6]. Concerning the distribution of rods and cones in the retina remarkable differences exist between the species depending on their natural habitat. Humans and mice possess rod-dominated retinae. On average, the human retina is built of 20% cones and 80% rods while a typical mouse retina is composed of 97% rods and 3% cones. Humans are diurnal and mainly rely on cone vision during day time. In the center of the human retina, an area with a high density of cones exists which is termed the fovea. This area is crucial for visual acuity and color perception.

The mouse is a nocturnal animal, hence they mainly rely on rod-vision during night and they have no fovea [7].

1.1.3 The phototransduction cascade

Transmission of visual input starts with the detection of a light signal by the light sensing photoreceptor cells. The molecule being capable of detecting light is the visual pigment, i.e. rhodopsin and cone opsin. Opsins are seven-transmembrane G-protein coupled receptors that are incorporated into the disk membranes of the outer segments. The chromophore 11-cis retinal is attached within the transmembrane domain seven [8].

The cascade is initiated when a photon hits a rhodopsin (R) molecule and gets absorbed by the chromophore (Figure 4, step 1) [9]. Thereby the 11-cis retinal is isomerized into all-trans retinal which in turn triggers conformational changes within the protein leaving it in an excitated state (R*). Photoexcitated rhodopsin activates the heterotrimeric G-protein transducin (G) (step 2). Transducin is composed of a GDP/GTP-binding α-subunit and an undissociable $\beta\gamma$-subunit. Upon activation, the GDP bound to the α-subunit of transducin is exchanged by a GTP which in turn leads to dissociation of the α-subunit from the complex (G*) (step 3). α-Transducin now activates phosphodiesterase (PDE) by binding to the regulatory γ-subunit of this protein. PDE starts to hydrolyse cyclic GMP (cGMP) resulting in a lowered cGMP concentration (step 4). The cGMP-nucleotide gated channels (CNG) in the plasma membrane of the outer segments respond to the decrease of cGMP by closing of the channels. This leads to a hyperpolarization of the membrane and subsequent neuronal signalling. Of note, most retinal cells gradually release neurotransmitter, except the ganglion cells, which release action potentials.

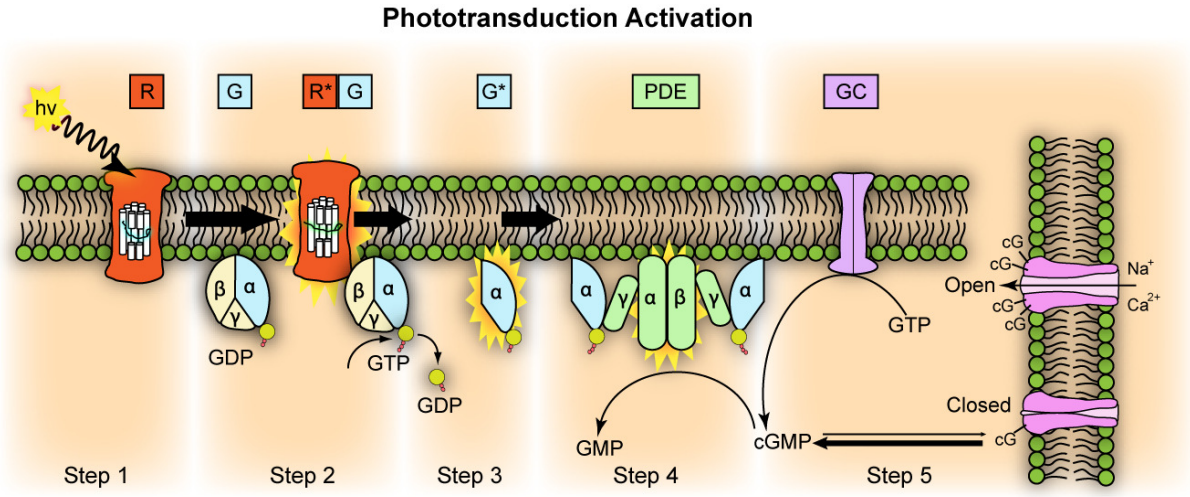

Figure 4: Sequence of the phototransduction cascade

A photon (hv) hits a rhodopsin (R) molecule and triggers a conformational change in the chromophore leaving rhodopsin in an excited state (R*) (step 1). Upon excitation of rhodopsin the heterotrimeric G-protein of the phototransduction cascade transducin (G) binds to R* thereby GDP is exchanged by GTP (step 2). This in turn activates G and the α-subunit with bound GTP (G*) dissociates from the trimeric complex (step 3). Two molecules of G* then bind to phosphodiesterase (PDE), which is also a heterotrimeric protein. Binding of G* results in enzymatic activation of PDE thereby catalyzing hydrolysis of cyclic GMP (cGMP) (step 4). The intracellular decrease in cGMP leads to closing of cGMP-gated cation channels (CNG). Subsequently, guanylate cyclase (GC) is activated regenerating cGMP from GTP (step 5). (source: http://upload.wikimedia.org/wikipedia/en/d/de/Phototransduction.png)

Of note, unlike every other neuron photoreceptors hyperpolarize upon signal transduction initiated by light. Thus, actually the dark state has to be regarded as the signalling event depolarizing the cell and therefore triggering neurotransmitter release. Transmission of the light stimuli to the bipolar cells can occur via two pathways. In the ON-pathway propagation occurs via ON-bipolar cells. ON-bipolar cells depolarize following reduced glutamate release from the photoreceptor upon light stimulation. Subsequently, they transmit the signal further to ON-ganglion cells, which finally generate an action potential. In contrast, OFF-bipolar cells hyperpolarize under light conditions, hence being inhibited in transmission to the OFF-ganglion cells [1].

The whole cascade has to be tightly controlled and restored to guarantee the very quick response to different light conditions. Several termination mechanisms operate to shut down phototransduction and restore the resting membrane potential. First, the photoexcitated rhodopsin (R*) is phosphorylated by rhodopsin kinase (RK) which allows arrestin to bind which in turn inhibits further activation of transducin molecules.

Second, the transducin heterotrimer is re-assembled by the return of the α-subunit upon hydrolysis of GTP to GDP during the interaction with PDE. Third, the decrease of intracellular Ca^{2+} upon channel closing activates Ca^{2+}-sensitive proteins like guanylate cyclase activation protein (GCAP), which again act on the guanylate cyclase (GC) that finally restores cGMP levels (step 5). Recoverin, another Ca^{2+}-sensing molecule regulates the activity of the rhodopsin kinase. Finally, the all-trans retinal chromophore has to be restored to 11-cis retinal for regeneration of the visual pigment. This restoration is accomplished in the visual cycle which mainly takes place within the RPE (Figure 5) [10]. Briefly, all-trans retinal is reduced and subsequently transported to the RPE, where the enzymatic steps of isomerization occur. One crucial enzyme within the visual cycle is RPE65, which catalyzes the isomerization step from all-trans retinyl ester to 11-cis retinol [11]. In mice, a polymorphism in this gene was described leading to an amino acid exchange (p.M450L). The leucine variant increases rhodopsin regeneration kinetics, therefore enhancing photon catch capacity and consequently rendering BALB/c mice more susceptible to light damage due to very fast rhodopsin regeneration [12,13]. The presence of RPE65 in cones is still a matter of debate [14-16]. It is worth mentioning, that recent research provided some evidence for a visual cycle regenerating the chromophore for cones photoreceptors [17,18].

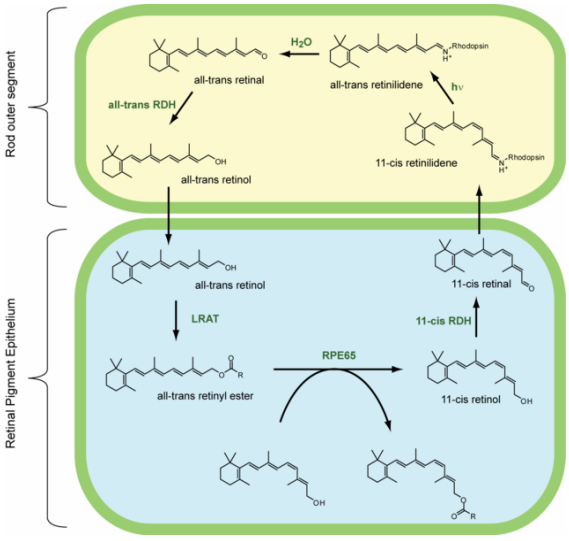

Figure 5: Schematic representation of the most important steps in the rod visual cycle

In the visual cycle the chromophore 11-cis retinal of the visual pigments is regenerated. In rods, the reactions take place in the photoreceptor outer segment and in the retinal pigment epithelium. Absorption of light leads to isomerization of 11-cis retinal to all-trans retinal (all-trans retinilidene). The

all-trans retinal dissociates from the opsin protein backbone and is reduced to all-trans retinol by all-trans retinol dehydrogenase (all-trans RDH). All-trans retinol is transported to the pigment epithelium and subsequently esterfied by lecithin retinol acyltransferase (LRAT) to form all-trans retinyl ester. The retinyl esters serve as a substrate for the isomerization process catalyzed by RPE65. The product of this reaction 11-cis retinol is oxidized by 11-cis retinol dehydrogenase to the aldehyde (11-cis retinal). 11-cis retinal is then finally transferred back to the outer segment where it binds to opsin (11-cis retinilidene) building the holoprotein rhodopsin now ready to start another cycle. In addition to the key proteins indicated above, several chaperones are participating in this complex cascade, which will not be described in detail. (modified after http://upload.wikimedia.org/wikipedia/en/thumb/0/09/Visual_cycle_v2.png/638px-Visual_cycle_v2.png)

Beside the quick restoration after photoexcitation the photoreceptors possess a fine-tuned mechanism allowing them to operate at a broad range of illumination levels. In this light adaptation process the sensitivity of photoreceptors decreases with increasing illumination levels in order to prevent saturation. The main mechanism that is thought to contribute to adaptation is the light-dependent drop of Ca^{2+} within the cell. As mentioned before the Ca^{2+} sensitive proteins recoverin and GCAP lead to inactivation of rhodopsin and restoration of cGMP, respectively, thereby contributing to lowered responsiveness in light. In addition, an astonishing physiological re-distribution of proteins of the phototransduction cascade in response to light has been identified. Arrestin, transducin and recoverin were found to translocate upon illumination, a process that is thought to contribute to adaptation to bright light [19]. In the dark adapted rod, arrestin is located in the inner segment and the inner plexiform layer while transducin is in the outer segment. Upon illumination arrestin moves to the outer segment for cessation of the phototransduction cascade and transducin moves in the opposite direction to prevent its activation by rhodopsin. Recoverin shifts from the outer segments to the synapse upon a light trigger. During dark adaptation, the proteins move back to their respective dark compartment. Of note, in cones arrestin has been described to compartmentalize as well. A recent study could prove that cone transducin redistributes as well however only at high light intensities [20]. The mechanism of transport is still a matter of debate. Basically, either active transport or diffusion is the cellular means of protein transportation. Studies providing evidence for either diffusion or active transport or both depending on the transport direction exist [21]. Thus, no definite answer to the mechanism of transport exists to date.

1.1.4 Electroretinography (ERG)

The membrane potential changes that are generated during phototransduction can be measured by electroretinography (ERG). Contribution of the rod and cone system can be discriminated by applying scotopic or photopic light conditions, respectively. The recorded response consists of several components originating from different cell types (Figure 6). They were described in detail in 1933 by Ragnar Granit, who was honoured with the Nobel prize in Physiology and Medicine in 1967 for his work on ERG [22].

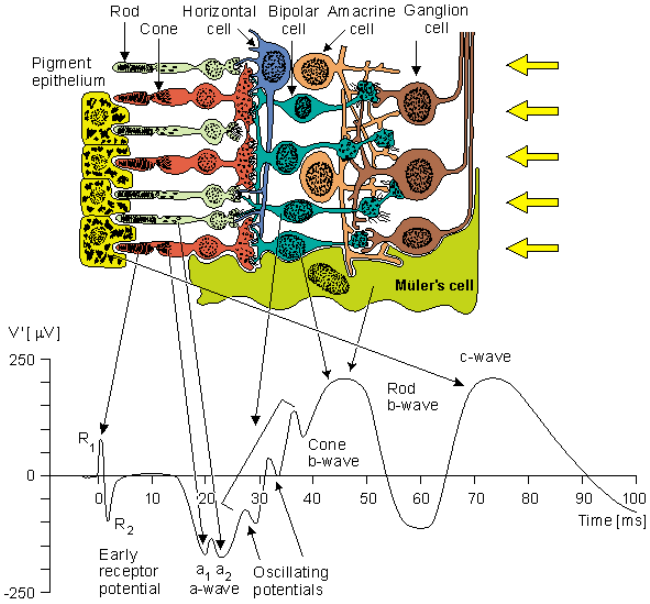

Figure 6: Retinal cells and their originating ERG components

An electroretinographic profile consists of several peaks. The early receptor potentials R_1 and R_2 are thought to evolve directly from the photoreceptors during conformational changes of the visual pigment. The cornea-negative a-wave component results from changes in the current in the rod or cone outer segment depending on the flash intensity and background illumination (a_1 and a_2 wave, respectively). Subsequent current changes in the second-order neurons (mainly from the ON-bipolar cells) are reflected in the cornea-positive rod or cone b-wave. In between, fast wavelets can be detected when bright light is applied. These oscillatory potentials are thought to originate presumably from cells of the inner plexiform layer. Finally, a cornea-positive c-wave can be monitored that is elicited by the retinal pigment epithelium. (http://butler.cc.tut.fi/~malmivuo/bem/bembook/28/fi/2802.gif)

An electroretinogram is recorded by placing a recording electrode on the cornea and a reference electrode to the forehead, temple, or earlobe. Light stimuli of a broad range of intensity are usually presented within a Ganzfeld bowl. The current changes from light signaling within the retina can then be detected by amplification of the signal.

The cornea-negative a-wave is the first prominent signal that can be recorded [2]. It is thought to derive from the rod and/or cone photoreceptors (a2 and a1 wave, respectively) due to closing of cyclic nucleotide gated channels (CNGs) upon light exposure. Thus, it directly reflects the integrity of the photoreceptor cells. The second prominent signal is the cornea-positive b-wave which is interpreted to be elicited mainly from the ON-bipolar cells therefore reflecting signal transmission from photoreceptors to ON-bipolar cells. However, Mueller cells are also thought to contribute to the signal. Based on the application of different light regimens (scotopic or photopic), the rod and the cone responses can be discriminated. When a bright light stimulus is applied, an array of low amplitude oscillating wavelets can be recorded. These oscillatory potentials (OP) are thought to originate from the inner retina [23]. Application of a flicker stimulus can also discriminate rod and cone responses as they respond temporally differently. Finally, a late cornea-positive c-wave signal can be detected, which presumably is generated by the RPE.
For diagnostic purposes of retinal diseases, the ERG has become a very important tool as many cell types and putative aberrations in the responses can be specifically monitored. In addition, several sophisticated variations of the method exist allowing further clinical discrimination of distinct phenotypes [24].

1.1.5 The photoreceptor connecting cilium

The connection between the inner and outer segment of the photoreceptor cell is a non-motile cilium termed the connecting cilium (Figure 7). Thus, the outer segment of photoreceptors can be regarded as the distal part of a non-motile cilium [25,26]. The connecting cilium corresponds to the transition zone of motile cilia, but possessing a “9+0” axoneme. Like in prototypic cilia the axoneme grows from the basal bodies which are located at the most apical side of the inner segment.

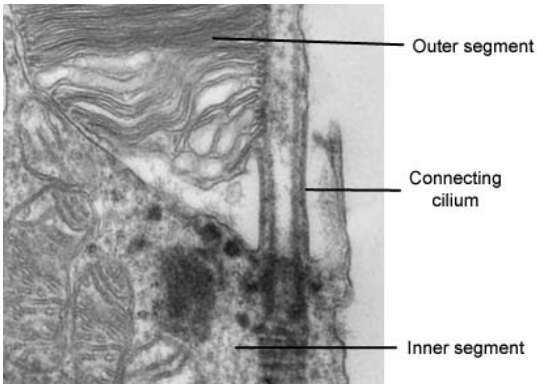

Figure 7: Electronmicrograph of a rod photorceptor
The connection between the inner and outer segment of rod and cone photoreceptors is the connecting cilium. The ciliary axoneme extends fro the inner segment into through the cilium into the outer segment. (modified with kind permission of Dr. Holger Jastrow (http://www.unimainz.de/FB/Medizin/Anatomie/workshop/EM/eigeneEM/Retina/HRet2.jpg)

The most important function of the connecting cilium beside its structural importance is the transportation of proteins and other components to the outer segment. The outer segment disks are constantly renewed and proteins destined for the outer segment have to be massively transported from the protein synthesizing inner segment through this slender connection. One of the main cargoes being transported is the opsin molecule as it is the most abundant protein in the outer segment. The mechanism of opsin transport is well studied and revealed some principles of the ciliary transport mechanisms.

Membrane-bound proteins like rhodopsin have to pass two transportation steps. Following synthesis in the endoplasmatic reticulum (ER) and modification and sorting in the Golgi network, they are delivered to the trans-Golgi network (TGN). In the first transport passage, vesicles bud off the TGN and undergo vesicle transport to the apical membrane of the inner segment where they fuse with the ciliary membrane [27]. Rhodopsin contains a VXPX-COOH sequence that is mandatory for correct targeting to the outer segment [28]. Of note, other ciliary proteins are assumed to have a ciliary targeting sequence as well [29]. Several Rab GTPases are involved in regulation processes of vesicle budding and fusion [30]. In addition, the small GTPase ARF4 specifically binds to the C-terminal VXPX sequence which is an essential step for vesicle budding from TGN [31]. The motor protein responsible for the retrograde transport to the ciliary base is thought to be cytoplasmic dynein as interaction of rhodopsin with the dynein light chain Tctex-1 was shown [32]. In the second step the rhodopsin molecules have to be transported through the cilium to the distal part in order to be incorporated into the disk membranes. The transport along the ciliary membrane is accomplished by motor proteins Myosin VIIa and Kinesin II [33,34]. Kinesin II is a microtubular motor protein involved in anterograde transport from the base to the tip of the cilium. The transport system through the cilium is also called intraflagellar transport (IFT) and is essential for assembly and maintenance of cilia and flagella (see chapter Intraflagellar transport).

1.2 The retina and photoreceptors in disease

The retina is a highly organized and specialized tissue as described in the chapter before. Hence, any disturbance of this versatile system leads to impairment or loss of vision. The sense of vision is one the most important senses for humans, thus an impairment of vision has a huge impact on the patients life. Many diseases affecting

the visual system are known and they occur in each structure of the eye. The most severe impairment of vision however arises from defects in the retina. Of interest, it is now known that retinal degenerations have underlying genetic defects (http://www.sph.uth.tmc.edu/Retnet/).

The retinal degenerations can be classified into two major groups based on the photoreceptor cell type mainly affected. Degeneration of rod photoreceptors occur in several diseases including Retinitis pigmentosa (RP, OMIM 268000), Leber congenital amaurosis (LCA, OMIM 204000) and syndromes associated with RP like Usher syndrome (USH, OMIM 276900) and Bardet-Biedl syndrome (BBS, OMIM 209900). Degenerations affecting primarily the cone photoreceptors occur in cone-rod degeneration (CORD, OMIM 120970), cone dystrophy (COD, OMIM 180020), Stargardt's disease (STGD, OMIM 248200), Sorsby fundus dystrophy (SFD, OMIM 136900), Best vitelliform macular dystrophy (VMD, OMIM 153700), and in the complex trait age-related macular degeneration (AMD).

1.2.1 Retinitis pigmentosa

The term Retinitis pigmentosa (RP) encompasses a group of retinal degenerations with highly variable clinical and genetic heterogeneity. The heterogeneity from the clinical point of view is based on the broad range of phenotypic manifestations found in affected individuals. The typical signs of early disease which usually manifest around the 2^{nd} – 3^{rd} decade of life are night blindness and tunnel vision with progressive constriction of the visual field. Later in disease the patients may become legally blind. However, central vision acuity is preserved until late stages of the disease as mainly rod photoreceptors are affected. In ophthalmoscopic examinations typical disease manifestations are usually evident. The most characteristic finding is changes in the pigmentation named "bone-spicules" based on their appearance (Figure 8).

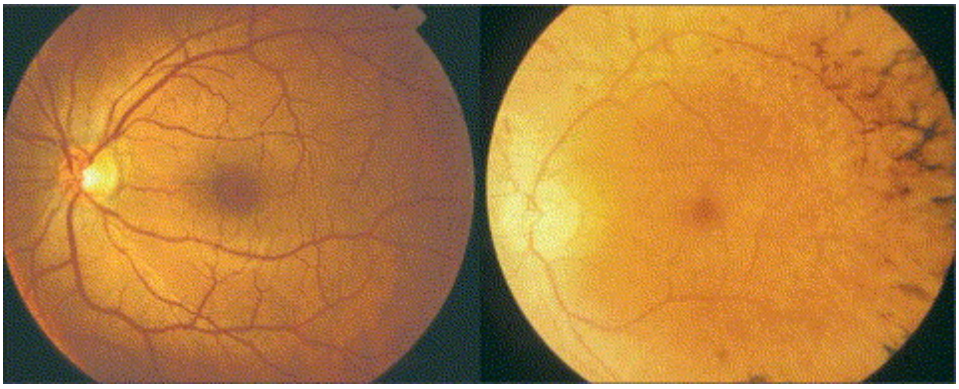

Figure 8: Fundus appearance in a patient suffering from RP

In contrast to the fundus of a healthy individual (left) patients suffering from RP (right) have attenuated retinal vessels, optic disc pallor and deposits of intraretinal pigment in the periphery which are termed "bone-spicules" (source: Hartong et al., 2006)

Electrodiagnostic testing of RP patients reveals significantly reduced scotopic ERG responses. In most cases, the photopic responses are severely diminished as well (Figure 9.). In addition, the latencies of the responses are also prolonged.

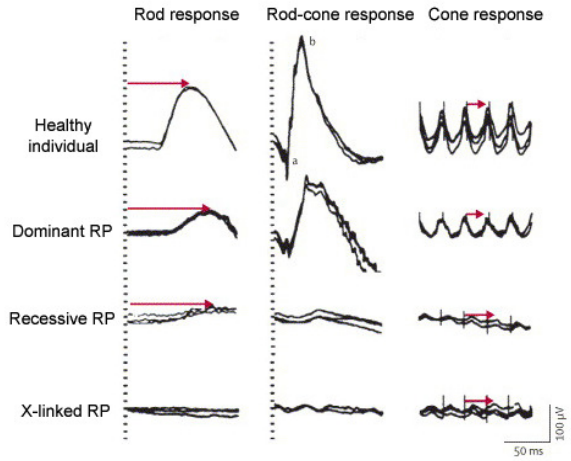

Figure 9: ERG panels from a healthy individual and three RP patients at the age of 9-14 years.

Different stimuli were applied in order to elicit isolated rod responses (left column), mixed rod-cone responses (middle column) and isolated cone responses (right column). Implicit times are indicated by arrows. Patients suffering from dominant RP displayed reduced amplitudes while in patients with recessive and X-linked RP responses were severely diminished or not recordable at all, respectively. (modified after Hartong et al., 2006)

Familial forms of RP and can be transmitted autosomal-dominant (AD; 50-60%), autosomal-recessive (AR; 30-40%) as well as X-linked (Xl; 5-15%) [35]. In addition, many sporadic cases have been described. All over, mutations in > 40 genes have been identified to date which lead to RP. Depending on the mutation either dominant or recessive inheritance is observed, sometimes even within one gene. Additional 10 genetic loci were assigned and the search for the underlying genes is a matter of

ongoing research. Still, these numbers represent only a portion of genes involved in RP and many others remain unidentified. The gene products involved in RP are partly retina-specific but also some widely expressed genes lead to this tissue-specific phenotype. The question of why mutations in ubiquitously expressed genes result in physiological dysfunctions only in the retina is one of the enigmas to be solved. One possible explanation is based on the extraordinary high metabolic demand of the retina which might imply a lower tolerance of irregularities than in other tissues. Interestingly, RP is observed as a condition in several recessive syndromes like abetalipoproteinemia (OMIM 200100), Alstrom syndrome (OMIM 203800), Refsum syndrome (OMIM 266500), Bardet-Biedl syndrome (OMIM 209900), Laurence-Moon syndrome (OMIM 245800), Usher syndrome (OMIM 276900), Cockayne syndrome (OMIM 216400), and pallidal degeneration (OMIM 260200). Some of them will be described in more detail in the "ciliopathies" section.
About 5-15% of all RP cases suffer from X-linked RP (XlRP), which displays the most severe disease course [36]. Affected males present early in life with the first symptoms. Carrier females manifest with a very broad spectrum of symptoms. Two genes had been found to harbour mutations leading to XlRP. The Retinitis pigmentosa 2 (RP2) gene was identified in 1998 by Schwahn et al. [37] and recent studies characterized the gene product to be a GTPase-activating protein (GAP) for Arl3 protein [38]. Mutations in RP2 were estimated to account for 20% of all XlRP patients. The major cause of XlRP is mutations in the Retinitis pigmentosa GTPase regulator (RPGR) gene. The remaining mutations not explained by those two genes might be found within the 4 linkage intervals for XlRP or in hitherto unknown genes/loci.

1.2.2 The Retinitis pigmentosa GTPase Regulator (*RPGR*) gene

The Retinitis pigmentosa GTPase regulator (*RPGR*) gene is a widely expressed gene and highly conserved throughout the species. It was cloned in 1996 and was initially reported to consist of 19 exons (Figure 10). However, it turned out that *RPGR* is subject to an extraordinary high degree of alternative splicing and many novel tissue-specific exons were described [39-41]. Exons 2-11 are homologous to the RCC1-like protein. RCC1 is a guanine nucleotide exchange factor for small GTPase Ran, involved in nuclear import and export pathways. Based on this homology the gene was designated "GTPase regulator" although putative GTPase regulating function has never been proven to date.

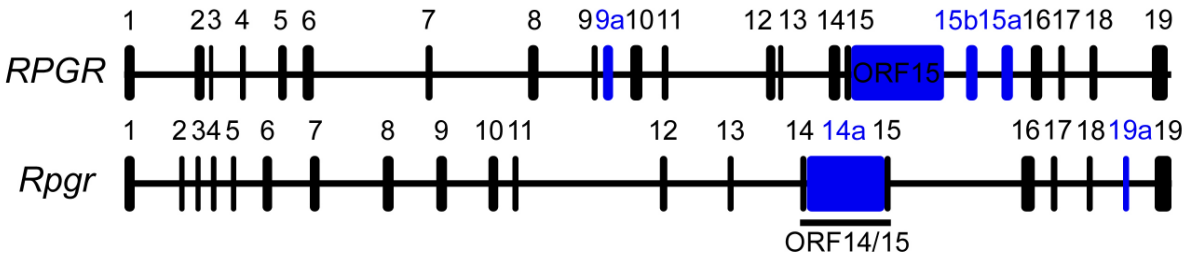

Figure 10: Schematic representation of the human and mouse *RPGR/Rpgr* gene

RPGR/Rpgr is known to consist of 19 constitutive exons (black boxes) in human (upper scheme) and mouse (lower scheme). However, additional exons have been discovered in both species (blue boxes). In humans, exon ORF15 is preferentially expressed in retina and is a mutational hot spot [39]. Exons 15b and 15a are additional exons within intron 15. Exon ORF15 and exon 15a introduce premature termination codons (PTC) [39,40]. Exon 9a was recently described to be expressed predominantly in cones introducing a premature stop codon [41]. In mouse, exons 14-14a-15 correspond to ORF14/15 [39]. Exon 19a is expressed in several tissues and also contains a PTC. In addition to inclusion of novel exons, several transcripts show skipping of exons.

On protein level two major isoforms are assumed to exist. The $RPGR_{1-19}$ isoform results from a transcript including exons 1-19 and has a molecular weight of about 95 kDa. It contains the RCC1-like domain (RLD) at its N-terminus and an isoprenylation motif at the C-terminus (Figure 11A). The RPGR-ORF15 isoform is produced when the alternative exon ORF15 is included into the transcript. This isoform is assumed to harbour the RLD at the N-terminus but an alternate C-terminus rich in acidic amino acids due to the unique repetitive composition of the exon ORF15 (Figure 11B). Recently, a third isoform RPGR-Int9 has been described containing exons 1-9a therefore possessing a truncated RLD (Figure11C) [41].

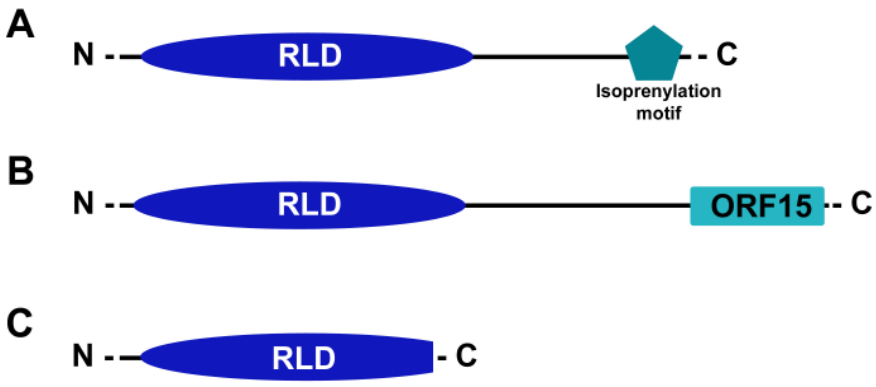

Figure 11: RPGR protein isoforms in human and mouse

On protein level, only few isoforms are known to exist in comparison to transcript isoforms. (A) Transcripts containing exons 1-19 result in a protein with the RCC1-like domain (RLD) at the N-terminus and an isoprenylation motif at the C-terminus, in both human and mouse. (B) When exon ORF15 in humans or exon ORF14/15 in mouse is included in the transcript, the protein carries an alternate C-terminus with the ORF15 domain, which is rich in acidic amino acids. (C) In humans, the alternative exon 9a results in a short protein with a truncated RLD.

One characteristic of the RLD is the seven-bladed propeller structure that was modelled based on the three-dimensional structure of RCC1 (Figure 12) [42]. In addition, most exons of the RLD are in-frame, therefore not disrupting the reading frame when deleted by alternative splicing or by mutations.

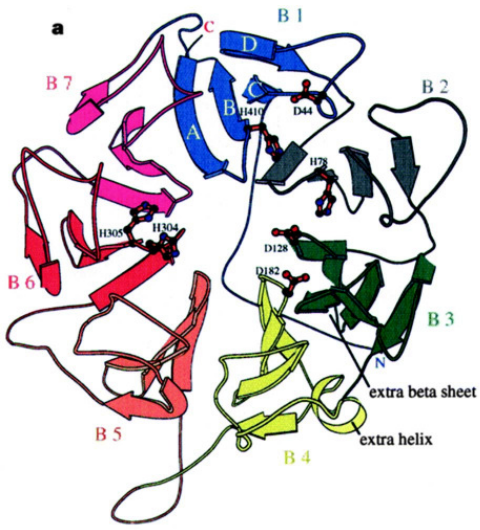

Figure 12: Seven-bladed propeller structure of RCC1 protein

The crystal structure of Regulator of Chromosome Condensation 1 (RCC1) protein with a 1.7 A resolution. The seven propellers are indicated in different colors and designated B1-B7. Conserved amino acid residues that are assumed to be important for connection of the blades and the interaction with Ran are indicated in “stick-and-ball” fashion. According to this model, the RLD of RPGR is assumed to posses a similar tertiary structure (Source: Renault et al, 1998)

Expression of *RPGR* was found in many tissues like retina, brain, kidney, lung and testis [40]. However, tissue-specific transcript and protein isoforms exist [39,40,43]. Localization of RPGR was investigated in some species and with different sets of antibodies. It was mainly found in the connecting cilium and at the basal bodies of

photoreceptor cells, indicating that it might exhibit its biological function in ciliary transport pathways [44-47]. Likewise, several interaction partners of RPGR are ciliary proteins and/or are involved in microtubular transport pathways (Figure 13) [46-50].

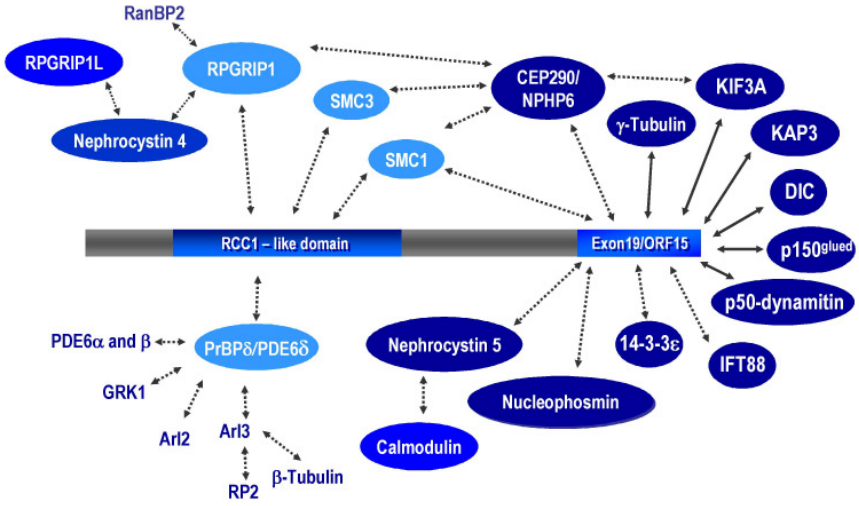

Figure 13: Scheme of RPGR and its known interaction partners

Several interaction partners of RPGR isoforms have been identified. Four have been found to interact with the RCC1-like domain (RLD). These are PDE6δ/PrBPδ, RPGRIP1, SMC1 and SMC3 proteins (light blue). RPGRIP1 in turn has been reported to be in a complex with nephrocystin-4 and thereby linked to RPGRIP1-like (RPGRIP1L) protein. For the C-terminus of both the $RPGR_{1-19}$ as well as the ORF15 many proteins have been found to interact (arrows). These are centrosomal/basal body proteins like CEP290/NPHP6, γ-tubulin, 14-3-3ε and IFT88. For the latter two, interaction was only found with the ORF15 isoform (doted lines). Several proteins of microtubular transport pathways were also found. Among them are subunits of anterograde (KIF3A and KAP3) as well as retrograde (dynein intermediate chain (DIC), $p150^{glued}$ and p50-dynamitin) motor proteins. They were found in a complex with both isoforms (black lines and arrows). Nephrocystin-5 which is a ciliary protein and nucleophosmin, a nuclear protein, were also found in a complex with RPGR-ORF15 isoform.

Patients suffering from X-linked RP (XlRP) were found to harbour mutations in *RPGR* [51,52]. Overall, it is known to be a major gene for XlRP. Mutations account for approximately 70-80% of all cases [39]. Recent reports described not only patients with classical RP, but also affected by cone-rod dystrophy, cone dystrophy, recessive atrophic macular degeneration and Coat's like exsudative vitreoretinopathy [53-56]. Interestingly, mutations do not only lead to retinal degenerations but also to syndromic phenotypes including hearing defects and recurrent sinorespiratory infections [57]. There were also patients described suffering from RP in conjunction of Primary Ciliary Dyskinesia (PCD) [58], a disease with symptoms of the respiratory tract

like rhinitis, sinusitis, otitis media and bronchiectasis [59]. In addition, patients may also develop situs inversus and male infertility. These findings further support the role of RPGR not only in the photoreceptor but also in other tissues.

1.3 Cilia and Flagella in health

Cilia and flagella are tiny, hair-like structures protruding from virtually every kind of cell. They are evolutionary highly conserved and can be found in simple protists as well as more complex multicellular organisms. Based on historical definition, cilia are short and numerous extensions on the cell surface responsible for the transportation of material across the cell or tissue. Their movements are a characteristic ciliary beats, which are episodes of an effective stroke and a recovery stroke. Flagella usually are only one or two long structures which are responsible for cell motility. The movements of a flagellum are successive waves that propagate along the entire length [60]. To date it is known that cilia/flagella are not only responsible for motility and fluid movement but also for chemo-, mechano-, and photosensation.

1.3.1 Structure and function of vertebrate cilia and flagella

Despite their different names, cilia and flagella share the same structure. Basically, a cilium/flagellum consists of a core microtubular structure (axoneme), which is anchored to the cell via the basal body (Figure 14). It is surrounded by a specialized membrane, which extends from the plasma membrane. The axoneme of motile cilia and flagella is built in the classical “9+2” arrangement, where nine outer microtubule doublets surround a central pair of singlet microtubules. The outer doublets are composed of an A and B tubule, both long polymers of heterodimeric α– and β tubulin monomers. The polymerisation of microtubules is a highly dynamic process. At one end (plus-end) fast assembly occurs leading to growing of the polymer and at the other end (minus-end) they assemble more slowly. Usually, the minus-end of the microtubule axoneme is anchored to the basal body resulting in growth direction into the cilium. Several other protein complexes are attached to the central microtubule structure for stability and force generation. These are the inner and outer dynein arms (IDA and ODA), the radial spokes and inter-doublet connections. The IDA and ODA are microtubular motor proteins that cause sliding of the microtubules with respect to each other generating bending of the axoneme.

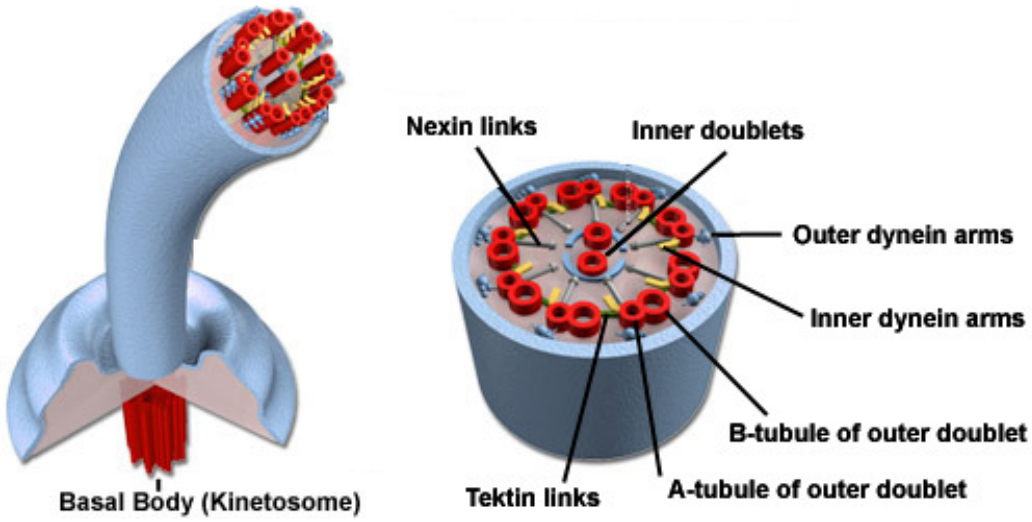

Figure 14: Schematic representation of the structure of "9+2" cilia and flagella

Motile cilia/flagella share a common architecture. The ciliary axoneme of motile cilia has a characteristic "9+2" structure with nine microtubule doublets surrounding two single central microtubules. The outer doublets are composed of an A and B tubule. Attached to the A-tubule are the inner and outer dynein arms connecting it to the B-tubule of the next doublet. In addition, the junction is strengthened by tektin links. Radial connections to the central pair of microtubules are built by nexin links. The axoneme is attached to the cell body via the basal body (kinetosome). (modified after http://micro.magnet.fsu.edu/cells/ciliaandflagella/images/ciliaandflagellafigure1.jpg).

The basal body is a post-mitotic centrosome consisting of two centrioles (Figure 15) [61]. In animal cells, centrioles are two barrel-shaped hollow cylinders composed of nine sets of triplet microtubules with no doublet in the center. At their proximal side, they are positioned close to each other in a right angle. The maternal (distal) centriole has appendages and is thought to serve as attachment site for microtubules. The two centrioles are surrounded by the pericentriolar matrix (PCM) which is the site for the nucleation of microtubules. Major constituents of the centrosomes are proteins like γ-tubulin and centrin.

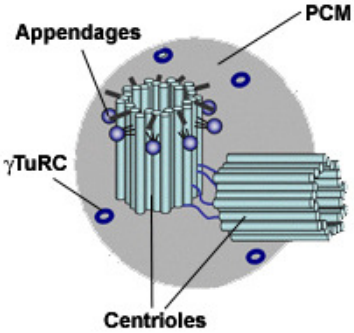

Figure 15: Scheme of a centrosome

The centrosome in animals is composed of two centrioles which are located perpendicular to each other. They have a triplet organization of microtubules. One centriole (the mother-centriole) has appendages. They are surrounded by the pericentriolar matrix, where γ-tubulin ring complexes (γTuRC) are a major protein constituent. (modified after http://www.irbbarcelona.org/files/Image/luders_fig3.jpg)

During mitosis centrosomes organize the mitotic spindles. In addition, they were reported to have regulatory functions in cell cycle progression [62]. In post-mitotic cells the centrosome moves to the plasma membrane to become the basal body. The maternal centriole serves as nucleation center for ciliogenesis. The triplet architecture of the microtubules of the basal body is converted into the doublet structure of the axoneme in the transition zone (Figure 16) [63]. Proximal transition fibers attached to each of the nine doublets of the basal body extend to the plasma membrane and serve as anchor of the complex.

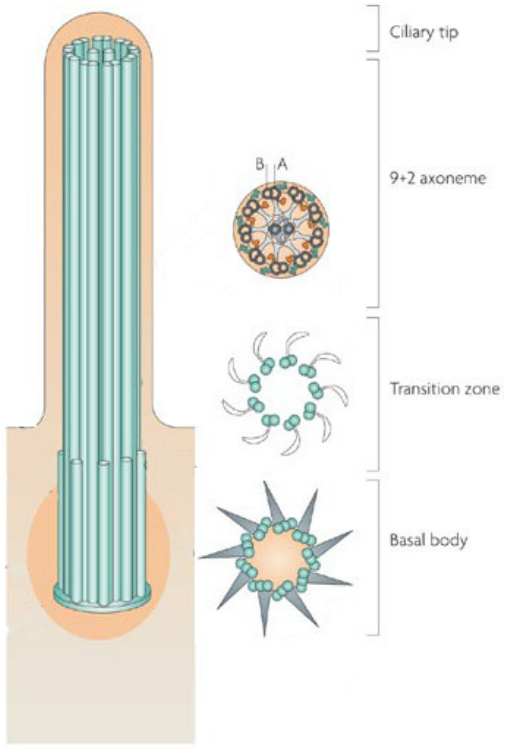

Figure 16: Compartments of a motile ciliary axoneme

Basically, a ciliary axoneme can be subdivided into four compartments. The basal body is a specialized centrosome consisting of a triplet microtubular structure (light green). At the distal end it is anchored to the plasma membrane by radial transitions fibers (grey). The centrioles are embedded in the pericentriolar matrix (orange). In the transition zone the triplet structure is converted into the doublet structure of peripheral microtubules of the axoneme. The transition fibers connect each doublet to the membrane. These fibers mark the border to the cilium. Proteins of the intraflagellar transport (IFT) machinery accumulate here. The "9+2" axoneme is present in the major part of the cilium. The most distal side of the axoneme is the ciliary tip where the switch between anterograde and retrograde transport is assumed to occur. (modified after Fliegauf et al., 2007).

Currently, vertebrate cilia are divided into four groups based on their axonemal structure [63-65]. Motile "9+2" cilia are present numerously on the cell surfaces of cells and beat in an orchestrated fashion to generate movement. They can be found on epithelial cells lining the upper and lower respiratory tract where they are necessary for mucociliary clearance, the ependymal cells lining the ventricles of the brain to move the cerebrospinal fluid as well as the reproductive tract in males for movement of sperm cells (sperm flagella and cilia of the testis efferent duct) and females (motile cilia from the fallopian tubes and the uterine lining for transportation of the oocyte). In contrast, primary cilia are present on virtually every kind of cell. Usually they are solely and immotile as their axoneme are built in a "9+0" arrangement lacking the

central doublets. These non-motile cilia are thought to play a role in sensation, like mechanosensation of tubular flow of renal cilia or sensation of light (photoreceptor connecting cilium), of odours (cilia of the olfactory epithelial cells) and of sound (kinocilium in the cochlea) [66]. The non-motile kinocilium is part of the hair cell bundle in the cochlea, which is involved in the transduction of a mechanical stimulus into an electrical signal. Although this monocilium is involved in mechanosensation, it retains the “9+2” architecture. One exception are nodal cilia with a “9+0” axoneme but still possessing the ability of beating in a propeller-like fashion as dynein arms are present. Beating of these cilia generates movement of extraembryonic fluid (nodal flow) which is required for left-right asymmetry [67]. Recent studies discovered links between primary cilia and receptor-dependent pathways like sonic hedgehog (SHH), platelet-derived growth factor receptor (PDGFR) and non-canonical Wnt/planar cell polarity (PCP) pathway [68-70].

1.3.2 Intraflagellar transport (IFT)

Proteins required for assembly and maintenance of cilia and flagella are synthesized within the cell soma and have then to be transported into the cilium/flagellum. The transport into the cilium can occur via several ways like diffusion or active transport. Membrane proteins are synthesized at the rough endoplasmic reticulum and processed via the Golgi and subsequently the trans-Golgi network (TGN) where protein-containing vesicles bud off. It is assumed, that ciliary proteins contain a targeting motif in order to be correctly sorted [29]. At the basal body region vesicles carrying the cargo are transported and dock at the transition zone. Transportation from the transition zone to their final destination site is accomplished by a specialized process called intraflagellar transport (IFT) [71-73] (Figure 17). The IFT motor proteins and IFT particles also accumulate at the transition zone [74]. Cargo, motor proteins and particles are assembled to build the IFT complex which is now ready to start the journey into the cilium. As IFT is a complex cellular process the components responsible for function and control of this transportation machinery are numerous.

Basically, transportation occurs bidirectional from the base of the cilium to the tip in anterograde direction (minus-end to plus-end) and in the opposite direction in retrograde direction (plus-end to minus-end). Hence, two different motor proteins were assumed to exist driving transport in either direction. The anterograde motor protein was identified to be kinesin II [75]. It is a heterotrimeric protein composed of the

KIF3A and the KIF3B motor subunits and a kinesin-associated protein KAP. However, recent studies point towards a second anterograde motor protein called OSM-3/Kif17 [76]. Studies on *Chlamydomonas* mutants revealed cytoplasmic dynein 1b as the corresponding retrograde motor protein [77]. The IFT particles consist of at least 16 polypeptides and can be subdivided into two complexes, whereby complex A is linked to retrograde transport and complex B to anterograde transport. Originally they were identified by particle fractionation in *Chlamydomonas* but performing database search on the derived amino acid sequences revealed that homologues of *Chlamydomonas* IFT proteins can be found in many organisms including worms (*Caenorhabditis.elegans*), fruit fly (*Drosophila melanogaster*), zebrafish (*Danio rerio*), mouse (*Mus musculus*) and human (*Homo sapiens*). One prominent example is IFT88, a protein of complex B that was identified in several species revealing identical function in IFT processes [78,79].

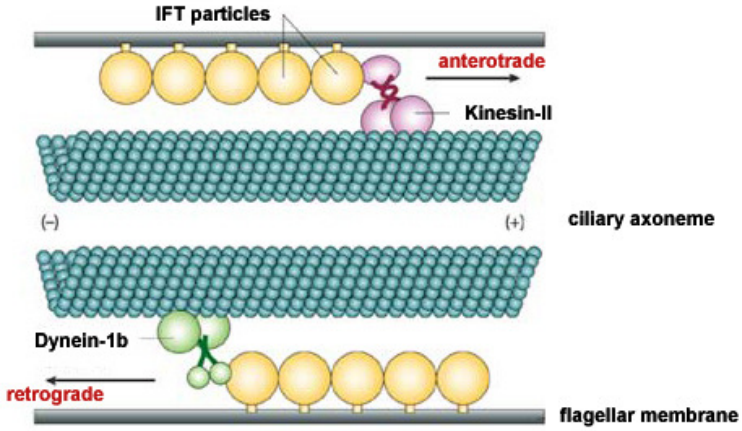

Figure 17: Scheme of intraflagellar transport

Transport of cargo in cilia in flagella is accomplished via intraflagellar transport (ITF). Motor proteins move along the ciliary axoneme. The cargo is suggested to be linked to the motor proteins via IFT particles. The motor protein for anterograde transport is kinesin-II and for retrograde transport dynein-1b. (modified after: http://www.nature.com/nrm/journal/v3/n11/images/nrm952-f2.jpg)

Despite the knowledge about the IFT components, many open questions concerning regulation of this process remain, e.g. entry of IFT complexes into the cilium and loading as well as unloading processes at the transition zone and the flagellar tip, respectively. However, some speculations about the gating function of the transition zone exist. The transition fibres are thought to build a “flagellar pore complex” which might serve as gate and docking site for proteins destined for the cilium[72]. In addition,

a lipid dense periciliary domain that might act as a second barrier for controlled entry of proteins to the cilium was described [80].

1.4 Cilia and Flagella in disease (Ciliopathies)

Cilia and flagella are involved in many biological processes. Thus, defects in those complex organelles have detrimental consequences for development and physiological homeostasis of an organism. Within the last years numerous studies reported on human disorders related to ciliary defects. In addition, many animal models were described having cilia abnormalities due to defects in ciliary proteins. This emerging class of diseases resulting from genetic defects is now termed ciliopathies. Ciliopathies include many different entities that affect many organ systems (Figure 18). They arise from mutations in genes coding for ciliary proteins involved in the assembly or maintenance of cilia and flagella. The clinical features and underlying genetic defects of the most common phenotypes will be described in detail in order to emphasize the common features reflecting the broad biological role of cilia and flagella.

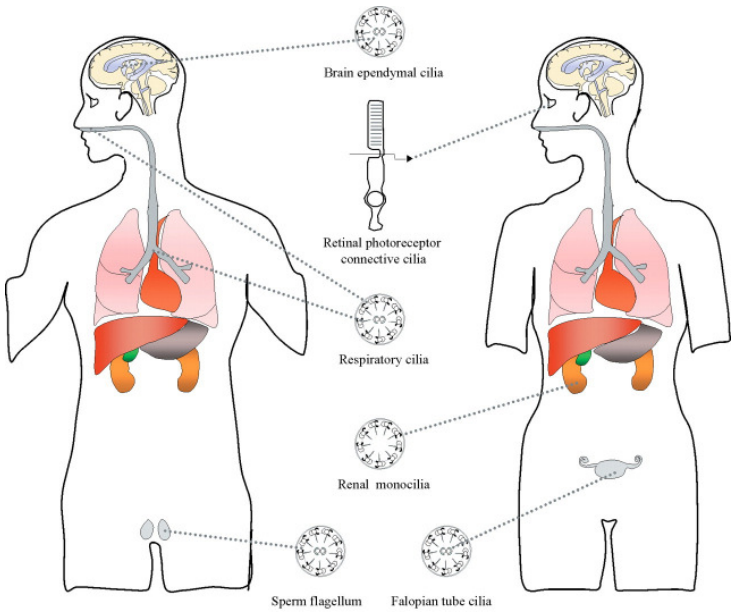

Figure 18: Cilia in the human body affected by ciliopathies

Different types of cilia are present in the human body. These are motile “9+2” cilia of the ependymal cells lining the ventricles in the brain, the photoreceptor connecting cilium in the retina with a “9+0” axoneme, the motile “9+2” cilia of the epithelial cells lining the respiratory tract, monocilia of the kidney with a “9+0” cilium, the motile cilia with a “9+2” structure of the fallopian tubes in the uterus (right) and the sperm flagellum and the efferent ducts of the testis also with a “9+2” structure (left). (Source: Ibanez-Tallon et al., 2003).

Retinal ciliopathies

Many forms of retinal degenerations can be considered as ciliopathies, as the photoreceptor outer segment is a specialized and modified cilium. Isolated retinal degenerations include RP, macular degeneration, cone-dystrophy (COD), cone-rod dystrophy (CORD) and Leber congenital amaurosis (LCA). These entities are molecularly based on mutations in ciliary genes like RPGR, RPGRIP1, RP1 and RP2 (for detailed information www.sph.uth.tmc.edu/retnet). Additionally, other systemic disorders present with retinal degenerations. It is worth mentioning, that some RP patients were described to have aberrant sperm cell flagella [81].

Usher syndrome (USH, OMIM 276900)

Usher syndrome is the most frequent syndromic form of retinal degeneration and is characterized by a combination of deafness and blindness (RP) [64]. The disease can be divided into three clinical subtypes USHI, II and III. To date, 11 loci have been linked this disease and some underlying genes have been identified. Mutations were found in the genes coding for MyosinVIIa, harmonin, SANS, whirlin, cadherin 23, protocadherin 15, usherin, VLRG1 and clarin-1. These proteins exhibit different functions, however, most of them were found to interact building a large interactome which localizes to the connecting cilium and associated compartments. Interestingly, some patients also show abnormalities in their sperm tails.

Bardet-Biedl syndrome (BBS, OMIM 209900)

The Bardet-Biedl syndrome is rare genetic disease with pleiotropic manifestations like obesity, retinal degeneration, renal abnormalities, polydactyly, male hypogonadism, learning disabilities and diabetes mellitus. Up to now, 14 different genes have been identified underlying BBS (BBS1-BBS14). A breakthrough in understanding the molecular basis was reported recently when 7 of the involved BBS proteins were found to interact in a large complex at the ciliary base [82]. It is though to participate in docking and fusion of vesicles, and subsequent intraflagellar transport. Three other but very similar syndromes to BBS had been described: McKusick-Kaufman syndrome (MKKS, OMIM 604869), Laurence-Moon syndrome (LMS, OMIM 245800) and Biemond syndrome type 2 (BS2, OMIM 210350).

Alstrom syndrome (ALMS, OMIM 203800)

Phenotypical manifestations are very similar to those of Bardet-Biedl patients including progressive cone-rod dystrophy, sensorineural hearing loss, and childhood obesity mostly associated with diabetes mellitus. Other frequent symptoms are renal failure, pulmonary, hepatic, and urologic dysfunction and dilated cardiomyopathy. In contrast to BBS, patients do not develop mental retardation, polydactyly or hypogonadism. The disease is autosomal-recessively inherited and mutations were found in the ALMS1 gene. Its gene product is a basal body protein and is supposed to function in intracellular transport and ciliary biogenesis [83].

Primary ciliary dyskinesia (PCD, OMIM 242650)

PCD is a genetic disorder affecting 1/20.000 individuals and is inherited in an autosomal recessive manner. Patients show defects in mucociliary clearance leading recurrent infections of the upper and lower respiratory tract, to hydrocephalus, to situs inversus but also to male infertility [65]. In most patients ultrastructural defects can be detected by electron microscopy. Defects can be found in the axoneme including total or partial absence of dynein arms, absence or dislocation of the central tubules, defects of radial spokes and peripheral microtubular abnormalities. Mutations were identified in the genes encoding axonemal dynein intermediate chain 1 (DNAI1), axonemal dynein heavy chain 5 (DNAH5) and axonemal dynein heavy chain 11 (DNAH11). Dyneins are involved in ciliary beating thus the phenotypic defects mainly affect motile cilia. Recently, a member of the thioredoxin family (TXNDC3) was also shown to be mutated in patients with PCD [84]. In some rare cases, patients were reported to carry mutations in RPGR and OFD1 [85,86].

Polycystic kidney disease (PKD, OMIM 173900 and 263200)

PKD is characterized by multiple cysts of the kidney. They arise from proliferating renal epithelial cells that form fluid-filled cysts which finally replace the renal tissue. Minor symptoms affect the cardiovascular and gastrointestinal system. PKD is further divided into two subclasses depending on the inheritance pattern. Autosomal-dominant PKD (ADPKD) is caused by mutations in the PKD1 and PKD2 genes encoding for polycystin 1 (PC1) and polycystin 2 (PC2), respectively. Both are located within the ciliary membrane and form a Ca^{2+} - permeable cation channel which is thought to be activated by fluid-induced ciliary bending [63]. The pathogenic

mechanism is explained by disturbed Ca^{2+} homeostasis, which in turn results in deregulation of cellular processes like proliferation and apoptosis. In addition, PC2 was linked to IFT processes and PC1 can form complexes with components of the Wnt signalling pathway, heterotrimeric G protein signalling and in the JAK-STAT pathway [87]. Autosomal-recessive PKD (ARPKD) arises from mutations in PKHD1 encoding fibrocystin. Fibrocystin is, like PC1 and PC2, a transmembrane protein; however the exact function still remains elusive.

Nephronophthisis (NPHP, OMIM 256100)

Nephronophthisis is an autosomal-recessive renal disease with renal cysts as the major clinical feature [88]. However, unlike PKD the cysts seem to develop from a loss of tissue. Additional features are tubular basement membrane disruption and tublointerstitial nephropathy. The disease can be classified into three categories depending on the age of onset (infantile, juvenile and adult form). To date, seven genes had been identified leading to NPHP when mutated. These are NPHP1/Nephrocystin-1, which accounts for 25% of all cases, NPHP2/Inversin, NPHP3/Nephrocystin-3, NPHP4/Nephroretinin, NPHP5/Nephrocystin-5, NPHP6/CEP290 and NPHP7/Nephrocystin-7. Of great interest, Nephrocystin-5 and CEP290 have been shown to interact with RPGR [48,49]. Accordingly, patients with mutations in NPHP5 and NPHP6 always display retinal degeneration. In general, patients displaying both nephronophthisis and severe retinal degeneration are referred to have Senior-Loken syndrome (SLS, OMIM 266900). Beside NPHP5 and NPHP6/CEP290, mutations had been identified in NPHP1 and NPHP4 leading to SLS.

Meckel-Gruber syndrome (MKS, OMIM 249000)

Patients suffering from Meckel Gruber syndrome display a combination of symptoms like renal cysts, developmental anomalies of the central nervous, hepatic ductal dysplasia and cysts, and polydactyly. It is inherited in an autosomal recessive fashion by mutations in MKS1, TMEM67, CEP290/NPHP6 and RPGRIP1L genes. A fifth locus was mapped to MKS2 region.

Joubert syndrome (JBTS, OMIM 213300)

The phenotype of Joubert syndrome is characterized by hypoplasia of the cerebellar vermis (“molar tooth sign”), neurological symptoms as well as retinal dystrophy and renal anomaly. A number of abnormalities found in JBTS are similar to those found in MKS. In addition, a significant portion of the patients also reveal nephronophthisis. Therefore, it is not astonishing that many known genes for those disorders also revealed mutations in JBTS patients. The underlying genes are AHI1, NPHP1, NPHP6/CEP290, TMEM67 and RPGRIP1L.

For the sake of completeness, some other rare symptoms presenting with retinal degeneration and putative ciliary abnormalities should be mentioned. These are Edwards-Sethi, Ellis-van Creveld (OMIM 225500), Jeune, Orofaciodigital Type 9, and Gurrieri syndromes (OMIM 601187)[83].

Male infertility

Last but not least, some forms of male infertility can also be accounted to the group of ciliopathies as they are based on defects in the flagellum. In addition, in some of the diseases mentioned above, male infertility is a possible symptom.

In summary, the spectrum of manifestations found in ciliopathies is very diverse. Still, some symptoms including retinal and renal dysfunctions are common to several entities. In these tissues the role of the cilia in sensation is basically understood. For other symptoms like polydactyly and obesity the link between the function of the cilium and the phenotype still remains elusive. First insights correlated an important role of cilia in signalling pathways. Based on the phenotypes it is now becoming clear that cilia and flagella significantly contribute in development and homeostasis of the human organism.

1.5 References of General Introduction

1. Purves D, Augustine G, Fitzpatrick D, et al. Neuroscience. In. Second Edition ed.: Sinauer; 2001.

2. Kolb H, Fernandez E, Nelson R. Webvision. In: National Library of Medicine; 2007.

3. Berg JM, Tymoczko JL, Stryer L. Biochemistry. In. Fifth Edition ed.: W.H. Freeman and Company; 2008.

4. Solomon SG, Lennie P. The machinery of color vision. *Nat Rev Neurosci*. 2007;8:276-286.

5. Peichl L. Diversity of mammalian photoreceptor properties: adaptations to habitat and lifestyle? *Anat Rec A Discov Mol Cell Evol Biol*. 2005;287:1001-1012.

6. Rohlich P, van Veen T, Szel A. Two different visual pigments in one retinal cone cell. *Neuron*. 1994;13:1159-1166.

7. Carter-Dawson LD, LaVail MM. Rods and cones in the mouse retina. I. Structural analysis using light and electron microscopy. *J Comp Neurol*. 1979;188:245-262.

8. Nathans J. In the eye of the beholder: visual pigments and inherited variation in human vision. *Cell*. 1994;78:357-360.

9. Arshavsky VY, Lamb TD, Pugh EN, Jr. G proteins and phototransduction. *Annu Rev Physiol*. 2002;64:153-187.

10. Lamb TD, Pugh EN, Jr. Dark adaptation and the retinoid cycle of vision. *Prog Retin Eye Res*. 2004;23:307-380.

11. Jin M, Li S, Moghrabi WN, Sun H, Travis GH. Rpe65 Is the Retinoid Isomerase in Bovine Retinal Pigment Epithelium. *Cell*. 2005;122:449-459.

12. Danciger M, Matthes MT, Yasamura D, et al. A QTL on distal chromosome 3 that influences the severity of light-induced damage to mouse photoreceptors. *Mamm Genome*. 2000;11:422-427.

13. Wenzel A, Reme CE, Williams TP, Hafezi F, Grimm C. The Rpe65 Leu450Met variation increases retinal resistance against light-induced degeneration by slowing rhodopsin regeneration. *J Neurosci*. 2001;21:53-58.

14. Muniz A, Villazana-Espinoza ET, Hatch AL, Trevino SG, Allen DM, Tsin ATC. A novel cone visual cycle in the cone-dominated retina. *Experimental Eye Research*. 2007;85:175-184.

15. Fleisch VC, Schonthaler HB, von Lintig J, Neuhauss SCF. Subfunctionalization of a Retinoid-Binding Protein Provides Evidence for Two

Parallel Visual Cycles in the Cone-Dominant Zebrafish Retina. *J Neurosci*. 2008;28:8208-8216.

16. Calvert PD, Strissel KJ, Schiesser WE, Pugh J, Arshavsky VY. Light-driven translocation of signaling proteins in vertebrate photoreceptors. *Trends in Cell Biology*. 2006;16:560-568.

17. Chen J, Wu M, Sezate SA, McGinnis JF. Light Threshold-Controlled Cone {alpha}-Transducin Translocation. *Invest Ophthalmol Vis Sci*. 2007;48:3350-3355.

18. Artemyev NO. Light-dependent compartmentalization of transducin in rod photoreceptors. *Mol Neurobiol*. 2008;37:44-51.

19. Granit R. The components of the retinal action potential in mammals and their relation to the discharge in the optic nerve. *J Physiol*. 1933;77:207-239.

20. Wachtmeister L. Oscillatory Potentials in the Retina: what do they Reveal. *Progress in Retinal and Eye Research*. 1998;17:485-521.

21. Bach M, Kellner U. [Electrophysiological diagnosis in ophthalmology]. *Ophthalmologe*. 2000;97:898-920.

22. Rohlich P. The sensory cilium of retinal rods is analogous to the transitional zone of motile cilia. *Cell Tissue Res*. 1975;161:421-430.

23. Horst CJ, Johnson LV, Besharse JC. Transmembrane assemblage of the photoreceptor connecting cilium and motile cilium transition zone contain a common immunologic epitope. *Cell Motil Cytoskeleton*. 1990;17:329-344.

24. Deretic D, Papermaster DS. Polarized sorting of rhodopsin on post-Golgi membranes in frog retinal photoreceptor cells. *J Cell Biol*. 1991;113:1281-1293.

25. Deretic D. A role for rhodopsin in a signal transduction cascade that regulates membrane trafficking and photoreceptor polarity. *Vision Research*. 2006;46:4427-4433.

26. Bloodgood RA. Protein targeting to flagella of trypanosomatid protozoa. *Cell Biology International*. 2000;24:857-862.

27. Deretic D. Rab proteins and post-Golgi trafficking of rhodopsin in photoreceptor cells. *Electrophoresis*. 1997;18:2537-2541.

28. Deretic D, Williams AH, Ransom N, Morel V, Hargrave PA, Arendt A. Rhodopsin C terminus, the site of mutations causing retinal disease, regulates trafficking by binding to ADP-ribosylation factor 4 (ARF4). *PNAS*. 2005;102:3301-3306.

29. Tai AW, Chuang JZ, Bode C, Wolfrum U, Sung CH. Rhodopsin's Carboxy-Terminal Cytoplasmic Tail Acts as a Membrane Receptor for Cytoplasmic Dynein by Binding to the Dynein Light Chain Tctex-1. *Cell*. 1999;97:877-887.

30. Wolfrum U, Schmitt A. Rhodopsin transport in the membrane of the connecting cilium of mammalian photoreceptor cells. *Cell Motil Cytoskeleton*. 2000;46:95-107.

31. Marszalek JR, Liu X, Roberts EA, et al. Genetic evidence for selective transport of opsin and arrestin by kinesin-II in mammalian photoreceptors. *Cell*. 2000;102:175-187.

32. Hartong DT, Berson EL, Dryja TP. Retinitis pigmentosa. *The Lancet*;368:1795-1809.

33. Neidhardt J, Glaus E, Lorenz B, et al. Identification of novel mutations in X-linked retinitis pigmentosa families and implications for diagnostic testing. *Mol Vis*. 2008;14:1081-1093.

34. Schwahn U, Lenzner S, Dong J, et al. Positional cloning of the gene for X-linked retinitis pigmentosa 2. *Nat Genet*. 1998;19:327-332.

35. Veltel S, Gasper R, Eisenacher E, Wittinghofer A. The retinitis pigmentosa 2 gene product is a GTPase-activating protein for Arf-like 3. *Nat Struct Mol Biol*. 2008;15:373-380.

36. Vervoort R, Lennon A, Bird AC, et al. Mutational hot spot within a new RPGR exon in X-linked retinitis pigmentosa. *Nat Genet*. 2000;25:462-466.

37. Kirschner R, Rosenberg T, Schultz-Heienbrok R, et al. RPGR transcription studies in mouse and human tissues reveal a retina-specific isoform that is disrupted in a patient with X-linked retinitis pigmentosa. *Hum Mol Genet*. 1999;8:1571-1578.

38. Neidhardt J, Glaus E, Barthelmes D, Zeitz C, Fleischhauer J, Berger W. Identification and characterization of a novel RPGR isoform in human retina. *Hum Mutat*. 2007;28:797-807.

39. Renault L, Nassar N, Vetter I, et al. The 1.7 A crystal structure of the regulator of chromosome condensation (RCC1) reveals a seven-bladed propeller. *Nature*. 1998;392:97-101.

40. Kirschner R, Erturk D, Zeitz C, et al. DNA sequence comparison of human and mouse retinitis pigmentosa GTPase regulator (RPGR) identifies tissue-specific exons and putative regulatory elements. *Hum Genet*. 2001;109:271-278.

41. Mavlyutov TA, Zhao H, Ferreira PA. Species-specific subcellular localization of RPGR and RPGRIP1 isoforms: implications for the phenotypic variability of congenital retinopathies among species. *Hum Mol Genet*. 2002;11:1899-1907.

42. Hong DH, Pawlyk BS, Shang J, Sandberg MA, Berson EL, Li T. A retinitis pigmentosa GTPase regulator (RPGR)-deficient mouse model for X-linked retinitis pigmentosa (RP3). *Proc Natl Acad Sci U S A*. 2000;97:3649-3654.

43. Khanna H, Hurd TW, Lillo C, et al. RPGR-ORF15, Which Is Mutated in Retinitis Pigmentosa, Associates with SMC1, SMC3, and Microtubule Transport Proteins. *J Biol Chem*. 2005;280:33580-33587.

44. He S, Parapuram SK, Hurd TW, et al. Retinitis Pigmentosa GTPase Regulator (RPGR) protein isoforms in mammalian retina: Insights into X-linked Retinitis Pigmentosa and associated ciliopathies. *Vision Research*. 2008;48:366-376.

45. Chang B, Khanna H, Hawes N, et al. An in-frame deletion in a novel centrosomal/ciliary protein CEP290/NPHP6 perturbs its interaction with RPGR and results in early-onset retinal degeneration in the rd16 mouse. *Hum Mol Genet*. 2006.

46. Otto EA, Loeys B, Khanna H, et al. Nephrocystin-5, a ciliary IQ domain protein, is mutated in Senior-Loken syndrome and interacts with RPGR and calmodulin. *Nat Genet*. 2005;advanced online publication.

47. Shu X, Fry AM, Tulloch B, et al. RPGR ORF15 isoform co-localizes with RPGRIP1 at centrioles and basal bodies and interacts with nucleophosmin. *Hum Mol Genet*. 2005;14:1183-1197.

48. Meindl A, Dry K, Herrmann K, et al. A gene (RPGR) with homology to the RCC1 guanine nucleotide exchange factor is mutated in X-linked retinitis pigmentosa (RP3). *Nat Genet*. 1996;13:35-42.

49. Roepman R, van Duijnhoven G, Rosenberg T, et al. Positional cloning of the gene for X-linked retinitis pigmentosa 3: homology with the guanine-nucleotide-exchange factor RCC1. *Hum Mol Genet*. 1996;5:1035-1041.

50. Demirci FY, Rigatti BW, Wen G, et al. X-linked cone-rod dystrophy (locus COD1): identification of mutations in RPGR exon ORF15. *Am J Hum Genet*. 2002;70:1049-1053.

51. Yang Z, Peachey NS, Moshfeghi DM, et al. Mutations in the RPGR gene cause X-linked cone dystrophy. *Hum Mol Genet*. 2002;11:605-611.

52. Ayyagari R, Demirci FY, Liu J, et al. X-linked recessive atrophic macular degeneration from RPGR mutation. *Genomics*. 2002;80:166-171.

53. Demirci FY, Rigatti BW, Mah TS, Gorin MB. A Novel RPGR Exon ORF15 Mutation in a Family With X-linked Retinitis Pigmentosa and Coats'-like Exudative Vasculopathy. *American Journal of Ophthalmology*. 2006;141:208-210.

54. Zito I, Downes SM, Patel RJ, et al. RPGR mutation associated with retinitis pigmentosa, impaired hearing, and sinorespiratory infections. *J Med Genet*. 2003;40:609-615.

55. Moore A, Escudier E, Roger G, et al. RPGR is mutated in patients with a complex X linked phenotype combining primary ciliary dyskinesia and retinitis pigmentosa. *J Med Genet*. 2006;43:326-333.

56. Gravesande KS, Omran H. Primary ciliary dyskinesia: Clinical presentation, diagnosis and genetics. *Ann Med*. 2005;37:439-449.

57. Dawe HR, Farr H, Gull K. Centriole/basal body morphogenesis and migration during ciliogenesis in animal cells. *J Cell Sci*. 2007;120:7-15.

58. Chapman MJ. One hundred years of centrioles: the Henneguy-Lenhossek theory, meeting report. *Int Microbiol*. 1998;1:233-236.

59. Doxsey S. Re-evaluating centrosome function. *Nat Rev Mol Cell Biol*. 2001;2:688-698.

60. Fliegauf M, Benzing T, Omran H. When cilia go bad: cilia defects and ciliopathies. *Nat Rev Mol Cell Biol*. 2007;8:880-893.

61. Roepman R, Wolfrum U. Protein networks and complexes in photoreceptor cilia. *Subcell Biochem*. 2007;43:209-235.

62. Ibanez-Tallon I, Heintz N, Omran H. To beat or not to beat: roles of cilia in development and disease. *Hum Mol Genet*. 2003;12:R27-R35.

63. Pan J, Wang Q, Snell WJ. Cilium-generated signaling and cilia-related disorders. *Lab Invest*. 2005;85:452-463.

64. Okada Y, Takeda S, Tanaka Y, Belmonte JCIa, Hirokawa N. Mechanism of Nodal Flow: A Conserved Symmetry Breaking Event in Left-Right Axis Determination. *Cell*. 2005;121:633-644.

65. Huangfu D, Liu A, Rakeman AS, Murcia NS, Niswander L, Anderson KV. Hedgehog signalling in the mouse requires intraflagellar transport proteins. *Nature*. 2003;426:83-87.

66. Schneider L, Clement CA, Teilmann SC, et al. PDGFR[alpha][alpha] Signaling Is Regulated through the Primary Cilium in Fibroblasts. *Current Biology*. 2005;15:1861-1866.

67. Ross AJ, May-Simera H, Eichers ER, et al. Disruption of Bardet-Biedl syndrome ciliary proteins perturbs planar cell polarity in vertebrates. *Nat Genet*. 2005;37:1135-1140.

68. Kozminski KG, Johnson KA, Forscher P, Rosenbaum JL. A Motility in the Eukaryotic Flagellum Unrelated to Flagellar Beating. *PNAS*. 1993;90:5519-5523.

69. Rosenbaum JL, Witman GB. Intraflagellar transport. *Nat Rev Mol Cell Biol*. 2002;3:813-825.

70. Scholey JM. Intraflagellar transport. *Annu Rev Cell Dev Biol*. 2003;19:423-443.

71. Deane JA, Cole DG, Seeley ES, Diener DR, Rosenbaum JL. Localization of intraflagellar transport protein IFT52 identifies basal body transitional fibers as the docking site for IFT particles. *Current Biology*. 2001;11:1586-1590.

72. Scholey JM. Kinesin-II, a membrane traffic motor in axons, axonemes, and spindles. *J Cell Biol*. 1996;133:1-4.

73. Insinna C, Pathak N, Perkins B, Drummond I, Besharse JC. The homodimeric kinesin, Kif17, is essential for vertebrate photoreceptor sensory outer segment development. *Developmental Biology*;In Press, Accepted Manuscript.

74. Pazour GJ, Wilkerson CG, Witman GB. A Dynein Light Chain Is Essential for the Retrograde Particle Movement of Intraflagellar Transport (IFT). *J Cell Biol*. 1998;141:979-992.

75. Pazour GJ, Dickert BL, Vucica Y, et al. Chlamydomonas IFT88 and Its Mouse Homologue, Polycystic Kidney Disease Gene Tg737, Are Required for Assembly of Cilia and Flagella. *J Cell Biol*. 2000;151:709-718.

76. Qin H, Rosenbaum JL, Barr MM. An autosomal recessive polycystic kidney disease gene homolog is involved in intraflagellar transport in C. elegans ciliated sensory neurons. *Current Biology*. 2001;11:457-461.

77. Vieira OV, Gaus K, Verkade P, Fullekrug J, Vaz WL, Simons K. FAPP2, cilium formation, and compartmentalization of the apical membrane in polarized Madin-Darby canine kidney (MDCK) cells. *Proc Natl Acad Sci U S A*. 2006;103:18556-18561.

78. Hunter DG, Fishman GA, Kretzer FL. Abnormal axonemes in X-linked retinitis pigmentosa. *Arch Ophthalmol*. 1988;106:362-368.

79. Nachury MV, Loktev AV, Zhang Q, et al. A Core Complex of BBS Proteins Cooperates with the GTPase Rab8 to Promote Ciliary Membrane Biogenesis. *Cell*. 2007;129:1201-1213.

80. Adams NA, Awadein A, Toma HS. The Retinal Ciliopathies. *Ophthalmic Genetics*. 2007;28:113-125.

81. Duriez B, Duquesnoy P, Escudier E, et al. A common variant in combination with a nonsense mutation in a member of the thioredoxin family causes primary ciliary dyskinesia. *Proc Natl Acad Sci U S A*. 2007;104:3336-3341.

82. Moore A, Escudier E, Roger G, et al. RPGR is mutated in patients with a complex X linked phenotype combining primary ciliary dyskinesia and retinitis pigmentosa. *J Med Genet*. 2006;43:326-333.

83. Budny B, Chen W, Omran H, et al. A novel X-linked recessive mental retardation syndrome comprising macrocephaly and ciliary dysfunction is allelic to oral-facial-digital type I syndrome. *Hum Genet*. 2006;120:171-178.

84. Bisgrove BW, Yost HJ. The roles of cilia in developmental disorders and disease. *Development*. 2006;133:4131-4143.

85. Hildebrandt F, Zhou W. Nephronophthisis-Associated Ciliopathies. *J Am Soc Nephrol*. 2007;18:1855-1871

2. Aim of the thesis

The knowledge about the heterogeneity of phenotypes associated with mutations in the Retinitis pigmentosa GTPase regulator (*RPGR*) gene as well as the complexity of expression on transcript and protein levels provided basic insights into the function and molecular characteristics of *RPGR*. The importance of mutations in *RPGR* leading to a class of diseases termed ciliopathies highlighted the significance not only in retina but also in other tissues. Still, the exact molecular function of *RPGR* is poorly understood.

The aim of the present work was to characterize two mouse models for *RPGR*-related diseases. Both mouse models have been generated and initially characterized in former work. The first model is an *Rpgr* transgenic mouse line. Phenotypic characterizations revealed infertility of male mice with high copy numbers of the transgene due to apparent lack of sperm flagella. The second mouse line carries a knock-in mutation of exon 4 of *Rpgr* thereby mimicking the situation of RP patients with mutations leading to exon 4 skipping. Initial functional and histological studies indicated no significant retinal phenotype in the BL/6 background.

The transgenic mouse line was the first *Rpgr* model exhibiting an infertility phenotype. Therefore, the intention of this study was to elucidate the infertility phenotype on a molecular level and to find potential functional links to *RPGR* overexpression. For the mouse line with the knock-in mutation on the BL/6 background a detailed examination of the phenotype was pursued. Furthermore, the mutation was crossed into the BALB/c mouse strain in order to gain information about the influence of modifier genes on the expressivity of the retinal phenotype. In patients, the clinical heterogeneity due to mutations in *RPGR* has been described before. Comprehensive phenotypical investigations of the two mouse strains and investigations of the underlying molecular mechanisms was a second major goal of this study. In addition, a set of RPGR-specific antibodies should be generated in order to provide a valuable tool for protein analysis. These objectives were set into the following schedule:

1) Generation and characterization of RPGR-specific antibodies
2) Characterization of transgenic mouse line with infertility phenotype
3) Breeding of knock-in mutation in two genetic backgrounds and examination of the phenotypes

The following three manuscripts of this thesis describe the studies and results that were accomplished according this schedule to assess the defined aims of the thesis.

3. Results

3.1 Generation and characterization of isoform-specific RPGR antibodies

Sandra Brunner[1], Silke Feil[1], John Neidhardt[1], Manfred Fliegauf[2], Sergej Skosyrski[3], Heymut Omran[2], and Wolfgang Berger[1]

[1]Division of Medical Molecular Genetics and Gene Diagnostics, Institute for Medical Genetics, University of Zurich, CH-8603 Schwerzenbach, Switzerland; [2]Department of Paediatrics and Adolescent Medicine, University Hospital Freiburg, 79106 Freiburg, Germany; [3]Department of Ophthalmology, Charité Campus Virchow Clinic, University Medical Center, Berlin, Germany;

Additional manuscript, not published

3.1.1 Introduction

The *RPGR/Rpgr* gene and its multitude of gene products and protein isoforms are poorly understood in their biological function. The transcript is known to be alternatively spliced to an extraordinary high degree. In addition, alternative splicing and expression of the corresponding protein isoforms are regulated in a tissue- and species-specific manner [1-3].

In human and mouse, the constitutive *RPGR/Rpgr* transcript contains 19 exons and is widely expressed. The respective protein has a molecular weight of about 90 kDa [4,5]. Partial retention of intron 15 results in an alternative transcript, RPGR-ORF15, which is abundantly expressed in the human retina[6]. The deduced protein is of high molecular weight ranging from 150-200 kDa and has an alternate C-terminus, which is rich in acidic amino acids. Recently, a novel isoform was reported including a novel exon located in intron 9 (RPGR-9a isoform) [2]. This exon introduces a premature termination codon. The deduced protein isoform has a molecular weight of 45 kDa and is predominantly found in cone photoreceptors.

In mice, the constitutive transcript contains two alternative translation initiation sites, which were shown to be utilized resulting in proteins of about 80 kDa [7]. In testis, brain and eye several transcript isoforms were found [1]. They mainly arise from skipping of exons in the 3' region of *Rpgr*, and lead to a diversity of transcripts. A similar transcript to RPGR-ORF15 in humans has also been described in mice; however intron 14 is retained as well as parts of intron 15 (ORF14/15)[6] (Chapter 1, Figure 10). Even within the highly repetitive ORF14/15 region alternative splicing was detected which produces a variety of ORF14/15 transcripts[8].

The different protein isoforms that could potentially be generated by the multitude of transcripts have also been investigated in several studies. Nevertheless, some discrepancies regarding protein size and number of detected RPGR isoforms seem to exist depending on the set of antibodies used. Most studies were able to detect the major isoforms at about 90 kDa ($RPGR_{1-19}$) and 150-200 kDa (RPGR-ORF15)[8-11]. However, in some studies additional bands potentially corresponding to distinct isoforms have been described[12]. With regard to the localization of the different RPGR isoforms similar incongruities exist. The common finding in most localization studies of retinal tissue is a defined staining pattern along the photoreceptor connecting cilium and at the basal bodies[10,11,13]. It is noteworthy, that RPGR-ORF15 was almost

exclusively found at basal bodies. In cultured mammalian cells, this isoform was found to localize at the centrosomes, which are the precursors of basal bodies [9,11]. Nevertheless, the $RPGR_{1-19}$ as well as RPGR-ORF15 variant have also be found within the photoreceptor inner and outer segments[12].

To gain more insight into the generation and distribution of RPGR isoforms, a set of isoform-specific antibodies was generated and characterized. They were applied to tissue preparations and/or protein extracts from eyes and retinae of wild type and mutant mice, zebrafish eye and human tracheal epithelial cells.

3.1.2 Materials and Methods

Generation of a set of isoform-specific RPGR antibodies

Several epitopes within the human RPGR (hRPGR, NCBI – Accession: NP_000319 and NP_ 001030025) and the mouse RPGR (mRPGR, NCBI – Accession: NP_035415) protein were chosen to generate isoform-specific antibodies (Eurogentec, Seraing, Belgium). These were hRPGR/mRpgr Ab4 (ALKPEKVKLAACGRNHTLVST), mRPGR Ab5 (NEGQLGLGDTDDRDTF)[14], hRPGR Ab4/5 (RNHTLVSTEGGNVYATGGNNE), mRPGR Ab19 (NLQDSTTPNMEGKSKSC) hRPGR ORF15 AbC1 (KNGPSGSKKFWNNILPHYLELK) and hRPGR ORF15 AbC2 (HKTYQKKSVTNTQGNGKE). The RPGR peptide was linked to a carrier protein (keyhole limpet hemocyanin, KLH) to enhance the immunogenicity. Animals were injected 5 times with the RPGR-KLH complex to induce immunresponse and a high antibody titer. Blood samples were taken at 3 distinct time points (0, 38 and 66 days) for testing the antibody titer and finally after 87 days the whole serum was isolated for purification of the specific antibodies. Peptides were derived from the human sequence when high homology to the mouse sequences was given, otherwise the murine sequence was taken.

Affinity purification

The antisera were affinity-purified against the cognate peptide according to manufacturer's instructions (Sulfolink; Pierce Biotechnology, IL, USA). The respective RPGR peptides were bound via disulfide bonds to the column. The column consists of a beaded agarose with free iodoacetyl groups. These react specifically with free sulfhydryl groups of the respective peptides. Unspecific binding sites were blocked with cystein solution. The antisera were incubated on the column for 1 h at room temperature to allow binding. The columns were washed with PBS to eliminate unbound serum constituents. After washing, the antibodies were eluted from the column by pH-shift. Elution fractions were collected and IgG concentration of affinity purified antibodies was determined using a Nanodrop device (ND-3300, Witec AG, Littau, Switzerland). Fractions with the highest peak were used in further studies.

Dot Blot analyses

For determination of the antibody titer of each bleed, the reactivity of the respective serum against its cognate peptide was tested. Therefore, RPGR peptide solutions in different concentrations (125, 250, 500 and 1000 ng) were applied in 1 µl droplets on stripes of nitrocellulose membrane. The stripes were air-dried at RT for 30 min, blocked in 10% skim milk in PBS (1h at RT) and incubated o/n at 4°C with the respective antisera in different dilutions (1:10, 1:100 and 1:1000). After rinsing with PBS, membrane stripes were incubated with a 1:2000 dilution (10% skim milk in PBS) of anti-rabbit IgG coupled to horseradish peroxidase for 2h at RT (Dianova, Hamburg, Germany). Membrane stripes were developed with Western Lightning Chemiluminescence Reagent Plus (Perkin Elmer, Boston, USA) and chemiluminescence detection film (Lumi-Film, Roche Diagnostics, Mannheim, Germany).

Western Blot analyses

Whole retinas from wild type and mutant animals (wt n=6, mut n=8) were homogenized on ice in 30µl sample buffer per retina (50mM Tris, 150 mM NaCl, 1mM EDTA, 0.2% NP40, Complete Protease Inhibitor (Roche Diagnostics, Mannheim, Germany)). The protein homogenate was obtained by centrifugation (20.000 at 4°C). Protein concentration was determined by a bicinchoninic acid assay (BCA, Sigma-Aldrich, Steinheim, Germany). For Western blots 75 µg – 100 µg of retinal protein extract were boiled in loading buffer (120mM Tris (pH 6.8), 2% w/v SDS, 5% v/v β-mercaptoethanol, 50% v/v glycerol, bromophenolblue), separated on a 10% SDS-PAGE and blotted on a PVDF membrane (Roche Diagnostics, Mannheim, Germany) by semi-dry blotting (Bio-Rad, Munich, Germany). Membranes were incubated with dilutions of RPGR antibodies (1:10, only RPGR ORF15 AbC2.1 1:20). Blocking of the antibody was done by adding 50 µg of cognate peptide for 2 hours at RT before incubation of the blotting membrane. Detection of primary antibodies was performed by incubation with anti-rabbit and anti-mouse IgG coupled to horseradish peroxidase (1:500, Dianova, Hamburg, Germany). Blots were developed with Western Lightning Chemiluminescence Reagent Plus (Perkin Elmer, Boston, USA) and chemiluminescence detection film (Lumi-Film, Roche Diagnostics, Mannheim, Germany).

Immunohistochemistry

Animals were anesthetized by inhalation of CO_2 and subsequently sacrificed by cervical dislocation. For staining of the photoreceptor connecting cilium, eyes were removed and embedded in O.C.T. without prior fixation (Tissue Tek, Digitana, Horgen, Switzerland). Sections of 8-10 µm were cut on a cryostat (Leica Microsystems, CM3050S, Glattbrugg, Switzerland) and gently fixed by air-drying o/n at RT. After blocking with 10% normal goat serum (NGS), sections were incubated o/n at 4°C with primary antibody and washed with PBS. Then, Cy3-labeled anti-rabbit (1:500) or Cy3-labeled anti-mouse (1:500) antibody (Dianova, Hamburg, Germany) was applied for 2h at RT. All RPGR antibodies were used in a 1:10 dilution, with exception of AbC2.1 (1:25). They were applied on retinal sections from wild type and mutant animals of both mouse strains ($2 \geq n \geq 4$/genotype). Slides were photographed with a Zeiss microscope equipped with ApoTome Technology (Zeiss, Axioplan 2, Feldbach, Switzerland) and processed in PhotoShop.

Tracheal epithelial cells from wild type and mutant BL/6 mice were prepared from isolated longitudinally incised trachea by scraping the interior tracheal wall using forceps (n=3/genotype). Human respiratory epithelial cells were obtained by transnasal brush biopsy (Cytobrush Plus; Medscand Medical, Malmo, Sweden). Cells were suspended in RPMI1640 cell culture medium without supplements. Samples were spread onto glass slides, air dried, and stored at –80°C until use. Cells were treated with 4% paraformaldehyde, 0.2% Triton X-100, and 0.5% skim milk before incubation with primary antibody (at least 2 hours) and secondary antibody (30 minutes) at room temperature. Appropriate controls were performed by omitting the primary antibody. Secondary antibodies (Alexa Fluor 488 and Alexa Fluor 546) were from Molecular Probes/Invitrogen (Karlsruhe, Germany). DNA was stained with Hoechst 33342 (Sigma). Confocal images were taken on a Zeiss laser scanning microscope (Axiovert 200 LSM510 META) using a 63 x 1.2 numerical aperture water immersion objective. A four-channel, eightbit multitracking scan mode was used with a 1024 x 1024 frame size and four-fold average line scan settings. Images were processed with the Zeiss LSM510 software.

3.1.3 Results

Generation of RPGR polyclonal antibodies

Six epitopes were selected in order to be able to distinguish between the $RPGR_{1-19}$ and RPGR-ORF14/15 isoforms (Figure 1). Three peptide epitopes were located within the RCC1-like domain. The peptides are coded by exon 4 (Ab4) and by parts of exon 5 (Ab5). In addition, a previously published epitope was chosen bridging exon 4 and 5 (Ab4/5) [15]. The Ab4 was chosen based on the fact, that exon 4 is deleted in the *Rpgr* mutant mouse model therefore providing a reliable control for specificity. These antibodies are supposed to detect the $RPGR_{1-19}$ as well as the RPGR-ORF14/15 isoform as both are assumed to contain the RLD.

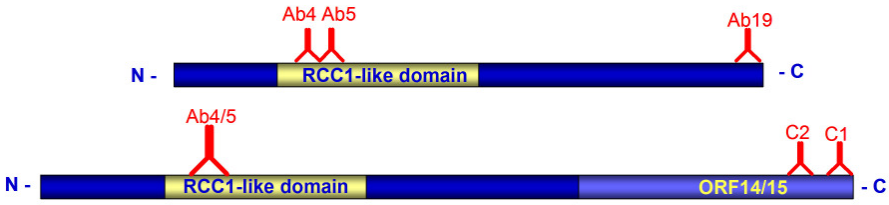

Figure 1: Schematic representation of peptide epitopes within the RPGR isoforms

Two major protein isoforms of RPGR are known to exist, which are the $RPGR_{1-19}$ (upper) and the RPGR-ORF14/15 isoform (lower). Six peptide epitopes were chosen for immunization of rabbits. Three of them (Ab4, Ab5 and Ab4/5) are located at the N-terminus within the RCC1-like domain which is common to both isoforms. They were drawn separately into the upper and lower protein schemes only for illustration purposes. The corresponding peptides are encoded by exon 4 (Ab4), part of exon 5 (Ab5) and by a sequence bridging exons 4 and 5 (Ab4/5). A fourth antibody is directed against a peptide encoded by part of exon 19. Therefore it only recognizes isoforms containing the C-terminus with the isoprenylation motif (Ab19). AbC2 and AbC1 exclusively detect isoforms with the alternate C-terminus encoded by exon ORF14/15.

The epitopes located at the C-terminus of RPGR were designed to distinguish between the $RPGR_{1-19}$ and RPGR-ORF14/15 isoform. Ab19 detects an epitope encoded by exon 19, which is included in the $Rpgr_{1-19}$ transcript. The two antibodies C1 and C2 are directed against two different epitopes within exon ORF14/15. Epitopes RPGR-C1 as well as RPGR-C2 have also been used for antibody generation before [13,16]. Prior to synthesis, the peptides were evaluated on several parameters like hydrophilicity (hydrophobicity), charges and antigenicity using a commercially available program (Lasergene, DNASTAR, Madison, U.S.). These *in-*

silico analyses were performed at the commissioned company (Eurogentec, Seraign, Belgium).

For immunization, two rabbits per peptide were booster-injected with a peptide-KLH complex according to a standard protocol (Figure 2). The injection scheme was slightly modified by adding a fifth boost. A pre-immune bleed was taken prior to first injection for control experiments. During the immunization program three bleedings (small bleed, large bleed and final bleed) were taken to determine antibody reactivity.

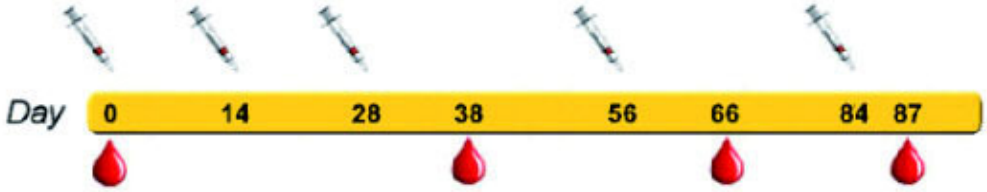

Figure 2: Temporal scheme of immunization program

During the immunization program the animals were injected at five different time points. These were done on day 0, day 14, day 28, day 56 and day 84. Blood samples were taken at day 0 (pre-immune), day 38 (small bleed), day 66 (large bleed) and day 87 (final bleed) within the immunization schedule. (modified after www.eurogentec.com/EGT/Images/Eurogentec-polyclonal-antibody-protocol-87-day-classic-530x120.jpg)

Determination of antibody titer

Reactivity of the four different bleeds (pre-immune, small, large and final) was determined by dot blot analyses. Series of serum dilutions were tested against different concentrations of peptide in order to determine the antibody titer (Figure 3).

All six antibodies were evaluated for their reactivity against the respective RPGR peptide. To determine unspecific reactivity, the pre-immune sera were tested in control reactions. The increase in reactivity was estimated by comparing the three different bleeds. Theoretically, the titer of the serum should raise upon booster-injections of the antigen. For the sera Ab4, Ab5 and AbC2 an increase in antibody titer could be observed (Figure 3A, 3C and 3F). In some cases the titer was slightly different between the two animals that were injected with the same peptide (e.g. 5.1 and 5.2, Figure 3C). The sera Ab4/5, Ab19 and AbC1 displayed no or only a very weak reactivity (Figure 3B, 3D and 3E). From those experiments only the antibody sera of the animal with the highest titer and the least background in the pre-immune serum were chosen for further affinity-purification and characterization. These were Ab4.2, Ab4/5.1, Ab5.1, Ab19.1 and AbC2.1.

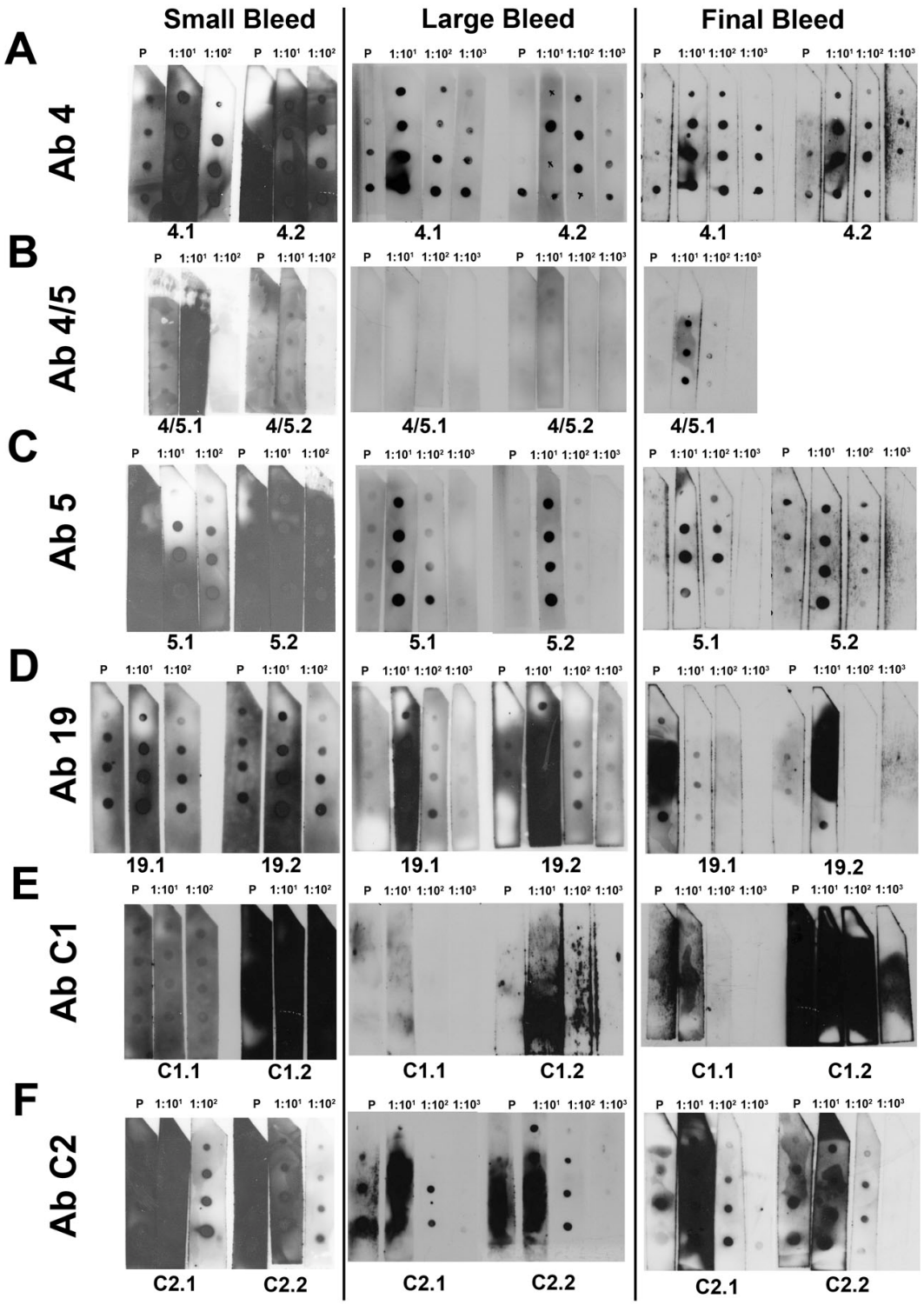

Figure 3: Dot blots of the small, large and final bleed of all RPGR antibodies

(A-F) Reactivity of the RPGR antisera Ab4, Ab4/5, Ab5, Ab19, AbC1 and AbC2 against their respective peptides was tested. Two animals per RPGR peptide X were immunized (X.1 and X.2). RPGR peptide solutions containing 125 ng, 250 ng, 500 ng and 1000 ng of peptide were applied in 1 µl drops on membranes (ascending concentrations from upper dot to lower dot on each stripe). Membranes were incubated with serum dilutions of the small bleed ($1:10^1$ and $1:10^2$), the large bleed ($1:10^1$, $1:10^2$ and $1:10^3$) and the final bleed ($1:10^1$, $1:10^2$ and $1:10^3$) from both animals of each serum, respectively. (A) Ab4 serum from both animals (Ab4.1 and Ab4.2) showed reactivity even at dilutions

of $1:10^3$ and a peptide concentration of 125 ng/µl. (B) Ab4/5.1 had a low titer only detectable in serum from the final bleed, while Ab 4/5.2 showed no reactivity. The animal died before taking the final bleed. (C) Ab5.1 and Ab5.2 revealed moderate titers detectable in the $1:10^2$ dilution in the final bleed serum. (D) Ab19.1 and Ab19.2 displayed weak signals only at the $1:10^1$ dilution in the final bleed and unspecific background signals in the pre-immune serum blots. (E) For both AbC1 sera no signal was detectable at all. AbC1.2 had high background signals on all membrane stripes. (F) AbC2.1 and AbC2.2 revealed reactivity on a peptide concentration of 125 ng/µl with a $1:10^2$ dilution with considerable unspecific signals in the pre-immune serum of AbC2.1 in the final bleed.

Characterization of antibodies on mouse protein extracts from different tissues

$RPGR_{1-19}$ and RPGR-ORF14/15 are known to be expressed in retina, kidney and testis [1]. In order to test the affinity-purified polyclonal antibodies for their specificity and affinity to RPGR proteins, they were applied on extracts from retina, testis and kidney. In addition, an extract from whole zebrafish eye was examined in order to evaluate for cross-reactivity with other species. For evaluation of specificity the antibody was blocked with its cognate peptide prior to application to the membrane.

Several immunoreactive bands could be detected in the three tissues with all antibodies tested (Figure 4A-J). However, most of those bands could not be blocked with the respective peptide and thus were classified to be unspecific to RPGR. Specificity of Ab4.2 could be additionally examined by comparing band patterns in protein extracts of wild type and mutant mice as the mutant protein is lacking 21 amino acids encoded by exon 4. In testis, one weak band at a high molecular weight (> 170 kDa) (Figure 4A, arrow) was apparently not present in mutant testicular protein extract (Figure 4B). A similar pattern was found for the corresponding band at > 170 kDa with Ab5.1 (Figure 4E and 4F). On the blot of Ab4/5.1 a band at 70 kDa was specific in retina and testis of wild type and mutant animals. In protein extracts from the zebrafish eye, an intense signal at >170 kDa was observed on unblocked but not on blocked membranes. Ab19.1 detected several bands at 60 kDa, 70 kDa and 130 kDa in mouse testis. The band at 60 kDa was also present in retina and the band at 130 kDa in zebrafish eye. All bands disappeared or appeared with reduced intensity when the antibody was blocked prior to incubation with the membranes (Figure 4C, 4D, 4G and 4H, arrows). The RPGR-ORF14/15 isoform was detected with AbC2.1. A high molecular band migrating at 170 kDa was visible which seemed to be specific as the signal could be blocked. This isoform seems most abundant in the retina, as it has also been described before [1].

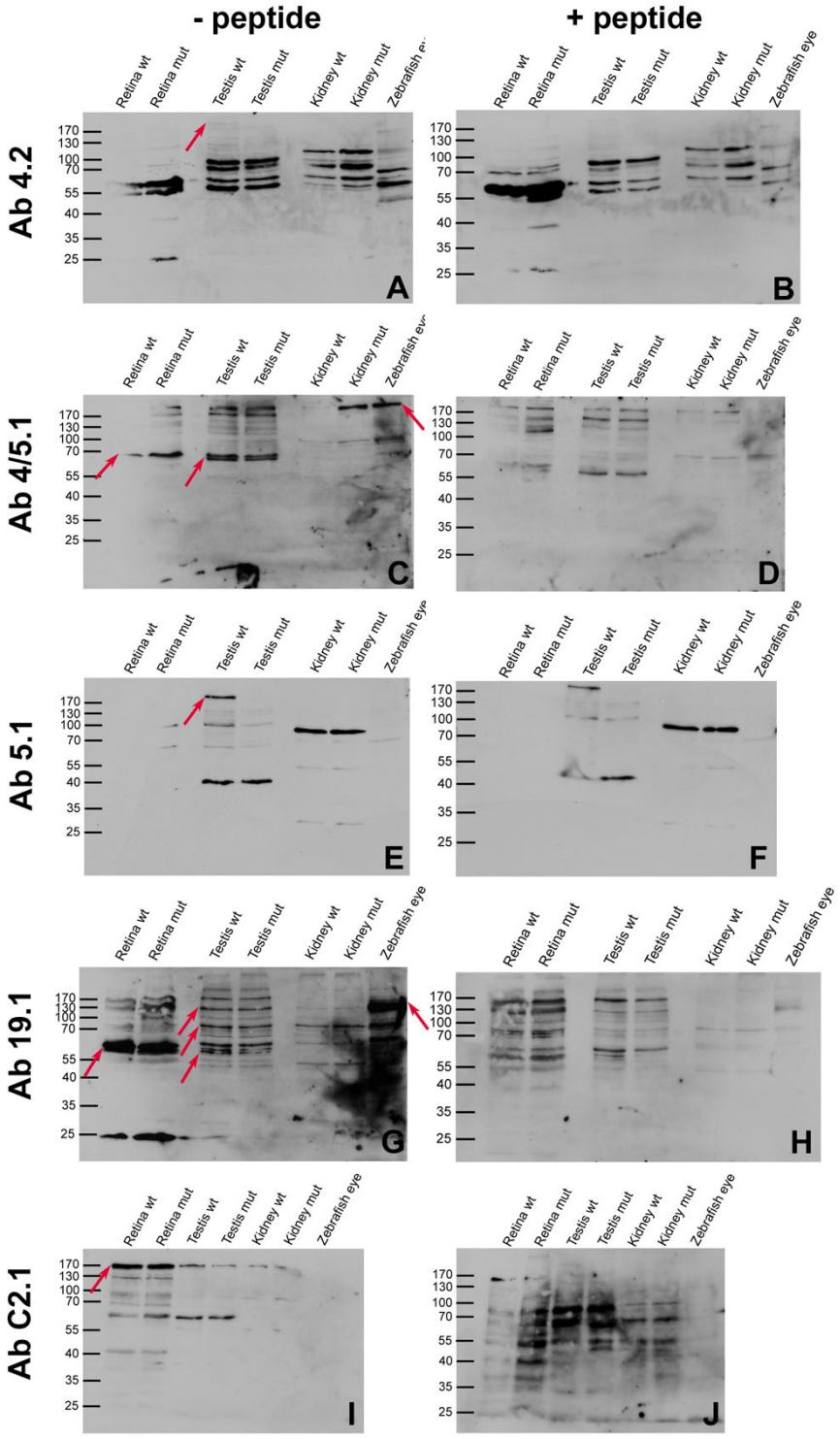

Figure 4: Western Blot analysis of RPGR antibodies on several tissues

Affinity-purified antibodies were applied on protein extracts from retina, testis and kidney of BL/6 wild type and mutant mice (A, C, E, G, and I). Equal amounts of 75 µg were loaded in each lane. In order to prove specificity, antibodies were blocked with an excess of the cognate peptide (B, D, F, H and J). (A and B) Ab4.2 detected several unspecific bands. One high molecular weight protein at 200 kDa was not present in mutant animals and on blocked membranes (arrow). (C and D) Ab4/5.1 detected immunoreactive bands at about 70 kDa in retina and testis. The signal intensity of the corresponding bands on the blocked membranes was reduced. In kidney of mutant animals and in zebrafish eye, a

protein with high molecular weight was present, a faint band of the appropriate size was visible when the antibody was blocked (arrow). (E and F) Ab5.1 revealed one band at about 200 kDa in testis that was only detectable in wild type (arrow). In retina, Ab5.1 failed to detect proteins. (G and H) A prominent band at 60 kDa with reduced intensity on the blocked membrane was detectable in wild type and mutant retinae (arrow). In testis, three bands at 60, 80 and 130 kDa were present with diminished signal intensity when the antibody was blocked. A corresponding intense signal was present on zebrafish eye extracts that could also be blocked. (I and J) An intense immunoreactive band at 170 kDa and a band at 130kDa of lower intensity were present in retina when AbC2.1 was applied. Highest intensity was detected in the retina of wild type and mutant animals (arrow). The bands could be reduced in signal intensity by blocking. In testis and kidney a band at 170 kDa but of lower intensity was detected.

Localization of RPGR in mouse retinal sections

Most isoforms of RPGR have been described to predominantly localize in the connecting cilium and basal bodies of photoreceptors (see chapter 1). Therefore, localization studies with RPGR antibodies were performed and focused on this particular region to obtain further insights regarding the specificity of the antibodies. For convenient staining of the connecting cilium, air-dried sections were used as other conditions were found to quench the signal (i.e. not treated with paraformaldehyde).

Four of the five affinity-purified antibodies that suggested specificity to RPGR isoforms in Western Blot analyses also revealed staining in immunohistochemical experiments (Figure 5A-D). However, for Ab4.2, Ab5.1 and Ab19.1 the signal was of very low intensity. This could not be improved by applying different antigen retrieval conditions (data not shown). The dot-like staining pattern characteristic for connecting cilium and basal body staining (see γ-tubulin and acetylated α-tubulin staining in chapter 3.3) was present with all four antibodies tested. For Ab4.2 the staining was judged to be unspecific as it was detected in mutant animals as well (Figure 5A). A similar staining pattern as for Ab4.2 was observed with Ab5.1 in wild type as well as mutant animals (Figure 5B). The blocking experiments that were performed on wild type animals showed a higher background staining which made it difficult to definitely judge on remaining staining within the area of the connecting cilium (Figure 5B). Ab19.1 also showed the dot-like staining in the connecting cilium area between the inner and outer segments (Figure 5C), which seemed to be extinguished by blocking except for one mutant BALB/c animal (Figure 5C). Hence, specificity of the staining was again not clear. In contrast, the staining pattern of the

AbC2.1 was very intense and detectable within the region of the connecting cilium (Figure 5D). Of note, the signal disappeared after blocking the antibody with the cognate peptide (Figure 5D). Thus, AbC2.1 seems to specifically stain the RPGR-ORF14/15 isoform in retinal sections.

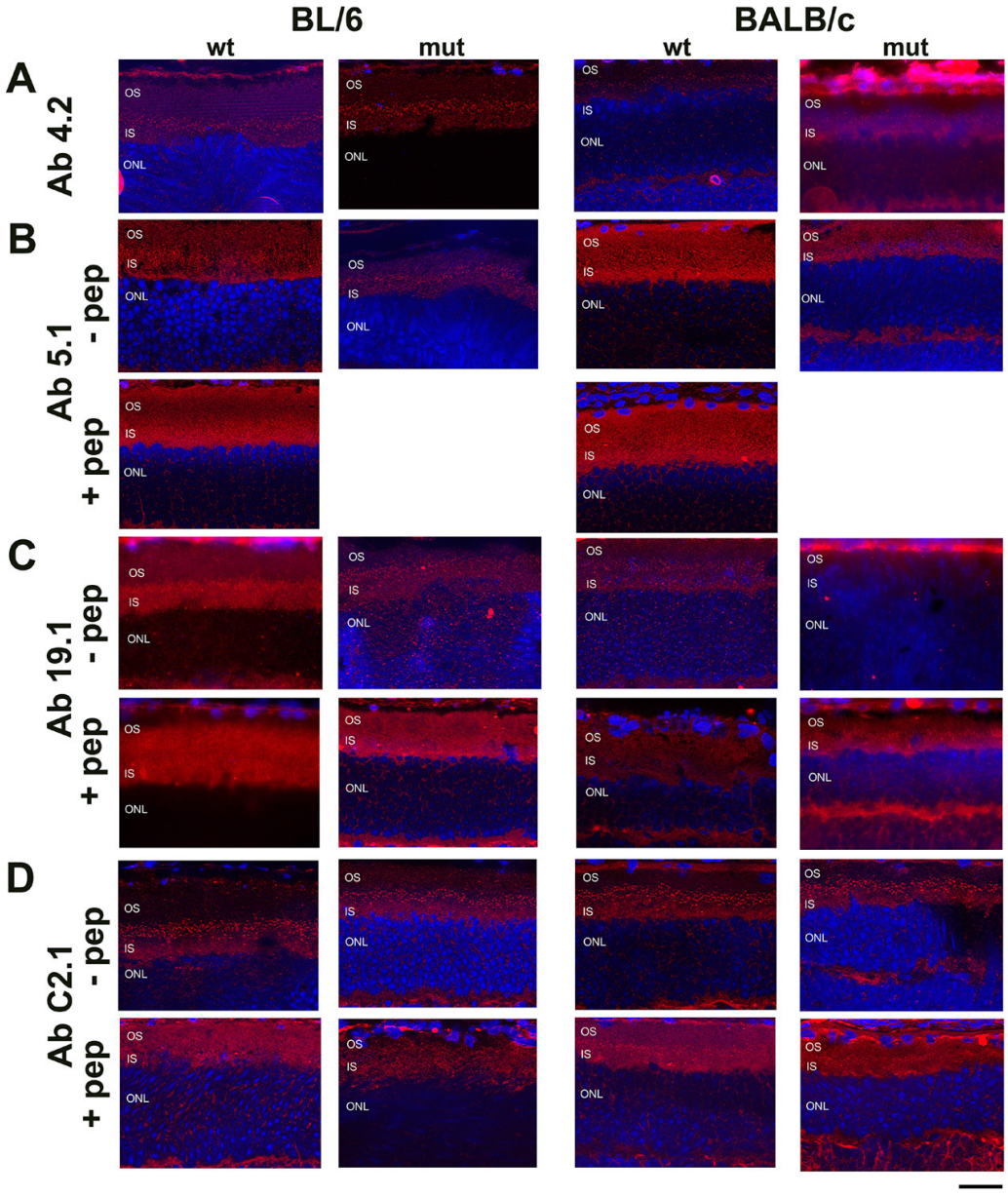

Figure 5: Antibodies Ab4.2, Ab5.1, Ab19.1 and AbC2.1 on retinal mouse sections

Localization of RPGR on retinal sections of wild type and mutant mice of the BL/6 and BALB/c backgrounds with isoform-specific antibodies. (A) Ab4.2 revealed punctuate staining pattern in the area between the inner and outer segments in wild type as well as mutant BL/6. This pattern was also visible in the BALB/c line. Of note, the mutant animals lack exon 4. (B) A weak but similar pattern was observed by staining with Ab5.1 in wild type and mutant animals of both strains (-pep). Blocking the signal with the cognate peptide in wild type mice resulted in elevated background fluorescence of the outer segments (+pep). Still, some remaining staining of the connecting cilium area seems to be

present. (C) Ab19.1 also faintly labelled the region at the junction between the inner and outer segments in wild type as well as mutant animals (-pep). Although background staining was higher in blocking experiments, the faint punctuate staining pattern disappeared. (D) An antibody directed against the ORF14/15 isoform showed an intense dot-like fluorescent pattern in the area of the connecting cilium. The signal was present in wild type and mutant animals of the Bl/6 and BALB/c line (-pep). Upon blocking, this characteristic punctuate fluorescence pattern disappeared or present with low signal intensity (+pep). Pictures of each antibody comparable retinal areas have been taken with similar exposure times. Scale bar = 50 μm.

Localization of RPGR in mouse tracheal epithelial cells

In order to determine if the antibodies might detect RPGR in tissues other than retina, they were additionally applied on mouse and human tracheal epithelial cells (collaboration with Professor Heymut Omran and Dr. Manfred Fliegauf, University Childrens Hospital, Freiburg, Germany). In these cells RPGR specifically was found to localize in the transition zone [17]. The transition zone is located at the base of the cilium and is the analogous structure of the photoreceptor connecting cilium [18].

Antibodies were applied on tracheal epithelial cells of human and wild type mice to examine specificity and putative species-specific differences (Figure 6A-J). In addition, acetylated α-tubulin was labelled as a marker of the ciliary axoneme.

In humans, Ab4.2 and Ab5.1 specifically stained the area of the transition zone (Figure 6A and C). The transition zone is located at the base of the ciliary axoneme, which was confirmed by the relative position of RPGR staining (red) to the staining of acetylated α-tubulin (green). In mice, the staining pattern was more diffusely distributed along the length of the cilia. Nevertheless, staining with Ab5.1 also revealed fluorescent signals at the ciliary base distally to acetylated α-tubulin. The staining pattern was vice versa for RPGR antibody Ab19.1 (Figure 6D and I). Here, in humans the cilia were labelled while the pattern in mice was more restricted to the transition zone. For Ab4/5.1 diffuse staining of the entire cell was found, while in mice apparently the cilia were detected (Figure 6B and G). The RPGR antibody directed against the ORF15 or ORF14/15 isoform in human or mice, respectively (AbC2.1), labelled the area of the transition zone in both human and mice (Figure 6E and J).

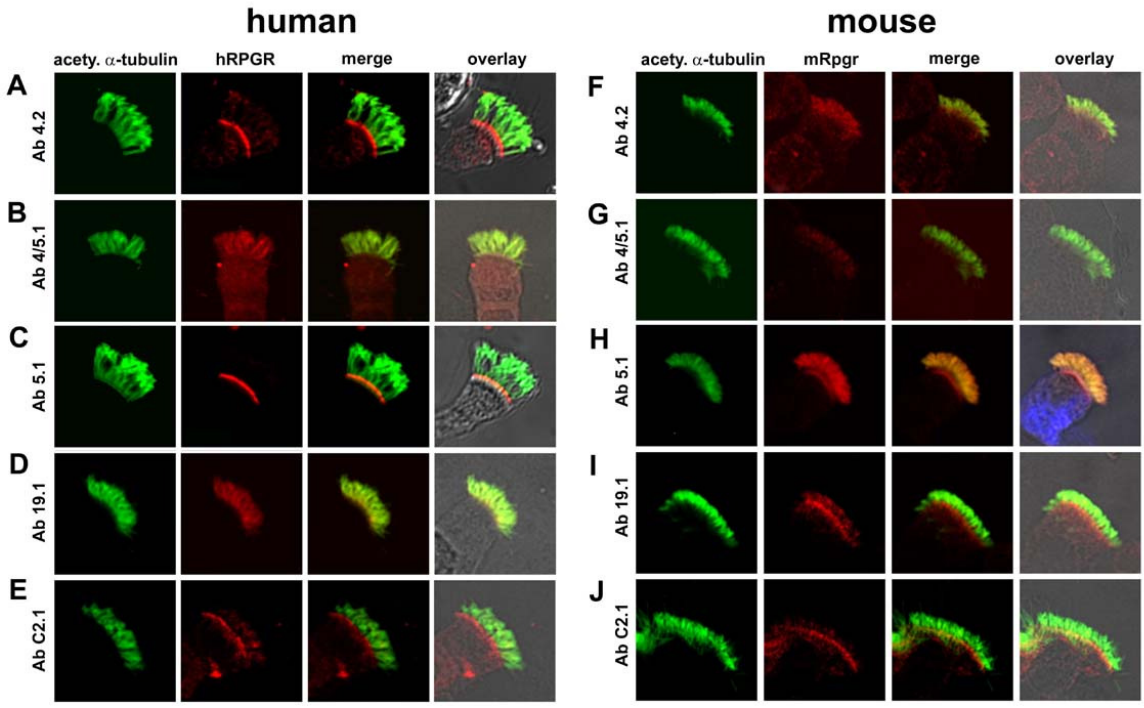

Figure 6: Comparison of RPGR staining of human and mice tracheal epithelial cells

The set of RPGR antibodies was used to stain mouse as well as human tracheal epithelial cells (red). Acetylated α-tubulin was used as a marker for the ciliary axoneme (green). Merged and overlay images are shown on the right. (A and F) In humans, Ab4.2 showed labelling at the transition zone at the base of the cilia, whereas in murine cells weak staining of the cilia was present (B and G) Ab4/5.1 weakly stained cilia in both species as indicated by co-localization with acetylated α-tubulin (C and H) An intense fluorescent pattern was visible distally to the ciliary axoneme staining in human cells with Ab5.1. In contrast, staining of cilia as well as a weak staining of the ciliary base was detected in mice. (D and I) In human cells, labelling with Ab19.1 indicated co-localization with acetylated α-tubulin. In murine cells, fluorescent staining pattern was observed distally to the cilium, i.e. in the transition zone (E and J). In human and mouse AbC2.1 revealed fluorescent signals predominantly in the area of the transition zone.

From the aforementioned localization studies of RPGR in human and mice, Ab5.1, Ab19.1 and AbC2.1 were chosen for further localization studies. This was based on the finding that staining was detected in the transition zone, in which RPGR has been described to localize before [17]. For identification of putative differences in the localization of mutant RPGR, these three antibodies were applied on tracheal epithelial cells of wild type and mutant mice.

Immunohistochemical staining with Ab5.1 revealed the same pattern as observed before (Figure 7A and D, Figure 6H). No obvious differences were noticed between

wild type and mutant mice. Similarly, labelling with Ab19.1 revealed an intense signal at the transition zone in both wild type and mutant animals (Figure 7B and E, Figure 6I).

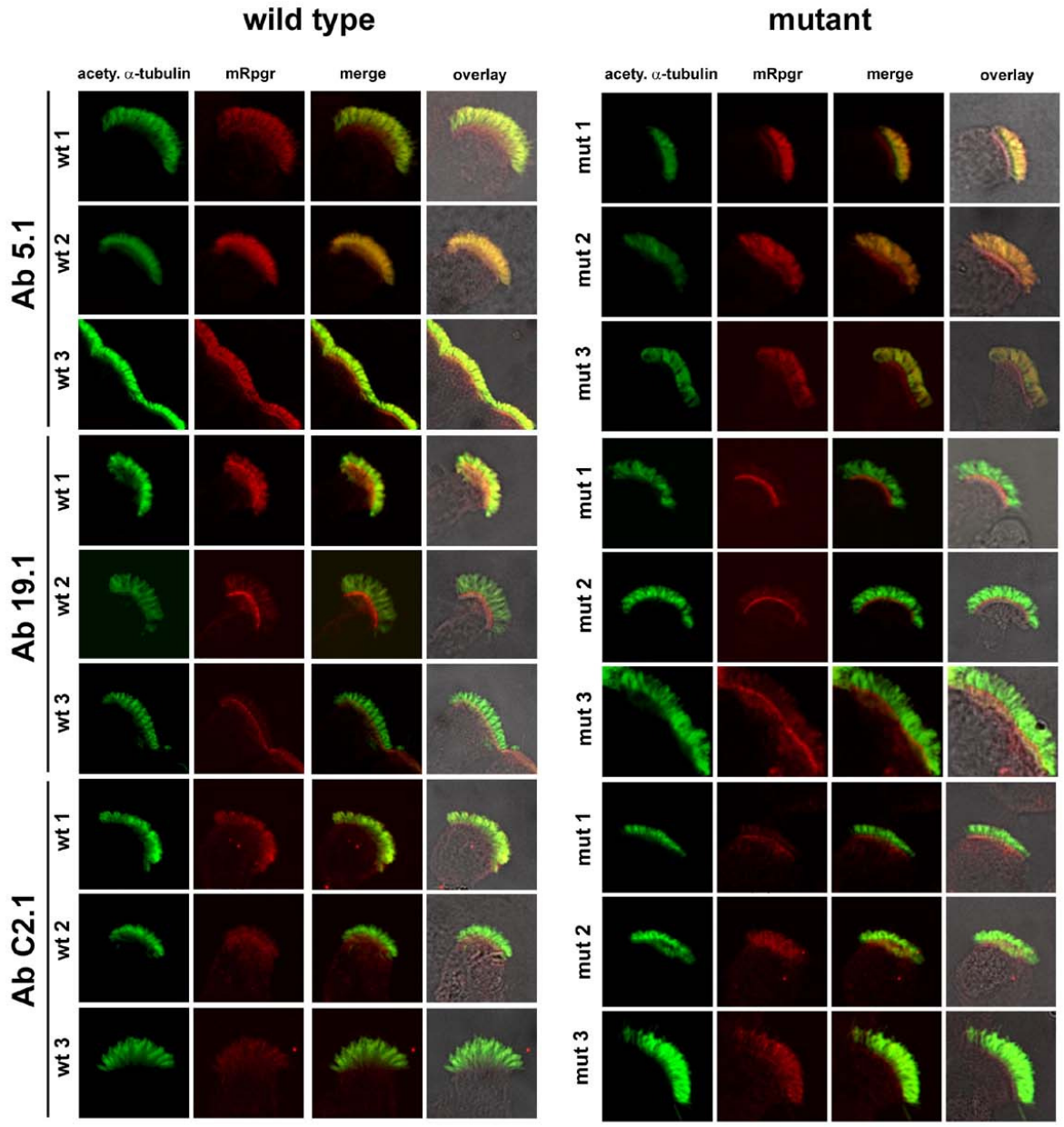

Figure 7: Immunohistochemistry with Ab5.1, Ab19.1 and AbC2.1 on murine tracheal epithelial cells

Murine tracheal epithelial cells from three wild type and three mutant BL/6 animals were stained with Ab5.1, Ab19.1 and AbC2.1 (red). Acetylated α-tubulin was used as a marker for the cilia (green). (A and D) Ab5.1 labelled the cilia in wild type and mutant mice, which can be seen in the overlay of the cilia marker and the staining with RPGR. The transition zone also seems to be faintly stained. (B and E). Staining with Ab19.1 showed defined red line at the base of the cilia which known to be the transition zone. No major differences seemed to be present between wild type and mutant animals. (C

and D) AbC2.1 revealed weak staining of the cilia. In one mutant animal (mut 1) the transition zone is labelled.

However, for AbC2.1 different results were obtained in the two stainings performed. In the first experiment the transition zone was labelled (Figure 6J) while in this series of experiments a more diffuse pattern along the cilia was found (Figure 7C and F). In two mutant animals (mut 1 and mut 3) there might be some labelling of the transition zone as well (Figure 7F). Nevertheless, the observed patterns were still consistent in the two genotypes.

3.1.4 Discussion

In this study, several isoform-specific RPGR antibodies were generated and characterized by immunostaining and Western blotting of tissue sections and protein extracts derived from several species.

Efficacy of immunization against RPGR peptides

Six peptides were used to immunize rabbits. Each peptide was injected into two different animals to ensure successful immunresponse and therefore antibody production. Out of these 12 animals, six displayed a higher titer than the others, i.e. detection of peptide at a dilution of $1:10^2$, at the end of the immunization program. These were both animals of Ab4 (4.1 and 4.2), Ab5 (5.1 and 5.2) and AbC2 (C2.1 and C2.2). In rabbits immunized with peptides of Ab4/5, Ab19 and AbC1, only a weak antigenic response against the peptide was observed. Therefore, half of the immunizations resulted in sufficient immune response for antibody production. Five of the 12 initial antisera were chosen to be further characterized. These were Ab4.2, Ab4/5.1, Ab5.1, Ab19.1 and AbC2.1.

Specificity and affinity to endogenous RPGR protein

The five antisera Ab4.2, Ab4/5.1, Ab5.1, Ab19.1 and AbC2.1 were affinity-purified against their cognate peptide for further applications. The affinity-purified antibodies against RPGR were then tested on protein extracts from different mouse tissues. These experiments revealed a few immunoreactive bands that might be specific to RPGR based on appropriate blocking controls. Beside the presumable specific bands of RPGR listed above, several unspecific bands were visible with the antibodies tested. The polyclonal antibodies might well cross-react with highly abundant proteins. However, these unspecific cross-reactions can be discriminated from specific bands by the blocking experiments that were conducted for each experiment. Ab4.2 and Ab5.1 detected a band at high molecular weight (>170 kDa) in murine testis, that was not present in mutant animals and that could be blocked. This isoform might represent the RPGR-ORF14/15 variant that was described to migrate at this size[12]. It is assumed that the RPGR-ORF14/15 isoform contains the N-terminal RLD where the epitopes/peptides are located. Of note, the RPGR-ORF14/15 isoform is known to be expressed in testis [11]. In wild type retina the Ab4.2 and 5.1 failed to

detect specific bands. This finding might be explained by low expression of *Rpgr* or by low affinity of the antibodies to the endogenous protein. Noteworthy, on testicular protein extracts from transgenic mice with overexpression of RPGR a band at 165 kDa was detected by Ab5.1 (see chapter 3.2). The intensity of this band correlated with *Rpgr* copy numbers. Hence, high amounts of protein are required to compensate the apparent low affinity in order to specifically detect RPGR.

Ab4/5.1 detected a protein of high molecular size similarly to Ab4.2 and Ab5.1 in kidney from mutant mice and zebrafish eye. The unexpected lack of this band in wild type kidney might be explained by degradation of the protein in this sample. An immunoreactive band migrating at 70 kDa was found with Ab4/5.1 and Ab19.1. These isoforms might correspond to each other, as the $RPGR_{1-19}$ variant should include exon 4, exon 5 and exon 19. Interestingly, a transcript isoform containing these exons was described to be expressed in eye, testis and brain[1]. The deduced protein would have a calculated size of 77 kDa and would fit to the observed band. The additional bands in retina at 60 kDa might correspond to a transcript found in mouse eye lacking exons 14, 14a, 15 and alternatively exon 19a [1]. The calculated size of those proteins would match the protein bands detected here. However, the study by Kirschner et al. described those transcripts only in the eye but not in testis. The band at 125 kDa, which is present in testis and zebrafish, exceeds the protein size that is assumed for the full-length $RPGR_{1-19}$ isoform (90kDa). This size discrepancy might be attributed to post-translational modification or alternative splicing. In accordance, a recent study also detected a band at that molecular weight in murine retina with an antibody directed against an epitope in close vicinity to the Ab19 peptide [12].

The RPGR-ORF14/15 variants detected by AbC2.1 correlate to the size range that is assumed for isoforms containing exons ORF14/15 [12]. The band at 170 kDa was detected in retina, testis and kidney; however expression was highest in retinal extracts. Strikingly, this isoform was reported to be abundantly expressed in retina [6]. A second isoform at 130 kDa was only seen in retina, indicating tissue specificity or expression levels in testis and kidney that are below detection limits. The ORF14/15 isoform at 170 kDa detected with AbC2.1 migrated at a smaller size range than the high molecular isoforms detected with Ab4.2, Ab4/5.1 and 5.1 (>170 kDa), which might also contain the exon ORF14/15 based on their molecular weight. This apparent discrepancy might be explained by the observation that exon ORF14/15

shows extensive alternative spliced [8]. Thus, antibodies directed against the N-terminus of the protein (Ab4.2, Ab4/5.1 and Ab5.1) might detect different ORF14/15 isoforms than the antibody directed against the very C-terminal part of the RPGR protein (AbC2.1).

Comparing the results of the present study of RPGR isoforms with a recent publication using a similar set of isoform-specific antibodies, different patterns with antibodies directed against the $RPGR_{1-19}$ isoform were found for murine retina [12]. However, some of the unspecific bands might mask specific staining. In addition, the Ab19.1 antibody might have lower affinity to the endogenous RPGR isoforms. Similarly, divergent sizes were identified for the ORF14/15 isoforms [12]. These findings might further indicate that indeed RPGR produces as many alternate isoforms as transcripts which is reflected by the diversity of bands which can be detected by different antibodies.

Localization of RPGR isoforms

In addition to discrimination of RPGR isoforms in various protein extracts, the localization of RPGR was investigated by localization studies. For this, antibodies were applied on retinal sections from wild type and mutant mice and on tracheal epithelial cells of mouse and human. In both tissues, localization of RPGR had been performed previously and thus provide additional criteria for determination of specificity [9,12,13,17].

Localization of RPGR isoforms with Ab4.2, Ab5.1 and Ab19.1 in mouse retina all revealed very faint signals in the area of the connecting cilium. However, signals of Ab4.2 were concluded to be unspecific as they were also visible in mutant animals. For Ab5.1 and Ab19.1 the faint signals were apparently extinguished when the antibody was blocked with its cognate peptide prior to application. It is worth mentioning that other studies using comparable epitopes within the N-terminus detected RPGR in the region of the connecting cilium in mice [13]. Another recent study using an antibody directed against a peptide encoded by exon 19 identified RPGR in a diffuse pattern along the ciliary axoneme [12]. Nevertheless, the obtained results for antibodies Ab4.2, Ab5.1 and Ab19.1 are preliminary and final conclusions about their specificity will require additional experiments. In contrast, AbC2.1 produced valuable results. With this antibody, that detects the ORF14/15 isoform, a specific dot-like fluorescent pattern reminiscent for basal body staining was observed. This

characteristic localization of this isoform has also been described before [13]. The localization pattern was comparable in the two mouse lines tested and between wild type and mutant animals.

The localization on tracheal epithelial cells revealed interesting insights into specificity. In human cells, Ab4.2 and Ab5.1 specifically labelled the area of the transition zone, which corresponds to the connecting cilium of photoreceptors. Several ciliary proteins had been described to specifically localizes in the transition zone [19]. Among them is IFT88, a known interaction partner of RPGR [11,20]. The RPGR-ORF15 isoform was also detected in the transition zone. Consistent with this finding the murine RPGR-ORF14/15 isoform also localizes there. However, Ab4/5.1 and Ab19.1 diffusely labelled cilia likely reflecting unspecific reactivity of the primary antibody (M.Fliegauf, personal communication). In contrast to the specific staining in humans, Ab4.2 and Ab5.1 stained the length of the cilia in murine cells, which is likely unspecific. In addition, the transition zone was marked with Ab5.1 indicating specificity. Ab19.1 revealed weak and diffuse staining of the cilia in humans while the transition zone was labelled in mice. Thus, species-specific differences in RPGR isoforms and their localization seem to be evident. Only the ORF15 and ORF14/15 isoforms showed comparable staining of the transition zone. Based on theses results, Ab4.2 and Ab5.1 are specific to RPGR in human tissues, while AbC2.1 revealed specific staining in both species.

In summary, several antibodies against RPGR were generated. Characterization indicated that only antibody AbC2.1 produced consistent results throughout all experiments that were performed. This antibody is currently tested on retinal sections of mutant dogs with deletions within the ORF15 sequence [21]. Two additional antibodies (Ab4.2 and Ab5.1) also provided some evidence that they might recognize specific bands on protein extracts and in human tissues. Therefore, these antibodies should be applied in future studies to evaluate their specificity.

3.1.5 References

1. Kirschner R, Rosenberg T, Schultz-Heienbrok R, et al. RPGR transcription studies in mouse and human tissues reveal a retina-specific isoform that is disrupted in a patient with X-linked retinitis pigmentosa. *Hum Mol Genet*. 1999;8:1571-1578.

2. Neidhardt J, Glaus E, Barthelmes D, Zeitz C, Fleischhauer J, Berger W. Identification and characterization of a novel RPGR isoform in human retina. *Hum Mutat*. 2007;28:797-807.

3. Brunner S, Colman D, Travis AJ, et al. Overexpression of RPGR Leads to Male Infertility in Mice Due to Defects in Flagellar Assembly. *Biol Reprod*. 2008.

4. Roepman R, van Duijnhoven G, Rosenberg T, et al. Positional cloning of the gene for X-linked retinitis pigmentosa 3: homology with the guanine-nucleotide-exchange factor RCC1. *Hum Mol Genet*. 1996;5:1035-1041.

5. Meindl A, Dry K, Herrmann K, et al. A gene (RPGR) with homology to the RCC1 guanine nucleotide exchange factor is mutated in X-linked retinitis pigmentosa (RP3). *Nat Genet*. 1996;13:35-42.

6. Vervoort R, Lennon A, Bird AC, et al. Mutational hot spot within a new RPGR exon in X-linked retinitis pigmentosa. *Nat Genet*. 2000;25:462-466.

7. Yan D, Swain PK, Breuer D, et al. Biochemical characterization and subcellular localization of the mouse retinitis pigmentosa GTPase regulator (mRpgr). *J Biol Chem*. 1998;273:19656-19663.

8. Hong DH, Li T. Complex expression pattern of RPGR reveals a role for purine-rich exonic splicing enhancers. *Invest Ophthalmol Vis Sci*. 2002;43:3373-3382.

9. Shu X, Fry AM, Tulloch B, et al. RPGR ORF15 isoform co-localizes with RPGRIP1 at centrioles and basal bodies and interacts with nucleophosmin. *Hum Mol Genet*. 2005;14:1183-1197.

10. Hong DH, Pawlyk B, Sokolov M, et al. RPGR isoforms in photoreceptor connecting cilia and the transitional zone of motile cilia. *Invest Ophthalmol Vis Sci*. 2003;44:2413-2421.

11. Khanna H, Hurd TW, Lillo C, et al. RPGR-ORF15, Which Is Mutated in Retinitis Pigmentosa, Associates with SMC1, SMC3, and Microtubule Transport Proteins. *J Biol Chem*. 2005;280:33580-33587.

12. He S, Parapuram SK, Hurd TW, et al. Retinitis Pigmentosa GTPase Regulator (RPGR) protein isoforms in mammalian retina: Insights into X-linked Retinitis Pigmentosa and associated ciliopathies. *Vision Research*. 2008;48:366-376.

13. Mavlyutov TA, Zhao H, Ferreira PA. Species-specific subcellular localization of RPGR and RPGRIP isoforms: implications for the phenotypic variability of congenital retinopathies among species. *Hum Mol Genet*. 2002;11:1899-1907.

14. Brunner S, Colman D, Travis AJ, et al. Overexpression of RPGR Leads to Male Infertility in Mice Due to Defects in Flagellar Assembly. *Biol Reprod*. 2008.

15. Roepman R, Bernoud-Hubac N, Schick DE, et al. The retinitis pigmentosa GTPase regulator (RPGR) interacts with novel transport-like proteins in the outer segments of rod photoreceptors. *Hum Mol Genet*. 2000;9:2095-2105.

16. Otto EA, Loeys B, Khanna H, et al. Nephrocystin-5, a ciliary IQ domain protein, is mutated in Senior-Loken syndrome and interacts with RPGR and calmodulin. *Nat Genet*. 2005;advanced online publication.

17. Schermer B, Hopker K, Omran H, et al. Phosphorylation by casein kinase 2 induces PACS-1 binding of nephrocystin and targeting to cilia. *EMBO J*. 2005;24:4415-4424.

18. Roepman R, Wolfrum U. Protein networks and complexes in photoreceptor cilia. *Subcell Biochem*. 2007;43:209-235.

19. Fliegauf M, Horvath J, von Schnakenburg C, et al. Nephrocystin Specifically Localizes to the Transition Zone of Renal and Respiratory Cilia and Photoreceptor Connecting Cilia. *J Am Soc Nephrol*. 2006;17:2424-2433.

20. Chang B, Khanna H, Hawes N, et al. An in-frame deletion in a novel centrosomal/ciliary protein CEP290/NPHP6 perturbs its interaction with RPGR and results in early-onset retinal degeneration in the rd16 mouse. *Hum Mol Genet*. 2006.

21. Beltran WA, Hammond P, Acland GM, Aguirre GD. A frameshift mutation in RPGR exon ORF15 causes photoreceptor degeneration and inner retina remodeling in a model of X-linked retinitis pigmentosa. *Invest Ophthalmol Vis Sci*. 2006;47:1669-1681.

3.1.6 Contributions of authors to the manuscript “Generation of RPGR-specific antibodies”

S.B.: selection of epitopes, affinity-purification, dot blots, Western blots (WB), immunohistochemistry (IHC), interpretation of data, writing of the manuscript

S.F.: technical assistance in affinity purification, WB and IHC

J.N.: technical and conceptual input, analysis of data, editing of the manuscript

M.F.: IHC on human and mouse tracheal epithelial cells, interpretation of IHC data

S.S.: preparation of animals

H.O.: data interpretation, supervision of IHC on human and mouse tracheal epithelial cells

W.B.: P.I., conceptual planning, design and supervision of the entire study, interpretation of data, writing and editing of the manuscript

3.2 Overexpression of RPGR Leads to Male Infertility in Mice Due to Defects in Flagellar Assembly

Sandra Brunner[1], Dvora Colman[1], Alexander J. Travis[2], Ulrich F.O. Luhmann[1,4],Wei Shi[3], Silke Feil[1], Coni Imsand[5], Jacquelyn Nelson[2], Christian Grimm[5], Thomas Rülicke[6], Reinald Fundele[3], John Neidhardt[1] and Wolfgang Berger[1*]

[1]Division of Medical Molecular Genetics and Gene Diagnostics, Institute for Medical Genetics, University of Zurich, CH-8603 Schwerzenbach, Switzerland; [2]Baker Institute for Animal Health, College of Veterinary Medicine, Cornell University, Ithaca, NY 14853, USA; [3]Department of Development and Genetics, Uppsala University, SE-75236 Uppsala, Sweden; [4]Division of Molecular Therapy, UCL Institute of Ophthalmology, London EC1V 9EL, United Kingdom; [5]Laboratory for Retinal Cell Biology, Department of Ophthalmology, University of Zurich, CH-8001 Zurich, Switzerland; [6]Institute of Laboratory Animal Science and Biomodels Austria, University of Veterinary Medicine Vienna, A-1210 Vienna, Austria;

Manuscript published, Biology of Reproduction, 2008 Jun 25., Epub ahead of print

3.2.1 Abstract

Male infertility is one possible consequence of a group of disorders arising from dysfunction of cilia. Ciliopathies include primary ciliary dyskinesia (PCD), polycystic kidney disease (PKD), Usher syndrome, nephronophthisis, Bardet-Biedl syndrome (BBS), Alstrom syndrome and Meckel-Gruber syndrome as well as some forms of retinal degenerations. Mutations in the retinitis pigmentosa GTPase regulator gene (*RPGR*) are best known for leading to retinal degeneration, but have also been associated with ciliary dysfunctions affecting other tissues. To further study the involvement of RPGR in ciliopathies, transgenic mouse lines overexpressing RPGR were generated. Animals carrying the transgene in varying copy number were investigated. We found that infertility due to aberrant spermatozoa correlated with increased copy numbers. In animals with moderately increased gene copies of *Rpgr*, structural disorganization in the flagellar midpiece, outer dense fibers, and fibrous sheath was apparent. In contrast, in animals with high copy numbers condensed sperm heads were present but the flagellum was absent in the vast majority of spermatozoa although early steps of flagellar biogenesis were observed. This complexity of defects in flagellar assembly suggests a role of RPGR in intraflagellar transport (IFT) processes.

3.2.2 Introduction

Male infertility is a common disease and to date about 10% of all cases are known to result from genetic defects. These can arise from chromosomal aberrations, microdeletions of the Y chromosome, or single gene mutations [1;2]. However, the underlying genes and molecular mechanisms are not well understood. In recent years many mouse models have shed some light on the molecular pathophysiology of infertlity [3;4]. In those, virtually all steps during spermatogenesis were found to be affected and include the spermatogonial/replicative and meiotic phases, spermiogenesis, as well as the spermiation process [3]. Spermiogenesis is the post-meiotic differentiation process during which the chromatin condenses, the acrosome is formed and the flagellum develops. Of interest, infertile men frequently display reduced or absent motility of the sperm cells resulting from abnormalities of flagellar morphogenesis [5;6]. The flagellum is the crucial structure for mobility of the sperm cell and thus an essential requirement to fertilize an oocyte. Flagellar assembly involves processes that proceed from the proximal to the distal side as well as others that proceed in the opposite direction, suggesting that regulated intraflagellar transport plays a prominent role [7-9].

The retinitis pigmentosa GTPase regulator gene (*RPGR*) gene is widely expressed, mainly in ciliated tissues, and is highly conserved throughout species [10;11] . At the protein level, exons 2-11 encode the regulator of chromosome condensation (RCC1)-like domain, which is homologous to the RCC1-protein, a guanine-nucleotide exchange factor involved in nuclear import and export [10-12]. This domain is thought to be common to the majority of both human and murine RPGR protein isoforms known to date. Mouse and man share 76.4% and 64% identity at the nucleotide and amino acid level, respectively [13]. The N- terminal RCC1-like domain retains 80% amino acid identity [14].

The murine *Rpgr* gene consists of 19 exons and shows an extraordinary high degree of alternative splicing, similar to the human ortholog [13;15]. The predicted size of the murine protein encoded by exons 1-19 is about 95kDa, whereas an alternative isoform retaining intron 14 (equivalent to human exon ORF15) results in a protein of about 150 - 200 kDa. In mouse, *Rpgr* expression analyses detected mRNA in the retina, brain, lung, kidney, liver and testis [16]. Among these tissues, testis displayed the highest level of expression as well as several alternatively spliced transcripts. On protein level, a testis-

specific isoform with a molecular weight of 165 kDa has been described [17]. These findings indicate that RPGR isoforms have tissue-specific functions, also in testis.

In human, bovine and mouse retina, RPGR isoforms were found mainly in the connecting cilium as well as in the basal body/transition zone of photoreceptors [17-22]. The connecting cilium is a narrow intracellular link between the inner and outer segments of photoreceptor cells with a crucial role in protein transport. In mouse sperm flagella, RPGR was localized along the length of the axoneme and the tip of the flagellum [22], structures involved in intraflagellar transport (IFT). In addition to its localization, some of the RPGR interacting proteins also suggest a role in transport. Proteins of cilia, the basal body, as well as the microtubule network were found in a complex with different RPGR isoforms [21-23] . Noteworthy, the association of proteins of the intraflagellar transport (IFT) complex has been identified for several human and bovine RPGR isoforms suggesting a role in IFT pathways [22;24-26] .

In humans, *RPGR* mutations account for approximately 70% of all X-linked retinitis pigmentosa (RP) cases and also for other retinal degenerations [27-32]. A cilia-associated role of RPGR is further indicated by mutations associated with RP, recurrent sinorespiratory infections, and hearing loss [33;34]. Of special interest, mutations in *RPGR* have also been associated with a complex phenotype combining RP and primary ciliary dyskinesia (PCD), a disease resulting from defects of cilia in the respiratory tract, embryonic node and sperm tail, the latter leading to male infertility [35-37]. Of note, patients suffering from X-linked RP were described to display alterations in sperm axoneme structure [38].

Taken together, these data suggest a role for RPGR in ciliary/flagellar transport pathways. Consequently, qualitative or quantitative alterations in RPGR may lead to an impairment of these processes and thus not only to the hitherto known ciliary phenotypes but also to dysfunctions of sperm flagella.

Here we report on infertility in RPGR overexpressing transgenic mice due to severely reduced sperm numbers as well as morphological and functional defects in the sperm flagellum. This infertility phenotype suggests a critical role of RPGR in spermatogenesis.

3.2.3 Methods

Animals

All animals used in this study were treated according to the NIH guide for Care and Use of Laboratory Animals as approved by the Swiss cantonal veterinary office. Wild type and transgenic adult male mice at the age of 12 months, in a mixed B6;C3 background, were anaesthetized by CO_2 inhalation and subsequently killed by cervical dislocation before removal of testes.

Generation of transgenic mice

For male pronucleus microinjection, a linearized P1 artificial chromosome (PAC) clone containing the *Rpgr* gene was used. The PAC was isolated by hybridization of a mouse 129 genomic PAC library with two cDNA probes covering exons 1-2 and 18-19, respectively [13]. Sequencing of the isolated PAC revealed that it contained the entire genomic region of *Rpgr* in addition to 7kb of the flanking 5' and 43kb of the flanking 3' end. After linearization with *NotI*, the PAC was purified by pulse-field electrophoresis (BioRad, Munich, Germany), Subsequently, DNA was processed for injection as described elsewhere [39]. Briefly, precipitated DNA was dissolved in TE buffer (40 mM Tris, 1mM EDTA, pH 7.6) containing 100 mM NaCl, 30 µm spermine, 30 µm spermidine to a concentration of 2 ng/µl. Aliquots were dialysed prior to injection on floating dialysis membranes (Millipore, pore size 0.05 µm, Schwalbach, Germany) for 2 h and then centrifuged in an Eppendorf microcentrifuge at maximum speed. The PAC was injected into male pronuclei of fertilised oocytes derived from B6C3F1 (C57BL/6 x C3H/J) x B6C3F1 matings using an Eppendorf FemtoJet injection system under constant positive flow (Eppendorf, Hamburg, Germany).

Southern blot analysis

Genotype analysis of founders and offspring was performed by Southern Blot analysis on mouse tail DNA. Briefly, HindIII digested DNA was separated on a 1% v/v agarose gel and blotted onto a nitrocellulose membrane (GeneScren Plus, NEN Life Science, Boston, Massachusetts, USA). A ^{32}P-labeled probe covering exons 3 – 5 of murine *Rpgr* was used for hybridization. In the C57BL/6 line, a 400 bp deletion in intron 4 of *Rpgr* occurred resulting in reduced fragment size. This polymorphism in the *Rpgr* gene allowed us to discriminate between the endogenous *Rpgr* locus and the transgene.

In-vitro fertilization

Males from transgenic and wild type mice were sacrificed by CO_2 euthanasia about 12 h after hCG injection of the egg donors. The cauda epididymis and vas deferens of each side were dissected to remove all fat and blood vessels and then placed in a culture dish with 0.5 ml preincubated HTF (human tubal fluid) medium covered with embryo tested mineral oil. To release the sperm from the epididymis it was immediately punctured several times with a 30-gauge needle. In addition, sperm in the vas deferens were gently squeezed out using forceps. All procedures were carried out quickly and on a warming plate (37°C) under sterile conditions. Afterwards the dish was placed for 50 minutes in the incubator (37°C, 5% CO_2 in air) to allow the spermatozoa to capacitate. The egg donors were superovulated by standard protocols and sacrificed about 12 ½ h after hCG treatment. The dissected oviducts were placed into HTF medium and the swollen ampullae were tore with a 30-gauge needle to release the cumulus masses, i.e. the oocytes surrounded by cumulus cells. The cumulus masses of several females were placed into fertilization dishes with 1.0 ml HTF medium. Before IVF the spermatozoa were inspected for concentration and 60 □l of the sperm suspension was added to the oocytes. After 5-6 h of incubation the oocytes were removed from the fertilization dish and washed several times in M16 medium (Sigma-Aldrich, Buchs, Switzerland) to leave behind as much cell debris as possible. Oocytes exhibiting normal morphology were cultured in M16 medium and incubated for an additional 20 h period to reach to two-cell-stage. The embryos were transferred together with two-cell embryos from control IVF into the oviduct of a d 0.5 p.c. pseudopregnant surrogate mother.

Copy number determination

Genomic DNA was isolated from rodent tails using the Qiagen DNeasy Tissue kit (Qiagene, Hombrechtikon, Switzerland). TaqMan primers and probes to exon 1 of the *Rpgr* gene (Forward - Primer: 5' TACAGGTGCTGTGTTTACGTTTGG 3'; Reverse Primer: 5' TCAAGCAACCTTTCCGTTCCT 3'; *Rpgr* probe exon 1: 5' CGTTCGCAGGCTTCGGCAT 3') and to exon 3 of the *Norrie* gene (Forward - Primer: 5' CACTGCAGCCAGGCATCAC 3'; Reverse Primer: 5' TCAAGCAACCTTTCCGTTCCT 3'; *Ndph* probe exon 3: 5' CTGAGCCCTTGGTGTC 3') were designed using the ABI Prism Primer Express 2.0 Software (Applied Biosystems, Rotkreuz, Switzerland). Norrie disease pseudoglioma gene homologue (*Ndph*) is a single copy X-linked gene and was chosen as the control. 10ng of genomic DNA was added to each TaqMan reaction

(250nM Probe, 900nM of each primer, 1x Universal TaqMan Master Mix, RNase-free water) in a final reaction volume of 25ul for both the *Rpgr* and *Ndph* genes. The ABI Prism 7000 Sequence Detection System (Applied Biosystems, Rotkreuz, Switzerland) was used and reactions were performed in 6 replicates for each individual DNA sample. Copy number was determined and calculated from the equation: $2^{\Delta Ct}$, where Ct is the PCR cycle number at which the accumulated fluorescence signal in each reaction crosses a threshold above background and $\Delta Ct = Ct_{Ndph} - Ct_{Rpgr}$

Expression studies using TaqMan

Testes were dissected from male wild type and transgenic littermates with 1 (wt), 2, 8, 10, and 12 copies of the *Rpgr* transgene. Total RNA was isolated using the RNeasy Midi kit (Qiagene, Hombrechtikon, Switzerland). After treatment with RNAse-Free DNase I (Invitrogen, Basel, Switzerland) the concentration and integrity of the RNA were checked on an Agilent Bioanalyzer 2100 (Agilent Technologies, Basel, Switzerland). Of each RNA sample five cDNA syntheses (1 µg RNA each) were performed with SuperScript III RNase H^- Reverse Transcriptase (Invitrogen, Basel, Switzerland) and random Hexamer Primers $pd(N)_6$ (Amersham Bioscience, Freiburg, Germany). Quantitative Real Time-PCR in a 384-well plate format was performed using the ABI PRISM 7900 Sequence Detection System. Five replicates for the target gene *Rpgr* (Forward - Primer: 5' TTTCCGAAGCAGGCACAGA 3'; Reverse Primer: 5' TACAGGTGCTGTGTTTACGTTTGG 3'; fluorchrome-labelled (Vic) *Rpgr* probe exon 1/2: 5' CCGTTCGCAGGCTTCGGCAT 3') and three replicates for the internal standard 18S rRNA (TaqMan Ribosomal RNA Control Reagent, ABI, Rotkreuz, Switzerland) were included for each sample. We used the ΔC_t-method for relative quantification and analysed the data by using the ABI Prism 7900HT SDS2.2 Software and Excel (Microsoft; Redmont, USA). Based on the mean relative expression values for the technical replicates, the mean value for the relative expression was calculated and used as the basis for the statistical analysis with the SPSS v.14 software (SPSS Inc., Chicago, IL). Outliers were omitted based on Grubbs test. Statistical analyses were done using Kruskal Wallis and Mann-Whitney U test.

Generation of anti-RPGR antibody

A polyclonal antibody was raised in rabbit against a short amino acid sequence coded by exon 5 of the murine RPGR sequence (^{153}NEGQLGLGDTDDRDTFH^{169}) (NCBI –

Accession: NP_035415) (Eurogentec, Seraing, Belgium). The antibody Ab5.1 was affinity-purified against the cognate peptide (Sulfolink; Pierce Biotechnology, IL, USA) according to manufacturer's instructions. Briefly, the peptide was coupled via disulfide bonds to a column, which was subsequently incubated with the rabbit antisera for 1 h at room temperature to allow binding to occur. After elution, the IgG concentration of affinity purified antibodies was determined using a Nanodrop (ND-3300, Witec AG, Littau, Switzerland).

Western blot analysis

Testes of transgenic animals were snap-frozen in liquid nitrogen. Frozen tissues were homogenized in a glass-teflon Potter in RIPA buffer (50mM Tris, 150 mM NaCl, 1mM EDTA, 0.2% NP40) containing Complete protease inhibitor cocktail (Roche Diagnostics GmbH, Mannheim, Germany) followed by centrifugation at 2000g at 4°C. Protein concentration was determined from the supernatant by a bicinchoninic acid assay (Sigma-Aldrich, Steinheim, Germany) and read-out on an ELISA-plate reader (ELx808, BioTek, Littau, Switzerland). Protein extracts were diluted with 5x SDS loading buffer (120mM Tris (pH 6.8), 2% w/v SDS, 5% v/v β-mercaptoethanol, 50% v/v glycerol, bromophenolblue), boiled and resolved on a 10% w/v SDS-PAGE. For testis, 33 µg of protein extract were loaded. After electrophoresis, proteins were transferred to a PVDF membrane (Roche Diagnostics, Mannheim, Germany) by semi-dry blotting (Bio-Rad, Munich, Germany). Detection was performed by using anti-RPGR Ab5.1 at 2.9 µg/ml and a mouse anti-GAPDH antibody was used as a loading control (Chemicon, Dietlikon, Switzerland). For blocking experiments the antibody was pre-absorbed with 50 □g peptide for 3 h at room temperature. As secondary antibody, anti-rabbit and anti-mouse IgG coupled to horseradish peroxidase (Dianova, Hamburg, Germany) were used at dilutions of 1:500. Blots were developed with Western Lightning Chemiluminescence Reagent Plus (Perkin Elmer, Boston, USA) and chemiluminescence detection film (Lumi-Film, Roche Diagnostics, Mannheim, Germany).

Quantification of western blots

Western blots were scanned (Epson Perfection 1660 Photo, Meerbusch, Germany) and used for quantification. Density of RPGR immunoreactive bands at different exposure times was measured with image analysis software (TL 100, Nonlinear Dynamics, Newcastle upon Tyne, UK) and used for further calculation. Comparison of GAPDH

immunoreactivity was used to ensure that equal amounts of protein extracts were loaded into each lane (data not shown). The fold change of RPGR-165 isoform in transgenic animals was calculated relative to wild type (1217/Wt) and 1217/Tg4 band density, respectively. Graphs show values of one representative experiment.

Histology

Testes from 12 month old wild type and transgenic mice were collected and immediately frozen in liquid nitrogen, and stored at -80°C until further usage. Tissues were fixed at 4°C for 6 h in serras fixative (60% v/v 100% v/v ethanol, 30% v/v 37% v/v formaldehyde, 10% v/v 100% v/v acetic acid), dehydrated in ascending concentrations of isopropanol, transferred into chloroform and embedded in paraffin. Sections of 5-6 µm were cut with a microtome (Leica Microsystems, RM2145, Glattbrugg, Switzerland). Slides were stained with hematoxylin and eosin and then examined and photographed with a Zeiss microscope (Zeiss, Axioplan 2, Feldbach, Switzerland) attached to a Zeiss camera (Zeiss, AxioCam HR, Feldbach, Switzerland).

Electron microscopy

Tissue was fixed in 2.5% Glutaraldehyde in 0.1 M cacodylate buffer, pH 7.3, at 4°C overnight, washed in cacodylate buffer, incubated in osmium tetroxide for 1 h, dehydrated in increasing ethanol concentrations, and embedded in Epon 812. Sections (50–60 nm) were prepared and contrasted with 4% uranyl acetate in 50% EtOH and 2.6% lead nitrate in 1 M NaOH. Sections were analyzed using a Hitachi 7000 electron microscope (Hitachi, Tokyo, Japan).

3.2.4 Results

Generation of Rpgr transgenic mice

A transgenic mouse line was generated by pronuclear injection of a mouse P1 artificial chromosome (PAC) clone that was entirely sequenced and used for comparative sequence analysis of *RPGR* in man and mouse [13]. In addition to the coding region of *Rpgr* derived from the mouse strain 129 (*Rpgr*^{129}), the PAC also contained flanking genomic sequence in the 5' and 3' end of 7kb and 43kb, respectively, which likely include regulatory elements of the *Rpgr* gene. For microinjection, zygotes from the mixed B6C3F1 strain were used. After transfer of microinjected embryos into carrier females, the offspring were genotyped for *Rpgr* and *Pde6β* on tail DNA. A nonsense mutation in the *Pde6β* gene is known to cause retinal degeneration (rd1) in several inbred strains including the C3H strain [40]. In addition to the nonsense mutation, the rd1 mice carry a proviral insertion in intron 1 of *Pde6β*, which cosegregates with the retinal phenotype [41]. This mutation can be detected by PCR and was used for genotyping purposes [42]. After exclusion of the Pde6β^{rd1} allele we determined if the transgene was present and identified two founders by Southern blot hybridisation (Figure 1). The two females were mated with C57BL/6 males to establish two independent transgenic lines with confirmed integration of the transgene, denoted B6;C3-Tg(*Rpgr*) 1217 and 1222. Analysis of the progeny revealed germ line transmission of the PAC transgene for both founders.

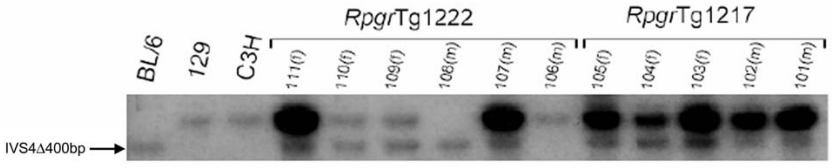

Figure 1: Southern blot analysis of founder female offspring

Germline transmission of the PAC transgene (*Rpgr*^{129}) was detected in offspring derived from two independent founders. Analysis of DNA derived from the progeny of *Rpgr* transgenic founder mice 1222 and 1217 was performed by Southern blot hybridisation. The reduced fragment size in B6 is due to a deletion polymorphism in intron 4 of *Rpgr*. This 400bp deletion allows one to discriminate if the *Rpgr* gene copy is derived from the transgene or C57BL/6 mice. The presence of the transgene is also indicated by an increased signal intensity of the non-deleted allele. According to these results, all offspring from founder 1217 (three females (f) and two males (m)) carry the transgene. In the progeny of founder 1222, we detected two transgenic mice, one female and one male. As the transgenic male mice have inherited the B6 allele of *Rpgr*, the upper band exclusively represents the transgene.

Determination of the Rpgr copy number in transgenic animals

To determine the number of integrated *Rpgr* copies into the genome of the individual animals, a quantitative real-time PCR assay (TaqMan) was used. The founder female 1222 had 20 and founder female 1217 had 24 transgenic *Rpgr* copies (animals were designated therefore as Tg20 and Tg24), respectively (Table 1). In the first litter of female 1222, one transgenic animal had 11 copies (1222/Tg11) and from female 1217 one male offspring had 8 transgenic copies of *Rpgr* (1217/Tg8). In the second litter, originating from the founder female 1222, three male mice were wild type and one had 10 copies of the transgene (1222/Tg10). In the second litter from the founder female 1217, six offspring inherited the transgene in variable copy numbers (1217/Tg2 – 1217/Tg13) (Table 1). One sibling of this litter was wild type and used as littermate control (1217/wt). For exclusion of effects on the phenotype due to integration site, experiments were done on animals deriving from both transgenic founder females.

Table 1: Copy numbers of founder females and their offspring

Founder female	Litter	Offspring Male ID	Copy number	Animal Name
1222			20	Tg20
1217			24	Tg24
1222	1st	107	11	1222/Tg11
1217	1st	102	8	1217/Tg8
1222	2nd	201	1	
1222	2nd	202	1	
1222	2nd	203	1	
1222	2nd	204	10	1222/Tg10
1217	2nd	205	2	1217/Tg2
1217	2nd	206	5	1217/Tg5
1217	2nd	207	1	1217/wt
1217	2nd	208	12	1217/Tg12
1217	2nd	209	13	1217/Tg13
1217	2nd	210	4	1217/Tg4
1217	2nd	211	8	1217/Tg8

Two transgenic founder females (#1222 and #1217) were mated to C57BL/6 males and two litters of each were genotyped for *Rpgr* transgene copy numbers. The *Rpgr* transgene was passed to the male offspring with varying copy numbers

Infertility in transgenic male mice

Two transgenic male mice from the first litter carrying 8 and 11 copies of *Rpgr* (1217/Tg8 and 1222/Tg11), respectively, were bred to wild type B6 females. Although mating occurred as indicated by the positive control of copulatory plugs, no progeny were produced. Consequently an *in-vitro*-fertilization (IVF) procedure was carried out. Four animals from the second litter were chosen that carried 2, 8, 10 and 12 copies of

Rpgr (1217/Tg2, 1217/Tg8, 1222/Tg10 and 1217/Tg12), respectively. Caudae epididymides of these animals were dissected and treated as described before. For the animals 1217/Tg8, 1222/Tg10 and 1217/Tg12 neither morphologically intact nor sperm cells with deformities were released from the punctured caudae epididymides. The cell debris found in the sperm dish had no obvious spermatogenic cells and was therefore not further analysed. In the male with 2 copies of the *Rpgr* transgene (1217/Tg2) sperm cells were present and used for (IVF). After IVF only one 2-cell embryo was produced out of approximately 200 oocytes incubated with the 1217/Tg2 sperm in contrast to about 73% fertilized oocytes of the control IVF using wild type sperm (data not shown). However, the single *Rpgr*-transgenic embryo did not develop to term after embryo co-transfer with control wild type 2-cell embryos as confirmed by the coat color and by genotyping of the offspring.

Expression levels of transgenic Rpgr/RPGR

To characterize the infertility phenotype on the molecular level, qRT-PCR and Western blot analyses were performed. Transcript analyses in testis extracts showed that all transgenic animals examined (1217/Tg2, 1217/Tg8, 1222/Tg10 and 1217/Tg12) had significantly elevated mRNA levels compared to wild type (Figure 2A). Transgene expression was increased significantly in 1217/Tg2 by 32-fold compared to wild type and also significantly higher in 1217/Tg8 and 1222/Tg10 compared to 1217/Tg2. We did not detect significant difference in the transgene expression in 1217/Tg8 and 1222/Tg10 and the expression level in testis of animal 1217/Tg12 was similar to 1217/Tg2. Overall, *Rpgr* was overexpressed in the testes of transgenic animals however, high levels of transgenic *Rpgr* copy numbers led to an attenuation of transcript expression.

Subsequently, the effect of elevated mRNA expression on testicular RPGR protein level was assessed by western blot analysis. A polyclonal RPGR-specific antibody recognizing a peptide derived from exon 5 was used for this purpose (Ab 5.1). In the wild type, the antibody recognized three proteins at 40 kDa, 65 kDa and 165 kDa (Figure 2B, left blot). The binding to the protein of 65 kDa was judged to be non-specific as it was not blocked by pre-absorption with the cognate peptide (Figure 2B, right blot). In testes from overexpressing males, additional immunoreactive bands were detected (80 kDa, 95 kDa and 125 kDa). Thus, those bands seem to be specific to RPGR. The amount of testis-specific [17] RPGR isoform of 165 kDa was significantly increased compared to wild type. An antibody against RPGR-ORF15 did not detect a protein of

that size indicating that this high molecular isoform might not contain exon ORF15 (data not shown). It is noteworthy that expression of exon ORF15 in testis has been reported [22]. A smaller product of approximately 125 kDa was observed in 1217/Tg4 and 1217/Tg5, suggesting either translation of alternatively spliced mRNA, post-translational modifications or sample degradation. However, this isoform was not detected in 1217/Tg13, which might indicate altered splicing in correlation with the expression level of RPGR. The amount of the two proteins of 95kDa and 100kDa was also increased in male 1217/Tg13 indicating specificity to RPGR. The transcript of *Rpgr* containing exon 1-19 is estimated to yield a protein of approximately 95 kDa [17;43]. Several minor immunoreactive fragments were also detected between 75 kDa - 100 kDa. Based on their loss of immunoreactivity when the antibody was pre-absorbed, these also appeared to be specific to RPGR and might also represent different post-translational modifications, alternative splicing, or sample degradation. The protein of 40 kDa might be either a different RPGR isoforms or degradation products.

Approximations of fold change of protein level of the highly overexpressed RPGR 165kDa isoform by semiquantitative densitometric analysis suggested that animals with 4 and 5 copies showed 30fold increase in protein amount (Figure 2C). Lower exposure times of the western blot revealed that 1217/Tg13 had about 1.4 – 1.6times higher protein levels compared to 1217/Tg4 and 12177Tg5, respectively (data not shown).

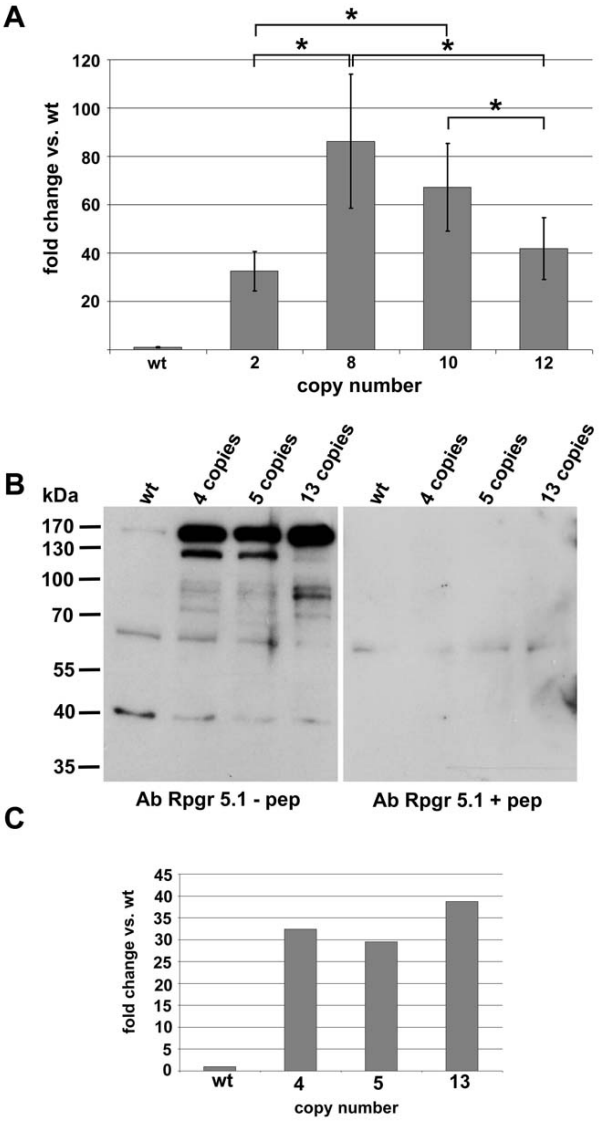

Figure 2: Expression levels of *Rpgr* transgene in testis

A) Transgenic *Rpgr* transcript levels were monitored by qRT-PCR and normalized to wild type expression level. Fold-change compared to wild type expression level are shown. All transgenic animals had significantly higher expression of *Rpgr*. Mean values +/- S.D. obtained from different cDNA syntheses (wt, Tg2, Tg10, Tg12: n=5; Tg8: n=4) are shown. Statistical analyses were performed using Kruskal Wallis and Mann-Whitney U tests ($p \leq 0.05$)

B) Western blot of Rpgr protein expression in wild type and transgenic animals carrying 4, 5 and 13 copies of the transgene (1217/Tg4, 1217/Tg5 and 1217/Tg13). Long exposure revealed several bands in wild type and transgenic animals (left). Western Blot incubated with pre-absorbed antibody was used for specificity testing (right). One representative experiment is shown.

C) Relative expression of the Rpgr-165 kDa isoform compared to wild type protein level observed in the blot of panel B).

Histological analysis of transgenic testes

We next examined whether spermatogenesis and/or morphology of transgenic sperm was disturbed due to overexpression of RPGR and whether any such changes could explain the observed infertility. Therefore, testis sections from wild type and different transgenic animals were examined. Wild type animals presented normal morphology with all maturation stages of sperm visible during spermatogenesis (Figure3, A and B). In the animal with two copies of *Rpgr* (1217/Tg2) morphology appeared unaltered as well (Figure 3, C and D). The lumina of seminiferous tubules contained normal-looking flagella (arrows). In contrast, in males carrying eight or ten *Rpgr* copies (1217/Tg8 and 1222/Tg10), the lumina of the seminiferous tubules were empty indicating a severely reduced number of mature spermatozoa (Figure 3, E – H). However, some spermatids

with condensed nuclei were present indicating that post-meiotic aspects of spermatogenesis were not entirely ablated (Figure 3 F and H, arrowheads).

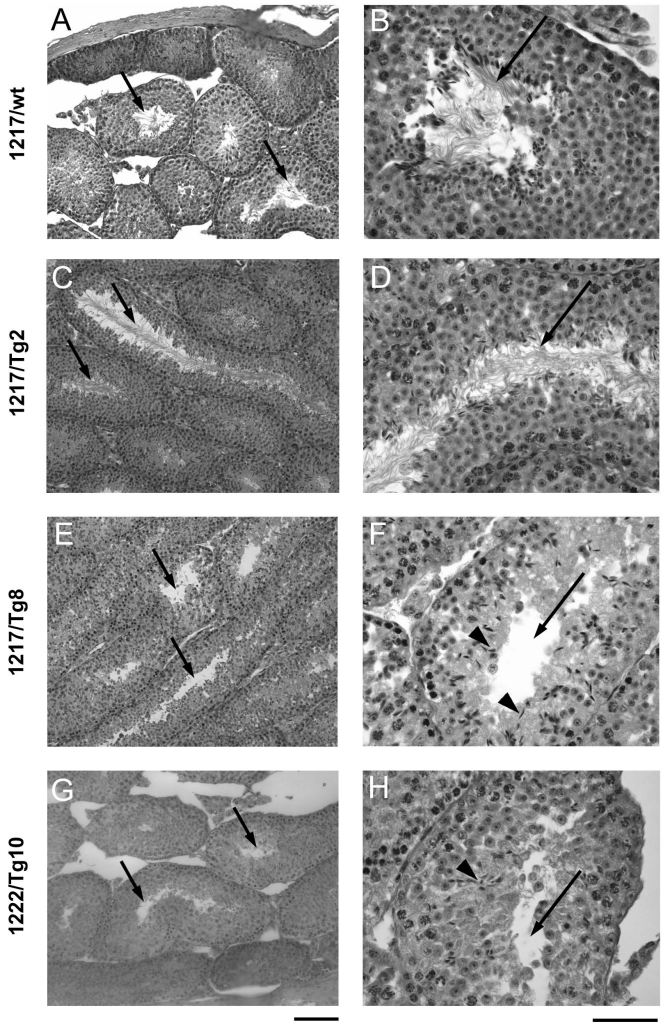

Figure 3: Histological analysis of testis from transgenic and wild-type mice

A) Hematoxylin and eosin staining of testis sections from wild type (A and B) and transgenic (C-H) mice. In the wild type, the lumina of the seminiferous tubules were filled with mature spermatozoa (arrows). In the animal carrying 2 copies of *Rpgr* mature spermatozoa were still present (C and D, arrows), whereas in the animals carrying 8 or more copies of *Rpgr* the lumen of the tubules were empty (E – H, arrows). Note that the heads of condensing spermatids were formed (F and H, arrowheads), but the flagella were absent. Scale bar = 100 µm (left) and 50 µm (right).

Ultrastructural changes in sperm flagellum

Structurally, the flagellum can be divided into four segments (connecting piece, midpiece, principal piece and endpiece) (Figure 4A)[44;45]. The axoneme extends through the whole length of the flagellum. In the midpiece it is surrounded by nine outer dense fibers (ODF) which correspond to the nine outer doublets of the axoneme (Fig 4B). The midpiece, the only region of mature spermatozoa to contain mitochondria, is encircled by the mitochondrial sheath (Figure 4B). The principal piece is surrounded by the fibrous sheath, which consists of two longitudinal columns that are attached to ODFs 3 and 8 and replace them such that moving distally the principal piece then has 7 ODF. Because in animals with moderate copy numbers (i.e. 4-5) mature spermatozoa were

still present, putative sub-structural defects were investigated by transmission electron microscopy. Males 1217/Tg4 and 1217/Tg5 were chosen as their copy number is between the morphologically normal looking flagella of animals with 2 copies and the lack of flagella seen with 8 or 10 copies. Sperm from wild type littermates showed normal flagellar sub-structural organization (Figure 4C). In the transgenic animal with 5 copies (1217/Tg5), defects were observed in several structures of both the midpiece and principal piece of the flagellum and varied between individual sperm within the same tissue section (Figure 4D-F). Occasionally, the mitochondria of the flagellar midpiece appeared abnormal in *Rpgr* transgenic mice in terms of their arrangement and contents. Moreover, derangements in the organization of the ODF were present (Figure 4D). In some other midpieces, the mitochondria had a relatively normal appearance, but there was an excess of cytoplasm under the plasma membrane, and the number of ODF was less than the nine that would be expected at this level in the flagellum (Figure 4E). Sections through the principal piece revealed derangements of the fibrous sheath, including asymmetry and thickening of the lateral ribs (Figure 4F). Occasionally, sperm exhibited an abnormal axoneme. In order to see whether flagellar formation was completely abolished in transgenic mice with high copy numbers we looked at the zone of the connecting piece in wild type (Figure 4G) and transgenic animals with 4 (Figure 4H) and 11 copies (4I and 4J). Although only very few sperm heads with condensed nuclei were present in those sections, some of the spermatids were informative and revealed that structures of the connecting piece associated with early flagellar biogenesis seemed to be present in animal 1217/Tg4 (Figure 4H, arrow) and animal 1222/Tg11 (4I and 4J, arrows). In both transgenic animals the basal plate was visible (Figure 4H and 4I, arrows). This finding might indicate that the defect is not due to a complete failure in flagellar formation but rather due to a disturbed organization.

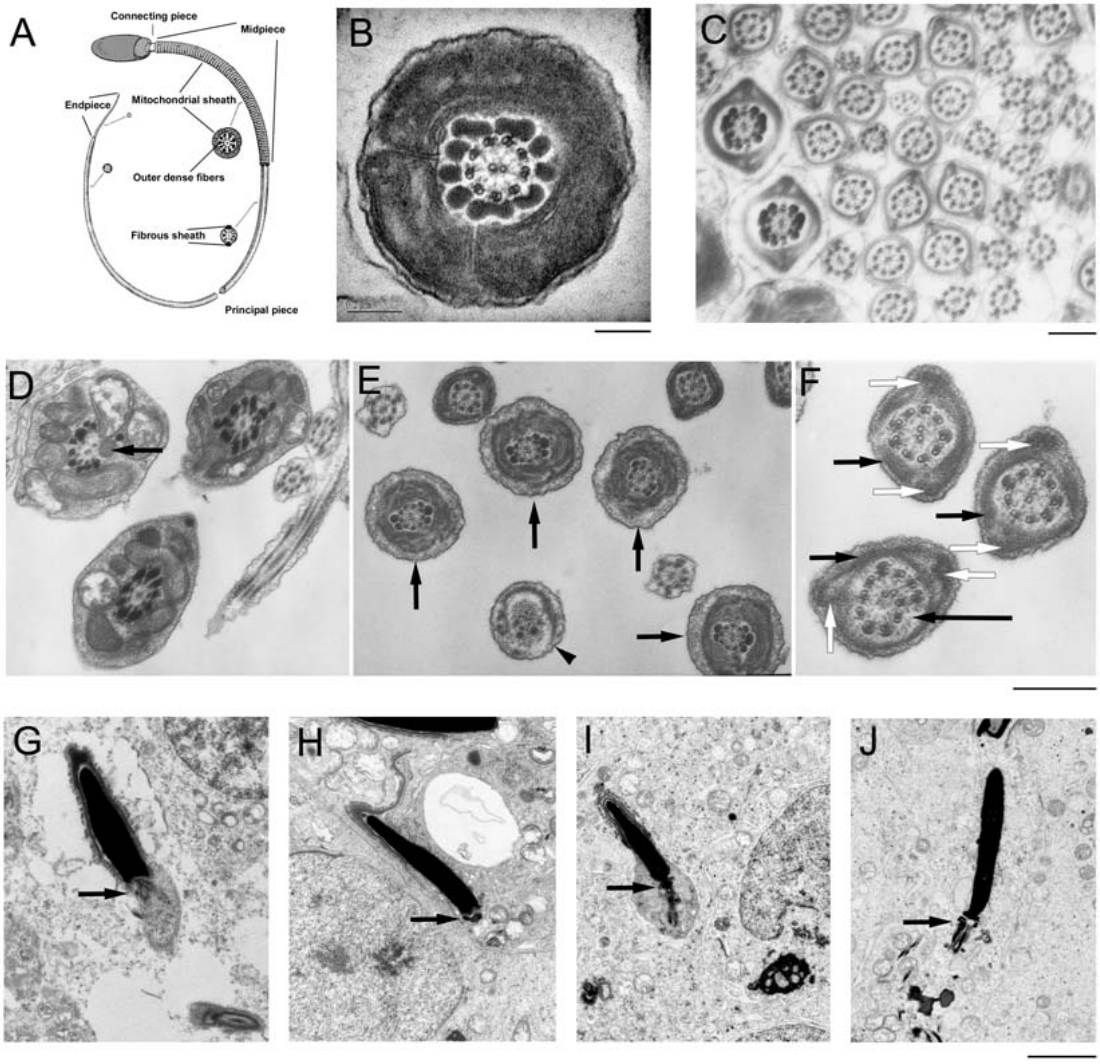

Figure 4: Transmission electron micrographs from transgenic *Rpgr* testes. A) Scheme of a mammalian sperm cell. The four major segments of the flagellum are indicated (connecting piece, midpiece, principal piece and endpiece). Schemes of cross sections show the typical composition of a flagellum in the different segments. Note the organized structure of the mitochondrial sheath (MS), the outer dense fibers (ODF) in the midpiece, the fibrous sheath and the outer dense fibers in the principle piece. Scheme modified after Fawcett D., 1975 B) Electron micrograph of a section through the midpiece of a wild type flagellum. The MS is regular and the ODF perfectly correlate with the outer doublets of the axoneme. C) Micrograph showing multiple cross-sections through the flagella of wild-type sperm as a control. The organization of the ODF in the midpiece and principal piece stands in strong contrast to the sperm from mice overexpressing RPGR. D) Cross-sections of three flagellar midpieces from transgenic mice carrying 4 *Rpgr* copies. The arrow points to a major defect in the organization of the axoneme and ODF within one sperm. E) In all cross-sections through the flagellar midpiece of a Tg5 animal abnormal numbers of ODF were found (arrows). There were also multiple defects observed in what appears to be a cross-section through a principal piece (arrowhead). F) Cross-sections through three abnormal principal pieces in a Tg5 animal. Each has defects in the fibrous sheath, including abnormal thickening of the

lateral ribs (black arrows) and varying degrees of asymmetrical positioning of the longitudinal columns (white arrows). A defect in the organization of an axoneme is marked by a grey arrow. Defects in the axoneme were rare relative to the abundance and severity of defects seen in the flagellar accessory structures. G-J) Condensed sperm head with the neck region of the sperm flagellum from a wild type mouse (G) and transgenic animals Tg5 (H) and Tg11 (I and J). In all sections some basic structures of the neck region/connecting piece such as the basal plate could be observed (arrows). Scale bars = 0.2 µm (B); 1 µm (C, D, E); 0.5 µm (F); 2 µm (G-J)

Together, these data suggest that overexpression of RPGR could be associated with multiple defects in flagellar assembly, rather than a specific defect in one flagellar structure.

3.2.5 Discussion

In this study, we demonstrated that overexpression of RPGR can result in infertility of male mice due to defects in spermiogenesis. The extent of the defect in flagellar formation, ranging from disorganization of accessory structures (ODF, FS and MS) to the complete lack of flagella, was dependent on the copy number of *Rpgr.*

Specificity of observed infertility

The strategy that was used to generate transgenic mice is based on random integration of the transgene into the genome. Therefore, the two founder females were expected to carry the transgene in varying number and at different chromosomal integration sites. This raises the possibility that the observed male sterility was caused by insertional mutagenesis. Nevertheless, male offspring of both founder females developed identical phenotypes. Second, the structural abnormalities in sperm cells correlated with the number of copies of *Rpgr*. Thus, males carrying two copies of the transgene still had motile sperm and the flagellum was built. However, in animals with an intermediate number of *Rpgr* copies, i.e. 4-5, and an elevated protein amount of at least 30-fold of wild type level, the flagellum was also built but accessory structures were not properly organized. In contrast, in animals with high copy numbers (i.e. 13) and an increased protein expression of another 40% - 60% compared to males 1217/Tg4 and 1217/Tg5, the flagellum was not built at all. This strict dose-dependent phenotype also supports the specificity of the effect. In a recent review of 23 knockout mouse models with abnormalities of the sperm flagellum, only three of those specifically resembled the noted absence of flagella while the sperm head was still formed and the nucleus underwent condensation [4]. They will be discussed below. Seven of the 23 models displayed disruptions either in the fibrous or mitochondrial sheath; however, none of these defects seemed to result directly from defects in flagellar assembly and transport.

Unstable transmission of transgene from founder females to male offspring

Genotyping of the transgenic animals revealed that transgenic *Rpgr* was not inherited in a stable fashion from the mothers to their offspring. While the two founder females had 20 and 24 copies, respectively, the male offspring showed a highly variable number of *Rpgr* copies. In each case they had lower numbers than the copy number carried by the mothers. Such loss is known to occur during meiosis due to either unequal crossover or

by slippage during DNA replication [46]. Alternatively, the transgenic loci at multiple insertion sites segregated independently.

Effect of copy number on transcript levels

On the transcript level we found an attenuation of overexpression in animals with high copy numbers. This might be due to genetic background effects, as the transgene was injected into B6C3F1 pronuclei and then backcrossed for only one generation to C57BL/6 background. In addition, the *Rpgr* transgene was derived from the 129 mouse strain and was expressed in a mixed C57BL/6 x C3H background. Furthermore, high copy number of transgenes have been reported to display reduced expression [47]. Alternatively, it seems possible that not all *cis*-acting elements were included beside the large genomic extend of the PAC. Since only one animal for each copy number has been generated the observed variations may reflect individual deviations of transgene expression. Precise regulation of excess transcriptional products was not relevant to the testing of overexpression of protein, so this line of inquiry was not pursued.

Isoform - specific overexpression of the Rpgr transgene

We detected several overexpressed protein isoforms of RPGR in testis. The highly overexpressed isoform of 165 kDa (RPGR-165) has been described as testis-specific in mouse [17]. Another isoform of lower molecular weight (RPGR-95), corresponding to the size of the $RPGR_{default}$ variant containing exons 1-19, was also elevated. The amount of the isoform of 130 kDa was elevated in animals 1217/Tg4 and 1217/Tg5 but could not be detected in 1217/Tg13. These differences might be attributed to different regulatory mechanisms due to high overexpression. In summary, these data further support previous findings of our and other groups that *Rpgr* is alternatively spliced and generate different isoforms in a tissue-specific manner [15;16;32]. These different isoforms might have distinct functions in the formation and maintenance of cilia and flagella.

Defects in periaxonemal structures

Previous studies described ultrastructural defects of the flagellum in infertile men [5;48]. Likewise, numerous genetically engineered mouse models also revealed a flagellar phenotype [4]. For example, Akap4 as well as Ube2b null mice have disturbed organization of the fibrous sheath [49;49;50]. Although those proteins are not directly involved in IFT, they presumably play a role in fibrous sheath organization. Indeed, the

asymmetry and FS disorganization seen in the Ube2b null mice resembles the mildly asymmetrical FS phenotype observed in RPGR overexpressing mice. In addition, failure in some cells to achieve or maintain complete encirclement of the flagellum with the lateral ribs of the FS was also seen in some Ube2b null sperm. In humans, some of the patients described by Chemes et al. and Escalier and David showed abnormalities of the axoneme [5;48]. This was only found very occasionally in our RPGR overexpressing mouse line. However, patients also exhibited defects in the periaxonemal structures like the fibrous sheath, a feature that was also present in our *Rpgr* transgenic mouse line with moderate copy numbers. Also of note, some of the patients described in these studies presented with additional symptoms of the respiratory system or with *situs inversus*, reminiscent of primary ciliary dyskinesia (PCD).

The disarrangement of structural components like the outer dense fibers (ODF), fibrous sheath (FS) and the mitochondrial sheath (MS) in animals with moderate *Rpgr* copy numbers (i.e. 5) rather than a principal failure in axoneme formation suggests that the assembly process of these structures was compromised. In animals with high copy numbers of *Rpgr* (i.e. >8) the assembly of the flagellum was completely abolished. Therefore, we examined round and condensing spermatids to determine whether development of flagella was initiated. These analyses were limited by the need for sections precisely through the developing connecting piece at a point that would be informative. We observed several examples in which the basal plate was identifiable, as were the initial aggregations of flagellar anlage, but no spermatids with amorphous tails of intermediate length. This suggests that very high *Rpgr* copy numbers lead to a lack of flagella but not to a short, stunted tail.

Our observations suggest an initiation of flagellar biogenesis and a failure in assembly. This distinguishes the RPGR overexpression phenotype from that of “easily decapitated sperm syndrome” (EDSS), where the basal plate does not form and the fully-developed flagellum loses its attachment to the sperm head [51].

RPGR in microtubular transport pathways

Transport of flagellar components is accomplished by intraflagellar transport (IFT) [25;52]. Several IFT proteins (IFT57, IFT52, IFT20 and IFT88) are abundantly expressed in murine testis and IFT88 was found in the manchette of mouse and rat spermatids [53;54]. Likewise, those proteins can be detected in mouse retina and it was shown that IFT complexes are present in both tissues [55]. Of note, the RPGR-ORF15

isoform associates with IFT88 (Polaris) [22]. Additionally, RPGR and RPGR-ORF15 isoforms both interact with microtubule motor protein subunits known to be responsible for IFT like KIF3A, KAP3, p150^{Glued}, dynein intermediate chain (DIC) and p50-dynamitin [22;24]. In *Tg737*(IFT88) mutant mice, mainly kidney and retina were affected [53;56]. Furthermore, these mice might have defects in spermiogenesis [54;57].

Of great interest is that in addition to aberrant sperm found in X-linked RP patients [38], that several mouse mutants of ciliary/flagellar proteins reveal a similar testicular phenotype as observed in our *Rpgr* transgenic mice with high copy numbers [58-62]. Knock-out mouse models for the Bardet-Biedl syndrome (BBS) affecting *Bbs2*, *Bbs4* and *Mkks (Bbs6)* fail to develop flagella, but condensed sperm heads can still be found suggesting that the transport machinery for flagellar formation is disrupted or that the connecting piece is formed inappropriately, and the developing flagellum breaks away from the body of the spermatid. In another mouse model for BBS, a knock-in mutation (M390R) was introduced into the *Bbs1* gene [61]. This loss-of-function mutation also led to the lack of sperm flagella whereas condensed sperm heads were present but no details about the flagellar phenotype were described. Just recently, Nachury et al. [63] found that seven of the twelve known BBS proteins form a complex with some additional proteins (referred to as the BBSome), including BBS1, BBS2 and BBS4. Additionally, this complex was shown to be involved in vesicular trafficking to ciliary membranes, a process which also involves small GTPases of the Rab and Arf families [63]. Recent studies proposed a functional link between the BBSome and IFT [63-65]. To date, RPGR has never been shown to interact with BBS proteins. However, most of the BBS proteins also locate at the base of the cilium [66-69], but presumably in a different ciliary compartment than RPGR [57]. A mouse model for primary ciliary dyskinesia (PCD) with a deletion of a region on chromosome 1 displayed absence of sperm flagellum and a novel ciliary/flagellar protein (PCDP1) was found to be responsible for the manifestations [62]. Notably, mutations in *RPGR* may also lead to PCD [36]. Although the testicular phenotypes of the mutant *Bbs* and *Pcdp1* mice is similar to our transgenic *Rpgr* mouse as all display a lack of flagella, the underlying mechanisms leading to this specific structural abnormality might be attributed to different pathogenic mechanisms. Whereas in the *Bbs* and *Pcdp1* mice the functional protein is absent, the mice described herein show an overexpression of RPGR. One possible explanation for the RPGR overexpression phenotype is that the excess of protein could lead to a cytoplasmic aggregation of RPGR which in turn could result in a lack of RPGR protein at the site

where it is normally required for proper function (i.e. the basal body/transition zone and/or the flagellum). The previously published *Rpgr* knockout mouse model did not address the investigations of a putative sperm flagellum phenotype, however it was stated that the k.o. mice were fertile [17]. It would be of great interest to see whether those mice show structural abnormalities in the flagellum as well. An alternative hypothesis is that the sensitive balance between RPGR and its interacting proteins has been disturbed due to overexpression. The relative abundance of RPGR might exert a dominant-negative effect by altering the stoichiometry of the components of multiprotein complexes consequently leading to their dysfunction. This might also account for the variety in sub-structural phenotypes, rather than a defect in the assembly of a specific component.

Taken together, the defects in flagellar formation displayed in the RPGR overexpressing mouse line described herein further strengthens the hypothesis that RPGR is involved in ciliary/flagellar assembly and/or transport pathways and fits to the general hypothesis that many ciliopathies result from defects in a large ciliary protein complex, also including RPGR. In addition, these data for the first time provide evidence that alterations in RPGR lead to a flagellar phenotype in mice and therefore might be considered as a novel candidate gene for isolated and syndromic male infertility.

3.2.6 Acknowledgements

We thank Barbara Kloeckener-Gruissem (PhD) for helpful discussions and critical reading of the manuscript.

3.2.7 References

[1] Tuttelmann F, Rajpert-De Meyts E, Nieschlag E, Simoni M. Gene polymorphisms and male infertility--a meta-analysis and literature review. Reprod Biomed. Online. 2007; 15: 643-658.

[2] Ferlin A, Raicu F, Gatta V, Zuccarello D, Palka G, Foresta C. Male infertility: role of genetic background. Reprod Biomed. Online. 2007; 14: 734-745.

[3] Cooke HJ, Saunders PTK. Mouse Models of Male Infertility. Nat Rev Genet 2002; 3: 790-801.

[4] Escalier D. Knockout mouse models of sperm flagellum anomalies. Hum Reprod Update 2006; 12: 449-461.

[5] Escalier D, David G. Pathology of the cytoskeleton of the human sperm flagellum: axonemal and peri-axonemal anomalies. Biol Cell 1984; 50: 37-52.

[6] Chemes HE, Olmedo SB, Carrere C, Oses R, Carizza C, Leisner M, Blaquier J. Ultrastructural pathology of the sperm flagellum: association between flagellar pathology and fertility prognosis in severely asthenozoospermic men. Hum Reprod 1998; 13: 2521-2526.

[7] Oko R, Clermont Y. Light microscopic immunocytochemical study of fibrous sheath and outer dense fiber formation in the rat spermatid. Anat. Rec. 1989; 225: 46-55.

[8] Irons MJ, Clermont Y. Formation of the outer dense fibers during spermiogenesis in the rat. Anat. Rec. 1982; 202: 463-471.

[9] Irons MJ, Clermont Y. Kinetics of fibrous sheath formation in the rat spermatid. Am J Anat. 1982; 165: 121-130.

[10] Meindl A, Dry K, Herrmann K, Manson F, Ciccodicola A, Edgar A, Carvalho MR, Achatz H, Hellebrand H, Lennon A, Migliaccio C, Porter K, Zrenner E, Bird A, Jay M, Lorenz B, Wittwer B, D'Urso M, Meitinger T, Wright A. A gene (RPGR) with homology to the RCC1 guanine nucleotide exchange factor is mutated in X-linked retinitis pigmentosa (RP3). Nat. Genet. 1996; 13: 35-42.

[11] Roepman R, van Duijnhoven G, Rosenberg T, Pinckers AJ, Bleeker-Wagemakers LM, Bergen AA, Post J, Beck A, Reinhardt R, Ropers HH, Cremers FP, Berger W. Positional cloning of the gene for X-linked retinitis pigmentosa 3: homology with the guanine-nucleotide-exchange factor RCC1. Hum. Mol. Genet. 1996; 5: 1035-1041.

[12] Renault L, Nassar N, Vetter I, Becker J, Klebe C, Roth M, Wittinghofer A. The 1.7 A crystal structure of the regulator of chromosome condensation (RCC1) reveals a seven-bladed propeller. Nature 1998; 392: 97-101.

[13] Kirschner R, Erturk D, Zeitz C, Sahin S, Ramser J, Cremers FP, Ropers HH, Berger W. DNA sequence comparison of human and mouse retinitis pigmentosa GTPase regulator (RPGR) identifies tissue-specific exons and putative regulatory elements. Hum. Genet. 2001; 109: 271-278.

[14] Yan D, Swain PK, Breuer D, Tucker RM, Wu W, Fujita R, Rehemtulla A, Burke D, Swaroop A. Biochemical characterization and subcellular localization of the mouse retinitis pigmentosa GTPase regulator (mRpgr). J. Biol. Chem. 1998; 273: 19656-19663.

[15] Neidhardt J, Glaus E, Barthelmes D, Zeitz C, Fleischhauer J, Berger W. Identification and characterization of a novel RPGR isoform in human retina. Hum. Mutat. 2007; 28: 797-807.

[16] Kirschner R, Rosenberg T, Schultz-Heienbrok R, Lenzner S, Feil S, Roepman R, Cremers FP, Ropers HH, Berger W. RPGR transcription studies in mouse and human tissues reveal a retina-specific isoform that is disrupted in a patient with X-linked retinitis pigmentosa. Hum. Mol. Genet. 1999; 8: 1571-1578.

[17] Hong DH, Pawlyk BS, Shang J, Sandberg MA, Berson EL, Li T. A retinitis pigmentosa GTPase regulator (RPGR)-deficient mouse model for X-linked retinitis pigmentosa (RP3). Proc Natl Acad Sci U. S. A 2000; 97: 3649-3654.

[18] Hong DH, Pawlyk B, Sokolov M, Strissel KJ, Yang J, Tulloch B, Wright AF, Arshavsky VY, Li T. RPGR isoforms in photoreceptor connecting cilia and the transitional zone of motile cilia. Invest Ophthalmol. Vis. Sci 2003; 44: 2413-2421.

[19] Hong DH, Yue G, Adamian M, Li T. Retinitis pigmentosa GTPase regulator (RPGRr)-interacting protein is stably associated with the photoreceptor ciliary axoneme and anchors RPGR to the connecting cilium. J. Biol. Chem. 2001; 276: 12091-12099.

[20] Mavlyutov TA, Zhao H, Ferreira PA. Species-specific subcellular localization of RPGR and RPGRIP1 isoforms: implications for the phenotypic variability of congenital retinopathies among species. Hum. Mol. Genet. 2002; 11: 1899-1907.

[21] Otto EA, Loeys B, Khanna H, Hellemans J, Sudbrak R, Fan S, Muerb U, O'toole JF, Helou J, Attanasio M, Utsch B, Sayer JA, Lillo C, Jimeno D, Coucke P, De Paepe A, Reinhardt R, Klages S, Tsuda M, Kawakami I, Kusakabe T, Omran H, Imm A, Tippens M, Raymond PA, Hill J, Beales P, He S, Kispert A, Margolis B, Williams DS, Swaroop A, Hildebrandt F. Nephrocystin-5, a ciliary IQ domain protein, is mutated in Senior-Loken syndrome and interacts with RPGR and calmodulin. Nat. Genet. 2005; 37: 282-288.

[22] Khanna H, Hurd TW, Lillo C, Shu X, Parapuram SK, He S, Akimoto M, Wright AF, Margolis B, Williams DS, Swaroop A. RPGR-ORF15, Which Is Mutated in Retinitis Pigmentosa, Associates with SMC1, SMC3, and Microtubule Transport Proteins. J. Biol. Chem. 2005; 280: 33580-33587.

[23] Chang B, Khanna H, Hawes N, Jimeno D, He S, Lillo C, Parapuram SK, Cheng H, Scott A, Hurd RE, Sayer JA, Otto EA, Attanasio M, O'toole JF, Jin G, Shou C, Hildebrandt F, Williams DS, Heckenlively JR, Swaroop A. In-frame deletion in a novel centrosomal/ciliary protein CEP290/NPHP6 perturbs its interaction with RPGR and results in early-onset retinal degeneration in the rd16 mouse. Hum. Mol. Genet. 2006; 15: 1847-1857.

[24] He S, Parapuram SK, Hurd TW, Behnam B, Margolis B, Swaroop A, Khanna H. Retinitis Pigmentosa GTPase Regulator (RPGR) protein isoforms in mammalian retina: Insights into X-linked Retinitis Pigmentosa and associated ciliopathies. Vision Research 2008; 48: 366-376.

[25] Rosenbaum JL, Witman GB. Intraflagellar transport. Nat Rev Mol Cell Biol 2002; 3: 813-825.

[26] Scholey JM. Intraflagellar transport. Annu. Rev Cell Dev. Biol 2003; 19: 423-443.

[27] Demirci FY, Gupta N, Radak AL, Rigatti BW, Mah TS, Milam AH, Gorin MB. Histopathologic study of X-linked cone-rod dystrophy (CORDX1) caused by a mutation in the RPGR exon ORF15. Am J Ophthalmol. 2005; 139: 386-388.

[28] Ebenezer ND, Michaelides M, Jenkins SA, Audo I, Webster AR, Cheetham ME, Stockman A, Maher ER, Ainsworth JR, Yates JR, Bradshaw K, Holder GE, Moore AT, Hardcastle AJ. Identification of novel RPGR ORF15 mutations in X-linked progressive cone-rod dystrophy (XLCORD) families. Invest Ophthalmol Vis. Sci 2005; 46: 1891-1898.

[29] Yang Z, Peachey NS, Moshfeghi DM, Thirumalaichary S, Chorich L, Shugart YY, Fan K, Zhang K. Mutations in the RPGR gene cause X-linked cone dystrophy. Hum. Mol. Genet. 2002; 11: 605-611.

[30] Ayyagari R, Demirci FY, Liu J, Bingham EL, Stringham H, Kakuk LE, Boehnke M, Gorin MB, Richards JE, Sieving PA. X-linked recessive atrophic macular degeneration from RPGR mutation. Genomics 2002; 80: 166-171.

[31] Demirci FY, Rigatti BW, Mah TS, Gorin MB. A Novel RPGR Exon ORF15 Mutation in a Family With X-linked Retinitis Pigmentosa and Coats'-like Exudative Vasculopathy. American Journal of Ophthalmology 2006; 141: 208-210.

[32] Vervoort R, Lennon A, Bird AC, Tulloch B, Axton R, Miano MG, Meindl A, Meitinger T, Ciccodicola A, Wright AF. Mutational hot spot within a new RPGR exon in X-linked retinitis pigmentosa. Nat. Genet. 2000; 25: 462-466.

[33] Zito I, Downes SM, Patel RJ, Cheetham ME, Ebenezer ND, Jenkins SA, Bhattacharya SS, Webster AR, Holder GE, Bird AC, Bamiou DE, Hardcastle AJ. RPGR mutation associated with retinitis pigmentosa, impaired hearing, and sinorespiratory infections. J. Med. Genet. 2003; 40: 609-615.

[34] Iannaccone A, Wang X, Jablonski MM, Kuo SF, Baldi A, Cosgrove D, Morton CC, Swaroop A. Increasing evidence for syndromic phenotypes associated with RPGR mutations. Am. J. Ophthalmol. 2004; 137: 785-786.

[35] Gravesande KS, Omran H. Primary ciliary dyskinesia: Clinical presentation, diagnosis and genetics. Ann. Med 2005; 37: 439-449.

[36] Moore A, Escudier E, Roger G, Tamalet A, Pelosse B, Marlin S, Clement A, Geremek M, Delaisi B, Bridoux AM, Coste A, Witt M, Duriez B, Amselem S. RPGR is mutated in patients with a complex X linked phenotype combining

primary ciliary dyskinesia and retinitis pigmentosa. J Med Genet 2006; 43: 326-333.

[37] Morillas HN, Zariwala M, Knowles MR. Genetic Causes of Bronchiectasis: Primary Ciliary Dyskinesia. Respiration 2007; 74: 252-263.

[38] Hunter DG, Fishman GA, Kretzer FL. Abnormal axonemes in X-linked retinitis pigmentosa. Arch Ophthalmol 1988; 106: 362-368.

[39] Schedl A, Larin Z, Montoliu L, Thies E, Kelsey G, Lehrach H, Schutz G. A method for the generation of YAC transgenic mice by pronuclear microinjection. Nucleic Acids Res. 1993; 21: 4783-4787.

[40] Pittler SJ, Baehr W. Identification of a nonsense mutation in the rod photoreceptor cGMP phosphodiesterase beta-subunit gene of the rd mouse. Proc Natl Acad Sci U. S. A 1991; 88: 8322-8326.

[41] Bowes C, Li T, Frankel WN, Danciger M, Coffin JM, Applebury ML, Farber DB. Localization of a retroviral element within the rd gene coding for the beta subunit of cGMP phosphodiesterase. Proc Natl Acad Sci U. S. A 1993; 90: 2955-2959.

[42] Gimenez E, Montoliu L. A simple polymerase chain reaction assay for genotyping the retinal degeneration mutation (Pdeb(rd1)) in FVB/N-derived transgenic mice. Lab Anim 2001; 35: 153-156.

[43] Roepman R, Bernoud-Hubac N, Schick DE, Maugeri A, Berger W, Ropers HH, Cremers FP, Ferreira PA. The retinitis pigmentosa GTPase regulator (RPGR) interacts with novel transport-like proteins in the outer segments of rod photoreceptors. Hum. Mol. Genet. 2000; 9: 2095-2105.

[44] Eddy EM, Toshimori K, O'Brien DA. Fibrous sheath of mammalian spermatozoa. Microsc. Res. Tech. 2003; 61: 103-115.

[45] FAWCETT DW. The mammalian spermatozoon. Developmental Biology 1975; 44: 394-436.

[46] Lovett ST. Encoded errors: mutations and rearrangements mediated by misalignment at repetitive DNA sequences. Molecular Microbiology 2004; 52: 1243-1253.

[47] Knotts S, Rindt H, Robbins J. Position independent expression and developmental regulation is directed by the beta myosin heavy chain gene's 5' upstream region in transgenic mice. Nucleic Acids Res. 1995; 23: 3301-3309.

[48] Chemes HE, Olmedo SB, Carrere C, Oses R, Carizza C, Leisner M, Blaquier J. Ultrastructural pathology of the sperm flagellum: association between flagellar pathology and fertility prognosis in severely asthenozoospermic men. Hum. Reprod. 1998; 13: 2521-2526.

[49] Escalier D. New Insights into the Assembly of the Periaxonemal Structures in Mammalian Spermatozoa. Biol Reprod 2003; 69: 373-378.

[50] Miki K, Willis WD, Brown PR, Goulding EH, Fulcher KD, EDDY EM. Targeted Disruption of the Akap4 Gene Causes Defects in Sperm Flagellum and Motility. Developmental Biology 2002; 248: 331-342.

[51] Emery BR, Thorp C, Malo JW, Carrell DT. Pregnancy from intracytoplasmic sperm injection of a sperm head and detached tail. Fertil. Steril. 2004; 81: 686-688.

[52] Kozminski KG, Johnson KA, Forscher P, Rosenbaum JL. A Motility in the Eukaryotic Flagellum Unrelated to Flagellar Beating. PNAS 1993; 90: 5519-5523.

[53] Pazour GJ, Baker SA, Deane JA, Cole DG, Dickert BL, Rosenbaum JL, Witman GB, Besharse JC. The intraflagellar transport protein, IFT88, is essential for vertebrate photoreceptor assembly and maintenance. J Cell Biol. 2002; 157: 103-113.

[54] Kierszenbaum AL. Intramanchette transport (IMT): managing the making of the spermatid head, centrosome, and tail. Mol. Reprod. Dev. 2002; 63: 1-4.

[55] Baker SA, Freeman K, Luby-Phelps K, Pazour GJ, Besharse JC. IFT20 Links Kinesin II with a Mammalian Intraflagellar Transport Complex That Is Conserved in Motile Flagella and Sensory Cilia. J. Biol. Chem. 2003; 278: 34211-34218.

[56] Taulman PD, Haycraft C, Balkovetz DF, Yoder BK. Polaris, a Protein Involved in Left-Right Axis Patterning, Localizes to Basal Bodies and Cilia. Mol. Biol. Cell 2001; 12: 589-599.

[57] Fliegauf M, Benzing T, Omran H. When cilia go bad: cilia defects and ciliopathies. Nat Rev Mol Cell Biol 2007; 8: 880-893.

[58] Nishimura DY, Fath M, Mullins RF, Searby C, Andrews M, Davis R, Andorf JL, Mykytyn K, Swiderski RE, Yang B, Carmi R, Stone EM, Sheffield VC. Bbs2-null mice have neurosensory deficits, a defect in social dominance, and retinopathy associated with mislocalization of rhodopsin. Proc Natl Acad Sci U. S. A 2004; 101: 16588-16593.

[59] Mykytyn K, Mullins RF, Andrews M, Chiang AP, Swiderski RE, Yang B, Braun T, Casavant T, Stone EM, Sheffield VC. Bardet-Biedl syndrome type 4 (BBS4)-null mice implicate Bbs4 in flagella formation but not global cilia assembly. Proc Natl Acad Sci U. S. A 2004; 101: 8664-8669.

[60] Fath MA, Mullins RF, Searby C, Nishimura DY, Wei J, Rahmouni K, Davis RE, Tayeh MK, Andrews M, Yang B, Sigmund CD, Stone EM, Sheffield VC. Mkks-null mice have a phenotype resembling Bardet-Biedl syndrome. Hum. Mol. Genet. 2005; 14: 1109-1118.

[61] Davis RE, Swiderski RE, Rahmouni K, Nishimura DY, Mullins RF, Agassandian K, Philp AR, Searby CC, Andrews MP, Thompson S, Berry CJ, Thedens DR, Yang B, Weiss RM, Cassell MD, Stone EM, Sheffield VC. A knockin mouse model of the Bardet Biedl syndrome 1 M390R mutation has cilia defects, ventriculomegaly, retinopathy, and obesity. Proc Natl Acad Sci U. S. A 2007.

[62] Lee L, Campagna DR, Pinkus JL, Mulhern H, Wyatt TA, Sisson JH, Pavlik JA, Pinkus GS, Fleming MD. Primary ciliary dyskinesia in mice lacking the novel ciliary protein Pcdp1. Mol. Cell. Biol. 2007; MCB.

[63] Nachury MV, Loktev AV, Zhang Q, Westlake CJ, Peranen J, Merdes A, Slusarski DC, Scheller RH, Bazan JF, Sheffield VC, Jackson PK. A Core Complex of BBS Proteins Cooperates with the GTPase Rab8 to Promote Ciliary Membrane Biogenesis. Cell 2007; 129: 1201-1213.

[64] Blacque OE, Reardon MJ, Li C, McCarthy J, Mahjoub MR, Ansley SJ, Badano JL, Mah AK, Beales PL, Davidson WS, Johnsen RC, Audeh M, Plasterk RH, Baillie DL, Katsanis N, Quarmby LM, Wicks SR, Leroux MR. Loss of C. elegans BBS-7 and BBS-8 protein function results in cilia defects and compromised intraflagellar transport. Genes Dev. 2004; 18: 1630-1642.

[65] Leroux MR. Taking Vesicular Transport to the Cilium. Cell 2007; 129: 1041-1043.

[66] Kim JC, Badano JL, Sibold S, Esmail MA, Hill J, Hoskins BE, Leitch CC, Venner K, Ansley SJ, Ross AJ, Leroux MR, Katsanis N, Beales PL. The Bardet-Biedl protein BBS4 targets cargo to the pericentriolar region and is required for microtubule anchoring and cell cycle progression. Nat Genet 2004; 36: 462-470.

[67] Ansley SJ, Badano JL, Blacque OE, Hill J, Hoskins BE, Leitch CC, Chul Kim J, Ross AJ, Eichers ER, Teslovich TM, Mah AK, Johnsen RC, Cavender JC, Alan Lewis R, Leroux MR, Beales PL, Katsanis N. Basal body dysfunction is a likely cause of pleiotropic Bardet-Biedl syndrome. Nature 2003; 425: 628-633.

[68] Kim JC, Ou YY, Badano JL, Esmail MA, Leitch CC, Fiedrich E, Beales PL, Archibald JM, Katsanis N, Rattner JB, Leroux MR. MKKS/BBS6, a divergent chaperonin-like protein linked to the obesity disorder Bardet-Biedl syndrome, is a novel centrosomal component required for cytokinesis. J Cell Sci 2005; 118: 1007-1020.

[69] Li JB, Gerdes JM, Haycraft C, Fan Y, Teslovich TM, May-Simera H, Li H, Blacque OE, Li L, Leitch CC, Lewis RA, Green JS, Parfrey PS, Leroux MR, Davidson WS, Beales PL, Guay-Woodford LM, Yoder BK, Stormo GD, Katsanis N, Dutcher SK. Comparative Genomics Identifies a Flagellar and Basal Body Proteome that Includes the BBS5 Human Disease Gene. Cell 2004; 117: 541-552.

3.2.8 Appendix: Electroretinography (ERG) and Histology of the Retina of *Rpgr* transgenic mice

Introduction

Mutations in *RPGR* are well known to lead to retinal dystrophies like Retinitis pigmentosa, cone-rod dystrophy, cone dystrophy, Coats'-like exsudative vitreoretinopathy and atrophic macular degeneration [1-7]. Accordingly, animal models for RPGR-related diseases also develop mild to severe retinal dystrophy [8-11]. Therefore, retinal function of transgenic mice with various copy numbers of *Rpgr* (Tg2, Tg8 and Tg13) was assessed by ERG. In addition, retinal morphology of several transgenic animals (Tg4, Tg5, Tg8, Tg11 and Tg13) was examined. These data were then correlated to the level of transgenic expression of *Rpgr*.

Materials and Methods

ERG measurements were performed in collaboration with the Eye Clinic Tuebingen, Germany (N. Tanimoto und M.Seeliger) [12]. ERG recordings were taken for both eyes under scotopic and photopic conditions, thereby assessing rod as well as cone photoreceptor responses. Single flash recordings and flicker responses were measured. Histological studies on plastic sections were performed as described in the Materials and Methods of the main manuscript. They were performed in collaboration with the Eye Clinic Zuerich, Switzerland (C.Imsand, C.Grimm). Expression studies on transcript and protein levels were carried out as described for the experiments on testis.

Results

Single ERG traces of scotopic and photopic conditions (flash and flicker, respectively) displayed standard responses of both rod and cone photoreceptor systems in the transgenic animals that were examined (Figure 1). Of note, photopic flash responses in Tg13 were slightly different as a late cornea-positive peak (c-wave) appears to be elicited earlier and/or at higher intensities in this mouse.

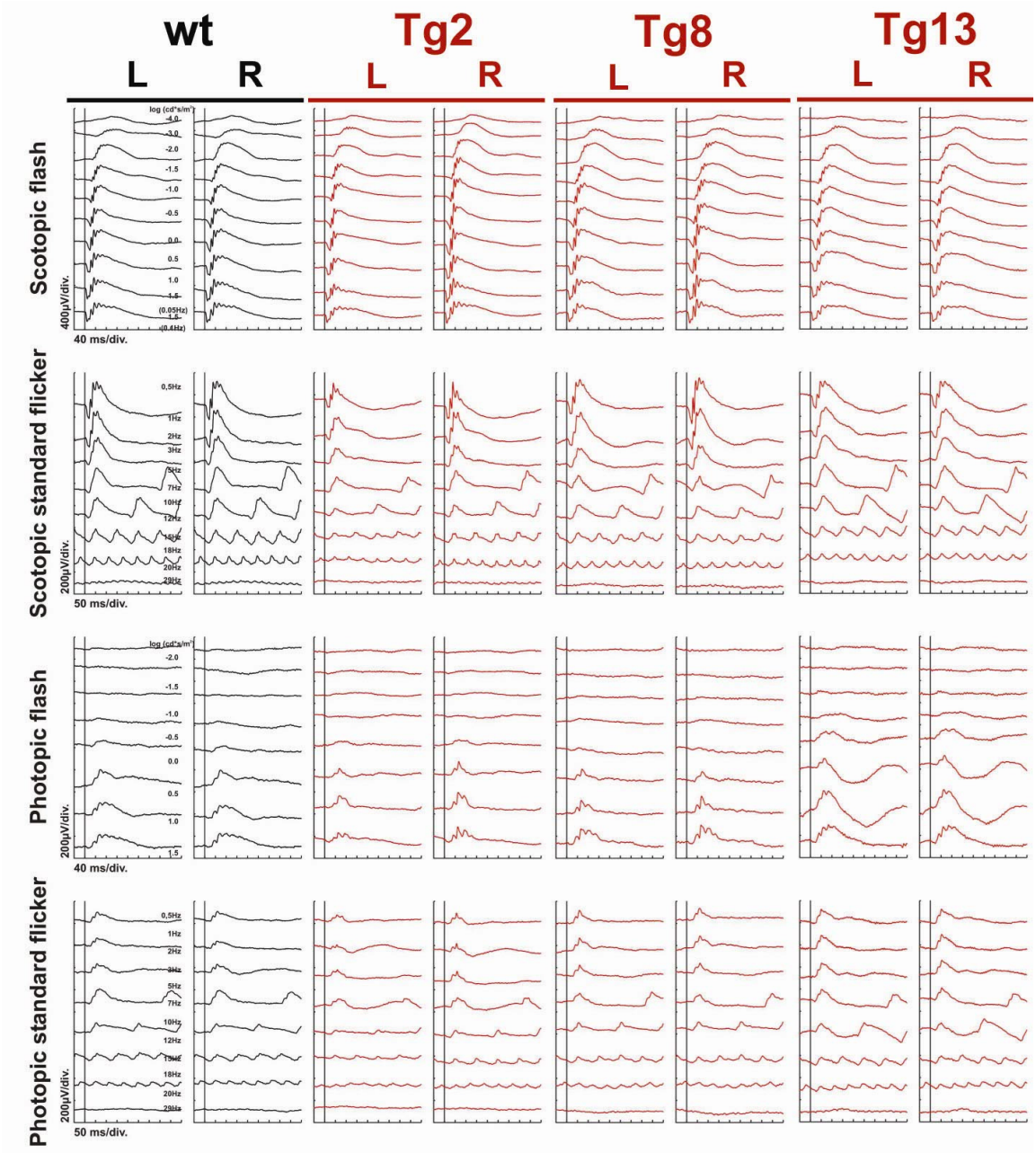

Figure 1: Single ERG traces of transgenic animals and a wild type littermate control

Scotopic and photopic responses were recorded under flash and standard flicker light conditions. Flash intensities were -4 – 1.5 log cds/m^2. Flicker stimuli reached from 0.5 – 29 Hz. The single ERG traces of the transgenic animals were comparable to the wild type littermate control. Some alterations in photopic flash responses at higher intensities were visible in animal Tg13.

Comparison of the rod and cone b-wave responses of the pooled transgenic and the wild type data indicated that there might be slight differences in the rod flicker amplitude and the cone responses of the second order neurons (Figure 2).

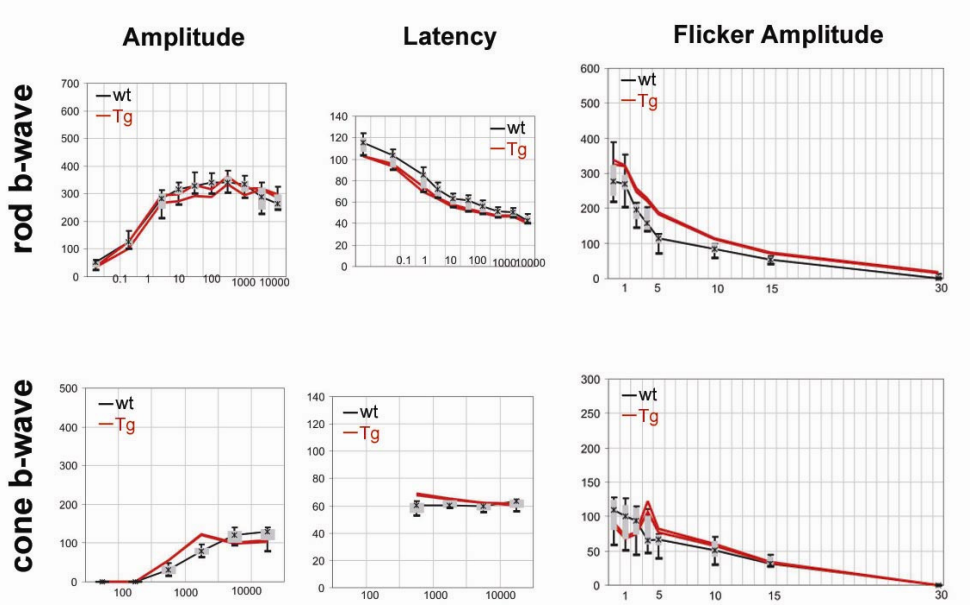

Figure 2: Mean rod and cone ERG responses and latencies of transgenic animals

The scotopic and photopic ERG b-wave amplitudes of all three transgenic animals and the wild type controls were pooled. The amplitude in [mV] was plotted against the flash intensity in [mcds]. The median (black cross), the 75% and 25% percentile (grey box) and the minima and maxima values (whiskers) are shown in the graph. Responses from transgenic animals were similar to wild type responses. Some variation at the rod flicker response and the cone b-wave amplitude are present.

For further evaluation of a putative retinal phenotype histological analyses were performed. Transgenic animals with various copy numbers of *Rpgr* revealed no obvious disarrangements or defects in retinal structure (Figure 3). All retinal layers were properly organized. This result corresponds to the findings of ERG measurements.

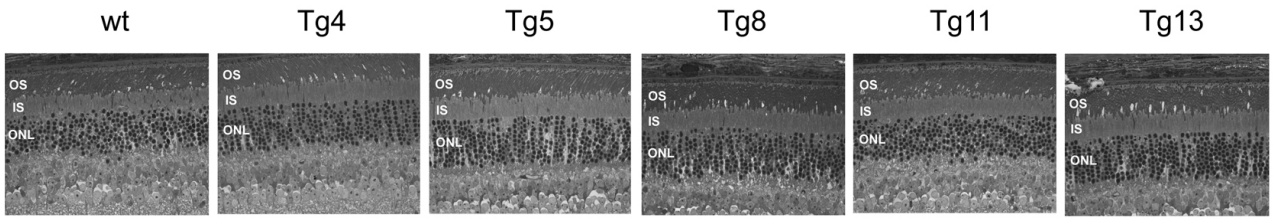

Figure 3: Histological analysis of retinae of transgenic animals

Retinae of a wild type control and transgenic animals of 12 months of age carrying 4, 5, 8, 11 and 13 copies of *Rpgr*, respectively, were investigated on semithin plastic sections. No obvious differences in retinal structure could be observed in all transgenic animals examined.

In order to confirm the phenotypical results gained by ERG and histological analyses, expression studies on transcript and protein levels were performed. Results of these

studies are preliminary as the data reflect one experiment. According to these experiments *Rpgr* transcript levels containing exons 1 and 2 were slightly elevated (5-7fold, Figure 4A). Similarly, intensity of immunoreactive bands migrating at 100 kDa and at >170 kDa that were detected with Ab5.1 was elevated (Figure 4B). Therefore, these bands might be specific to RPGR. In addition, the bands at about 100 kDa could be blocked (Figure. 2, main manuscript). The observed molecular size would correspond to the $RPGR_{1-19}$ and the ORF14/15 isoform, respectively. Semi-quantitative analysis of the 100 kDa band indicated that the amount of the protein was about 9-18times increased compared to the wild type band (Figure 4C).

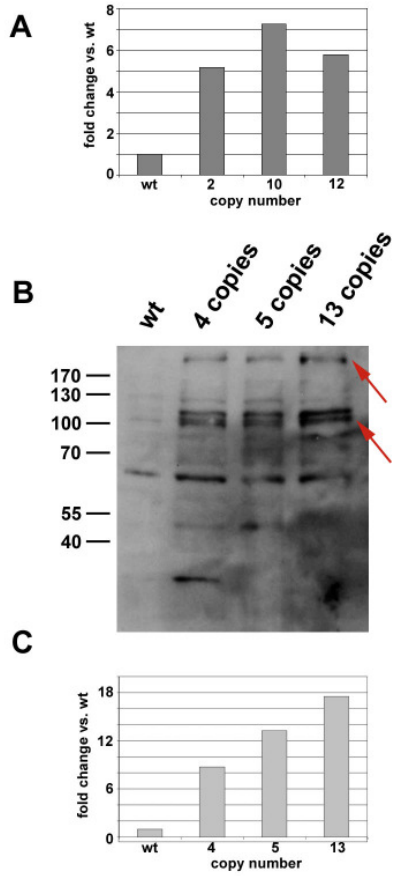

Figure 4: Expression levels of RPGR transgene in retina

A) Transgenic *Rpgr* transcript levels were assessed by qRT-PCR and normalized to wild type expression level. Transgenic animals with 2, 10 and 12 copies indicated to express slightly elevated levels of *Rpgr*.

B) Western blot of RPGR protein expression with Ab5.1 in wild type and transgenic animals carrying 4, 5 and 13 copies of the transgene (1217/Tg4, 1217/Tg5 and 1217/Tg13). Two immunoreactive bands at 100 kDa and >170 kDa showed higher intensity in retinae of transgenic animals. The band at 60 kDa was judged as unspecific as it could not be blocked (Figure 2, main manuscript). The bands at 50 kDa and 30 kDa might be degradation products.

C) Relative expression of the band at 100 kDa in transgenic animals compared to wild type protein level observed in the blot of panel B). Transgenic animals displayed approximately 9-18fold increased intensity depending on the genotype.

In summary, investigations on a putative retinal phenotype of mice with different copy numbers of *Rpgr* indicated that overexpression of might have no or only marginal effects on retinal function.

Discussion

The apparent lack of an obvious retinal phenotype in transgenic animals is in contrast to the severe phenotype found in their sperm flagella. Interestingly, another *Rpgr* overexpressing mouse model has been reported [9]. This model carries a cDNA

transgene and expresses the $RPGR_{1-19}$ variant in several fold higher level as compared to wild type. Histological evaluation of the retina revealed normal development followed by severe retinal degeneration. In addition, cone opsin was found to be mislocalized in young animals (P20 – 1.5 months). In contrast, the *Rpgr* overexpressing mouse model described herein carries a PAC transgene including the entire genomic region of *Rpgr* (gDNA) including flanking regulatory elements. Hence, the gDNA-based transgene is subjected to endogenous alternative splicing in contrast to the cDNA-based transcript of the *Rpgr* transgenic mouse line by Hong and Wright. The differences in phenotypical manifestations concerning the retina might therefore be explained by tissue-specific alternative splicing events of the *Rpgr* transcripts deriving from the PAC. Expression in the cDNA transgenic mouse was driven by a chicken beta-actin promoter resulting in ectopic expression. In contrast, the expression of the *Rpgr* PAC transgene was regulated by its endogenous promoter. Therefore, the transgene is expected to be expressed in a similar tissue-specific manner than the endogenous gene. Although preliminary expression analysis indicated slightly elevated transcript and protein levels, the amount of upregulated isoforms seems not to be sufficient to cause dysfunction in photoreceptor cells. The immunoreactive band at 100 kDa that might correspond to the $RPGR_{1-19}$ isoform, was expressed at higher amounts which might create a similar situation as in the cDNA transgenic line with overexpression of RPGR. The immunoreactive band at <170 kDa might reflect higher expression of the ORF14/15 variant. Nevertheless, these results are very preliminary and limited in their significance. Further experiments should be performed to exactly determine *Rpgr* expression and to evaluate putative defects in photoreceptors, e.g. localization of visual pigments

References

1. Demirci FY, Rigatti BW, Wen G, et al. X-linked cone-rod dystrophy (locus COD1): identification of mutations in RPGR exon ORF15. *Am J Hum Genet*. 2002;70:1049-1053.

2. Roepman R, van Duijnhoven G, Rosenberg T, et al. Positional cloning of the gene for X-linked retinitis pigmentosa 3: homology with the guanine-nucleotide-exchange factor RCC1. *Hum Mol Genet*. 1996;5:1035-1041.

3. Iannaccone A, Breuer DK, Wang XF, et al. Clinical and immunohistochemical evidence for an X linked retinitis pigmentosa syndrome with recurrent infections and hearing loss in association with an RPGR mutation. *J Med Genet*. 2003;40:e118.

4. Meindl A, Dry K, Herrmann K, et al. A gene (RPGR) with homology to the RCC1 guanine nucleotide exchange factor is mutated in X-linked retinitis pigmentosa (RP3). *Nat Genet*. 1996;13:35-42.

5. Moore A, Escudier E, Roger G, et al. RPGR is mutated in patients with a complex X-linked phenotype combining primary ciliary dyskinesia and retinitis pigmentosa. *J Med Genet*. 2005:jmg.

6. Yang Z, Peachey NS, Moshfeghi DM, et al. Mutations in the RPGR gene cause X-linked cone dystrophy. *Hum Mol Genet*. 2002;11:605-611.

7. Zito I, Downes SM, Patel RJ, et al. RPGR mutation associated with retinitis pigmentosa, impaired hearing, and sinorespiratory infections. *J Med Genet*. 2003;40:609-615.

8. Beltran WA, Hammond P, Acland GM, Aguirre GD. A frameshift mutation in RPGR exon ORF15 causes photoreceptor degeneration and inner retina remodeling in a model of X-linked retinitis pigmentosa. *Invest Ophthalmol Vis Sci*. 2006;47:1669-1681.

9. Hong D, Wright R. Overexpression of RPGR Default Variant Leads to Retinal Degeneration. *ARVO Meeting Abstracts*. 2008;49:2201.

10. Hong DH, Pawlyk BS, Adamian M, Li T. Dominant, gain-of-function mutant produced by truncation of RPGR. *Invest Ophthalmol Vis Sci*. 2004;45:36-41.

11. Hong DH, Pawlyk BS, Shang J, Sandberg MA, Berson EL, Li T. A retinitis pigmentosa GTPase regulator (RPGR)-deficient mouse model for X-linked retinitis pigmentosa (RP3). *Proc Natl Acad Sci U S A*. 2000;97:3649-3654.

12. Seeliger MW, Grimm C, Stahlberg F, et al. New views on RPE65 deficiency: the rod system is the source of vision in a mouse model of Leber congenital amaurosis. *Nat Genet*. 2001;29:70-74.

3.2.9 Contributions of authors to the manuscript “Overexpression of Rpgr Leads to Male Infertility in Mice due to Defects in Flagellar Assembly”

S.B.: generation of antibodies, Western blots (WB), electronmicroscopic (EM) micrographs, initiation of collaboration with A.T., interpretation of data, writing of the manuscript

D.C.: animal breeding, preparation of animals, HE histology, determination of copy numbers, transcript analyses (quantitative RT-PCR)

A.T.: evaluation and reproduction of antibody staining on testis sections, analysis of the EM micrographs, interpretation of data, writing and editing of the paper

U.L.: qRT-PCR experiments (Taqman), analysis of data, writing and editing of the manuscript

W.S.: pronucleus injection of PAC transgene into oocytes

S.F.: technical assistance in Southern Blot, genotyping of mice,

C.I.: preparation and cutting of epon sections, EM microscopy

Ja.Ne..: technical assistance in staining of testicular sections with antibodies

C.G.: analysis of EM micrographs

T.R.: *in-vitro* fertilization approach

R.F.: planning and supervision of generation of transgenic mice by pronucleus injection

Jo.Ne.: conceptual input, supervision of experiments, analysis of data, writing and editing of the manuscript

W.B.: P.I., conceptual planning, design and supervision of the entire study, interpretation of data, writing and editing of the manuscript

Appendix:

N.T.: performance and analysis of ERG measurements

M.S.: supervision and analysis of ERG measurements

3.3 Cone versus rod disease in two mouse strains with a knock-in mutation in the retinitis pigmentosa GTPase regulator (*Rpgr) gene*

Sandra Brunner[1], Sergej Skosyrski[2], Renate Kirschner-Schwabe[3], Klaus-Peter Knobeloch[4,5,] John Neidhardt[1], Silke Feil[1], Ulrich F.O. Luhmann[6], Klaus Rüther[2] and Wolfgang Berger[1*]

[1] Division of Medical Molecular Genetics and Gene Diagnostics, Institute for Medical Genetics, University of Zurich, CH-8603 Schwerzenbach, Switzerland; [2] Department of Ophthalmology, Charité Campus Virchow Clinic, University Medical Center, Berlin, Germany; [3] Department of Pediatric Oncology/Hematology, Charité - Universitätsmedizin Berlin, Germany; [4] Leibniz Institute for Molecular Pharmacology, Berlin, Germany; [5] *present address*: Institute of Pathology, University of Freiburg, Freiburg, Germany, [6]Division of Molecular Therapy, UCL Institute of Ophthalmology, London, United Kingdom

Manuscript submitted, Investigative Ophthalomolgy and Visual Science, 2008

3.3.1 Abstract

Purpose: To establish mouse models for *RPGR*-associated diseases by generating and characterizing an *Rpgr* knock-in mutation in two different genetic backgrounds (BL/6 and BALB/c).

Methods. Gene targeting in embryonic stem (ES) cells was performed to introduce a knock-in mutation in the *Rpgr* gene (in-frame deletion of exon 4, $Rpgr^{\Delta Ex4}$). Subsequently, the mutation was introduced in two different inbred mouse strains by successive breeding. Mutant and wild type mice of both strains were characterized by electroretinography (ERG) and histology at five time points (1, 3, 6, 9 and 12 months). RPGR transcript and protein expression was assessed by RT-PCR and Western Blot analyses. A variety of photoreceptor proteins, including RPGR-ORF15, RPGRIP1, PDE6δ/PrBPδ, rhodopsin and cone opsin were localized on retinal sections by immunohistochemistry.

Results. Mislocalization of rhodopsin and cone opsin was an early pathologic event in mutant mice of both lines. In contrast, RPGR-ORF15 as well as RPGRIP1 and PDE6δ/PrBPδ showed similar localizations in mutant and wild type animals. Functional and histological studies revealed a mild rod-dominated phenotype in mutant male mice on the BL/6 background while a cone-dominated phenotype was observed for the same mutation in the BALB/c background.

Conclusions. Both *Rpgr* mutant mouse lines developed retinal disease with a striking effect of the genetic background. The two lines provide models to study RPGR function in rods and cones, respectively. Mislocalization of visual pigments further supports the role of RPGR in ciliary transport in rod and cone photoreceptors.

3.3.2 Introduction

Degeneration of initially rod and later of cone photoreceptor cells is a common hallmark of a clinical and genetic heterogeneous disease termed Retinitis pigmentosa (RP). The X-linked form is the most severe form of RP (XlRP), in terms of onset and progression and predominantly male patients are affected although occasionally carrier females may show a variable expressivity of disease manifestations[1,2]. Mutations in the retinitis pigmentosa GTPase regulator gene (*RPGR*) are the major cause and account for approximately 70% of all XlRP cases[3]. The second major X-linked gene was also identified and designated *RP2*[4]. Expression of *RPGR* transcript isoforms were detected in many tissues including retina, brain, lung, kidney and testis of several species[5]. In humans as well as in mice, *RPGR* was described to consist of 19 constitutively expressed exons and to result in a protein of about 90 kDa ($RPGR_{1-19}$ variant)[6,7]. Exon 19 contains a conserved isoprenylation motif, indicating that this isoform might be post-translationally modified[6]. Several studies reported a high degree of alternative splicing and many novel exons were discovered, some of them being tissue-specific. The retina-abundant RPGR-ORF15 isoform has an alternate C-terminus, which is rich in acidic amino acids[8]. Another novel isoform, RPGR-9a, is predominantly expressed in cone photoreceptors of the human retina[9]. A common feature of most protein isoforms is the N-terminal RCC1-like domain (RLD)[7,10], encoded by exons 2-10. The regulator of chromosome condensation 1 (RCC1) is a guanine nucleotide exchange factor (GEF) for small GTPases and is involved in nuclear export and import pathways[11,12]. However, GEF activity has never been demonstrated for RPGR. The RLD has also been shown to interact with several proteins: the RPGR interacting protein 1 (RPGRIP1), structural maintenance of chromosomes (SMC) 1 and 3 proteins and prenyl-binding protein δ (PrBPδ) formerly known as phosphodiesterase delta subunit (PDE6δ) [13-15]. In addition, several ciliary/basal body as well as intraflagellar transport (IFT) proteins were found to interact with the C-terminus of the $RPGR_{1-19}$ as well as RPGR-ORF15 isoforms [15-18]. Accordingly, these isoforms mainly localize in cilia and basal bodies, suggesting a ciliary function [8,19].
RPGR mutations in the RLD and exon ORF15 account for approximately 32 % and 56 % of XlRP cases, respectively (http://rpgr.hgu.mrc.ac.uk). These pathogenic changes can lead to either classic RP or to cone-rod dystrophy, cone dystrophy and

macular degeneration, indicating that *RPGR* is essential also for cone function [20-22]. The phenotypic variability resulting from mutations in *RPGR* was expanded by patients displaying RP, recurrent sinorespiratory infections and hearing loss [23,24]. In addition, mutations were associated with RP in conjunction with primary ciliary dyskinesia (PCD) [25]. To date, no genotype-phenotype correlation could be assigned. Two recent studies reported on families carrying the same *RPGR* mutation but exhibited discordant phenotypes [26]. These cases indicate the involvement of modifier genes.

We generated a knock-in mouse model with an in-frame deletion of exon 4 of *Rpgr*. This alteration mimics mutations in RP patients that lead to exon 4 skipping [27,28]. In addition, we examined the mutation in two different mouse strains (BL/6 and BALB/c). Both developed retinal disease but displayed either a rod- or a cone-dominated phenotype.

3.3.3 Material and Methods

Animals

All experiments were performed in compliance with the National Institutes of Health guidelines, as approved by the Swiss cantonal veterinary office and the ARVO Statement for the Use of Animals in Ophthalmic and Vision research. Animals were born and maintained in controlled ambient illumination on a 12 hour light/dark cycle. For breeding, male wild type BL/6 animals were purchased from the Jackson Laboratory (Bar Habor, USA). Male wild type BALB/c animals were obtained from the Bundesinstitut für Risikobewertung (Berlin, Germany).

Generation of Rpgr$^{\Delta Ex4}$ mice

For construction of the *Rpgr*$^{\Delta Ex4}$ targeting vector a genomic region of 0.8 kb (Intron 2_F 5' GCTCTAGACCCAAAGAAGGTGATGGTCTACCA 3' to intron 3_R 5' CCGCTCGAGTCATGGATCTCACAGTCTGCAG 3') of the murine *Rpgr* gene was amplified from the 129 mouse strain and cloned into the 5' multiple cloning site of the neomycin cassette of the pTG1-vector (Transgenics, Berlin, Germany). Subsequently, a second genomic region of 5.5 kb of the 129 *Rpgr* gene (Intron 4_F 5' ACGCGTCGACGTGTTTTGTGGAAGCCATAGG 3' to intron 6_R 5' AGCCGTCGACTCACTCTTGTAGCATGCCTTGA 3') was cloned 3' of the neomycin cassette. The correct insertion direction of the fragments was confirmed by sequencing. The vector was linearized with *NotI* and transfected into a male ES cell line of the 129 mouse strain as described elsewhere [29]. Identification of ES clones carrying the recombinant *Rpgr* allele was done by Southern blot analysis using a 5' probe positioned outside of the targeting construct (exon 2_F 5' GCTCTAGACAGGTGCTGTGTTTACGTTTGG 3' to intron 2_R 5' CGTATCTTTCTGTGTTGAAGCAC 3'). The injection of mutant ES cells into BL/6 blastocysts was performed according to standard methods. Two recombinant ES cell lines (C2 and F10) produced chimeric offspring with germline transmission. These were used for establishing two independent mutant mouse lines by crossing to wild type BL/6 mice for at least 8 generations. In addition, the mutation was crossed into the albino BALB/c mouse strain for at least 7 generations. In generation F8 male and female mice heterozygous for the *Rpe65* polymorphism (p.M450L) were crossed to obtain homozygous leucine and methionine offspring.

Genotyping of Rpgr and Rpe65

Genotyping was performed by PCR on DNA isolated from tail biopsies. For *Rpgr*, two different forward primers were used to amplify a wild type specific (Exon 4: 5' GTGAAACTTGCTGCCTGTGGA 3') and a mutant specific product (Neomycin cassette: 5' AGCACGTACTCGGATGGAAG 3'), respectively. A third common reverse primer is located in intron 4 (5' AGCAGTCATCTCCGTTTTAATC 3'). The polymorphism in *Rpe65* was genotyped by sequencing using flanking primers (Rpe65_F 5' TGACAAGGTAATAAAGCATC 3' and Rpe65_R 5' ATTACCATCATCTTCTTCCA 3').

Morphometric analysis on plastic sections

Mice were anesthetized with CO_2 and subsequently killed by cervical dislocation. Eyes were marked at the superior pole, removed and fixed in 2.5% glutaraldehyde in 0.1 M cacodylate buffer (pH 7.3) at 4°C overnight. Eyes were bisectioned at the optic nerve head into a superior and an inferior part, washed in cacodylate buffer, post-stained in osmium tetroxide for 1h, dehydrated, and embedded in Epon 812 (SigmaAldrich, Buchs, Switzerland). Tissue sections of 0.5 µm were stained with toluidine blue and analyzed under a Zeiss microscope (Carl Zeiss AG, Feldbach, Switzerland).

For morphometric analysis of wild type and mutant mice of both strains, sections from the inferior central retina containing the optic nerve head and the ora serrata on both sides were chosen for retinal measurements. For each eye, three sections were examined. Four areas were chosen from each section (periphery temporal, center temporal, center nasal and periphery nasal). The central areas were defined being located 15° deg temporally and nasally from the optic nerve head (0° deg), the temporal region was chosen 30° deg from the ora serrata of each side. Measurements of the thickness of the outer nuclear layer (ONL) and the length of the rod inner and outer segment (RIS and ROS) were performed, each in triplicate. Additionally, the number of nuclei in the ONL was counted in an area of 100 μm^2. The mean value of ROS, RIS and ONL thickness and mean number of nuclei in the ONL for each area was calculated ($2 \geq n \geq 5$ per genotype). For quantification of cones, cone nuclei were counted in the whole area of one picture taken at 40x magnification. Statistical analysis was done using 95% confidence interval or Student's t-test.

Electroretinography (ERG)

ERG methodology has been described previously[30]. Mice were dark adapted (> 2h), pupils were dilated by tropicamide 0.5% and atropine 1% and mice were anesthetized by injection of xylazine [15 mg/kg body weight] and ketamine [100 mg/kg]. The recording electrode was a monopolar contact lens electrode and a subcutaneously fixed silver needle the reference and ground electrode. For recording the mouse was placed into a commercially available Ganzfeld bowl (Toennies Multiliner Vision, Höchberg, Germany), the examined eye facing the back of the globe. The signal was amplified by 10,000 with a bandpass filter including the range of 1 to 300 Hz. Oscillatory potentials were obtained by band-pass filtering from 100 to 300 Hz.

In the dark-adapted state, a flash series consisting of 8 steps started at –4.0 log $cdsm^{-2}$ and reached 0.48 log $cdsm^{-2}$. For a-wave recording additional six flash energies were applied ranging from 1.0 to 2.5 log $cdsm^{-2}$. These high intensity stimuli were provided by a photoflash mounted in the Ganzfeld globe. After recording the a-wave the background light (1.5 log cdm^{-2}) was turned on and the photopic ERG was recorded (1.2, 1.4 log $cdsm^{-2}$, average of 10 recordings at 1.5 Hz). Subsequently, the animals were further light adapted for ten minutes and the photopic ERG was recorded again using a series of flash energies (-0.3, 0.7, 1.2, 1.4, 1.7 and 2.0 log $cdsm^{-2}$). The b-wave amplitude was determined from a-wave trough to b-wave peak, behind the last prominent oscillatory potential. For the determination of b-wave amplitudes and implicit times the third oscillatory potential was chosen due to low variability. Statistical analysis was performed using ANOVA for repeated measurements, if applicable. Single recordings were tested by the two-tailed t-test. The critical p-value was set to 0.05.

Generation isoform-specific RPGR antibody

An epitope within the hRPGR-ORF15 protein (HKTYQKKSVTNTQGNGKE) (NCBI – Accession: NP_000319 and NP_ 001030025) was chosen to generate the isoform specific antibody AbC2.1 (Eurogentec, Seraing, Belgium). The antiserum was affinity-purified against the cognate peptide according to manufacturer's instructions (Sulfolink; Pierce Biotechnology, IL, USA). Briefly, the antiserum was incubated on a column with covalently bound peptide for 1 h at room temperature to allow binding to occur. After rinsing with PBS, the antibody bound to the column was eluted from the

column by pH-shift. IgG concentration of affinity purified antibodies was determined using a Nanodrop (ND-3300, Witec AG, Littau, Switzerland).

Western Blot analyses

Whole retinas from wild type and mutant animals were homogenized on ice in 30µl sample buffer per retina (50mM Tris, 150 mM NaCl, 1mM EDTA, 0.2% NP40, Complete Protease Inhibitor (Roche Diagnostics, Mannheim, Germany). The protein homogenate was extracted by fractionation centrifugation (20.000 at 4°C). Protein concentration was determined by a bicinchoninic acid assay (BCA, Sigma-Aldrich, Steinheim, Germany). For Western blots 75 µg – 100 µg of retinal protein extract were boiled in loading buffer (120mM Tris (pH 6.8), 2% w/v SDS, 5% v/v β-mercaptoethanol, 50% v/v glycerol, bromophenolblue), resolved on a 10% SDS-PAGE and blotted on a PVDF membrane (Roche Diagnostics, Mannheim, Germany) by semi-dry blotting (Bio-Rad, Munich, Germany). Membranes were incubated with 1:25 dilution of RPGR C2.1 antibody. Blocking of the antibody was done by adding 50 µg of cognate peptide for 2 hours at room temperature before incubation. Detection of primary antibodies was performed by incubation with anti-rabbit IgG coupled to horseradish peroxidase (1:500, Dianova, Hamburg, Germany). Blots were developed with Western Lightning Chemiluminescence Reagent Plus (Perkin Elmer, Boston, USA) and chemiluminescence detection film (Lumi-Film, Roche Diagnostics, Mannheim, Germany).

I*mmunohistochemistry*

Animals were anesthetized by inhalation of CO_2 or an injection of ketamin-xylacin and subsequently killed by cervical dislocation. Eyes were removed and either directly embedded in O.C.T. (Tissue Tek, Digitana, Horgen, Switzerland) or fixed in 4% PFA in PBS and subsequently cryoprotected by treatment with sucrose in ascending concentrations (10% w/v, 20% w/v and 30% w/v in PBS) at 4°C. Sections of 8-10 µm were cut on a cryostat and air-dried (Leica Microsystems, CM3050S, Glattbrugg, Switzerland). After blocking with 10% normal goat serum (NGS) sections were incubated overnight with primary antibody, washed with PBS and treated with Cy3-labeled anti-rabbit (1:500), Cy3-labeled anti-mouse (1:500) or Alexa488-labeld anti-mouse (1:500) antibody (Dianova, Hamburg, Germany). Primary antibodies against both rhodopsin (1:10.000, RetP1, Sigma, Saint Louis, U.S.), cone opsin

(1:4000, MWL cone opsin, kindly provided by C. Grimm) were applied to fixed eyes of wild type and mutant animals of the *Rpgr*$^{\Delta Ex4}$ BL/6 (n = 4/genotype) and BALB/c (n=2/genotype) strain. An anti-PrBPδ antibody (kindly provided by R. Cote) was used on fixed sections (n=2/genotype) in a 1:200 dilution. For detection of proteins in the connecting cilium unfixed eyes were used as other conditions were found to quench the signal. RPGR AbC2 was used in a 1:25 and RPGRIP1 in a 1:200 dilution (n=2/genotype). As markers for the connecting cilium and the centrosome/basal body, acetylated alpha-tubulin (Sigma, Saint Louis, U.S.) and gamma-tubulin (Abcam, Cambridge, UK) were used (n=2/genotype), respectively. Slides were photographed with a Zeiss microscope equipped with ApoTome Technology and processed in PhotoShop (Adobe, Munich, Germany).

3.3.4 Results

Generation of Rpgr mutant mice in two different genetic backgrounds

We have used gene targeting technology to generate a mouse line with a knock-in mutation in the *Rpgr* gene. In the gene targeting construct, exon 4 was replaced by a neomycin cassette, leading to an in-frame deletion of 63 bp of the *Rpgr* transcript and 21 amino acids of the RPGR protein (Figure 1A). The mutant mouse line was obtained after injection of two independently targeted embryonic stem cell (ES) clones (C2 and F10). The C2 and F10 ES clones were selected after testing for correctly targeted *Rpgr* gene copies (Figure 1B). From both ES cell lines we obtained chimeric animals. Germline transmission was confirmed for both and resulted in viable and fertile hemizygous male mice.

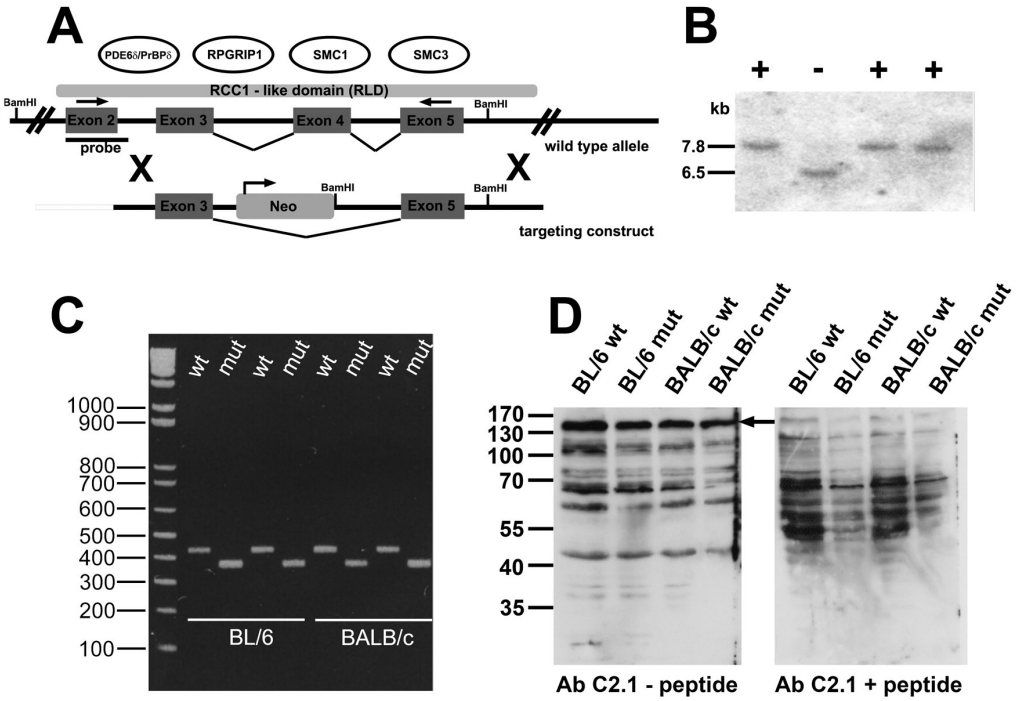

Figure 1: Generation of *Rpgr* knock-in mouse lines

(A) Scheme of wild type allele and targeting construct of the *Rpgr* gene and the four known interactions partners of the RCC1-like domain (RLD). Exon 4, which is located within the RLD, was replaced by a neomycin cassette (Neo) in the construct. This leads to a lack of exon 4 in the transcript of the targeted allele ($Rpgr^{\Delta Ex4}$). Direction of transcription of neomycin is the same as for *Rpgr*. (B). Digestion with BamHI and subsequent Southern blot analysis with a probe depicted in (A) resulted in a fragment of 7.8 kb for wild type (+) and a truncated fragment (6.5 kb) for mutant (-) *Rpgr*. This ES clone (C2) and a second one (F10) were chosen for further injection into blastocysts. (C) RT-PCR on mouse retinal cDNA using forward and reverse primers in exons 2 and 5 (as indicated in (A)). In the mutant animals only transcripts skipping exon 4 and thus showing 63 bp deletion were found. In wild

type animals only correctly spliced product was detected. (D) Western Blot analysis on retinal protein extracts from $^{P\pi\gamma p\Delta Ex4}$ BL/6 and *Rpgr*$^{\Delta Ex4}$ BALB/c wild type and mutant animals using Ab C2.1 directed against the RPGR-ORF15 isoform. Immunoreactive bands were present in both wild type and mutant animals (left panel). Specificity was judged upon blocking with the cognate peptide (right panel). The band at ~140 kDa (arrow) might represent the RPGR-ORF15 isoform.

The mutation was first bred into the pigmented BL/6 strain (C2 and F10 line) for at least 8 generations. Several studies reported on modifier genes influencing retinal degeneration as well as light damage susceptibility in BALB/c mice [31,32]. Thus, we decided to breed the *Rpgr*$^{\Delta Ex4}$ mutation into the albino BALB/c strain (C2 line) for additional 7-8 generations.

Expression of wild type and mutant Rpgr

Deletion of exon 4 in the mutant mice was verified by conventional RT-PCR using forward and reverse primers in exons 2 and 5, respectively. In wild type mice of both backgrounds, the expected band of 430 bp was found (Figure 1C). Mutant animals only showed a lower band corresponding to the deletion of 63 bp of exon 4. The bands were verified by sequencing. The deletion of exon 4 does not alter the reading frame, but would lead to a lack of 21 amino acids in the RLD (Figure 1A).

To show that protein is produced in the mutant animals, an RPGR ORF15-specific antibody (AbC2.1) was applied upon Western Blot analyses. We detected several immunoreactive bands on retinal extracts. One RPGR-ORF15 immunoreactive band at high molecular weight has been described before (~140 kDa) (Figure 1D, arrow)[19]. The ORF15 band was also detected in mutant animals and indicated the presence of RPGR. The signals were blocked with the cognate peptide. All other blocked bands might represent other RPGR isoforms however, specificity could not be determined. As expected, the difference of 21 amino acids between the wild type and the mutant protein isoforms was not resolved under these conditions. These results suggest that RPGR is expressed in wild type and mutant animals.

Assessment of retinal function by electroretinography (ERG)

For assessment of functional consequences of the *Rpgr*$^{\Delta Ex4}$ mutation in the two mouse lines, mutant male mice and their littermates were subjected to ERG measurements.

The *Rpgr*$^{\Delta Ex4}$ BL/6 line displayed a slightly progressive loss of amplitude of the scotopic a-wave from the age of 3 months onwards (Figure 2A). The scotopic b-wave remained unaffected at all ages examined, whereas the photopic b-wave was marginally reduced but only at 9 months of age. Surprisingly, functional measurements revealed a strikingly different result in the *Rpgr*$^{\Delta Ex4}$ BALB/c background. Here, the cone system was affected already at 1 month of age as indicated by the reduction of the photopic b-wave in mutant animals (Figure 2C). Simultaneously, the amplitudes of the scotopic a-wave were reduced. At three months, the *Rpgr*$^{\Delta Ex4}$ BALB/c line showed a cone-rod phenotype as compared to the isolated mild rod phenotype in *Rpgr*$^{\Delta Ex4}$ BL/6 mice at comparable age (Figure 2B and D). Over time, the decrease in the rod photoreceptor response in *Rpgr*$^{\Delta Ex4}$ BALB/c mice was progressive, whereas the scotopic b-wave was not affected at any time point examined. It is important to emphasize the stable photopic b-wave in wild type animals until 12 months of age (Figure 2C), while the wild type scotopic responses significantly declined during ageing. This age-related retinal degeneration is well known to occur in BALB/c and to a lesser extent also in BL/6 mice [33].

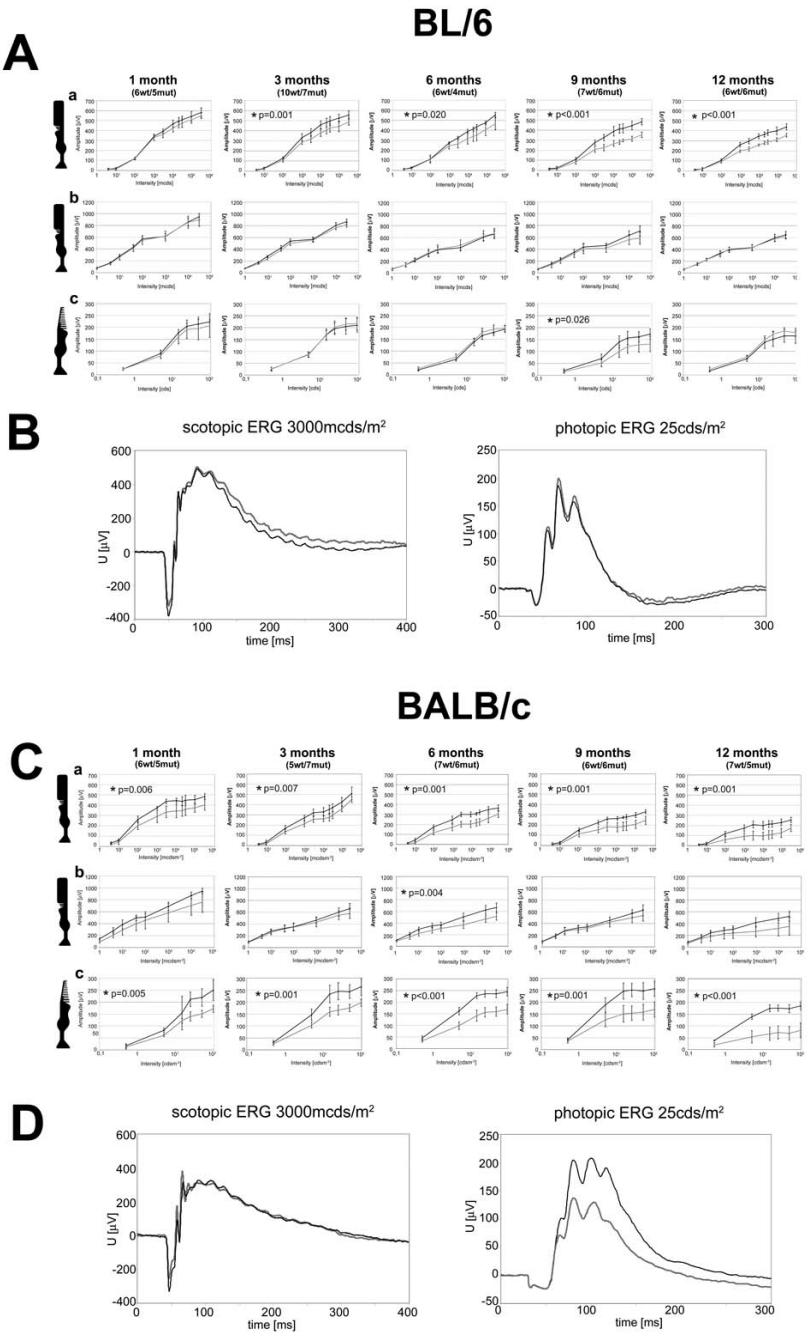

Figure 2: ERG measurements of the *Rpgr*$^{\Delta Ex4}$ BL/6 and *Rpgr*$^{\Delta Ex4}$ BALB/c mice

(A) ERG data from mutant animals (grey line) and their control littermates (black line) recorded in animals of 1, 3, 6, 9 and 12 months of age. Amplitudes [µV] from the scotopic a-wave (a), the scotopic b-wave (b) and the photopic b-wave (c) are plotted against the flash intensity ([mcds/m^2] for (a) and (b) and [cds/m^2] for (c)). In the *Rpgr*$^{\Delta Ex4}$ BL/6 line a mild progressive reduction of the scotopic a-wave was present in mutant animals starting at 3 month of age. The photopic b-wave was only marginally reduced in animals at 9 months of age. (B) Mean curve of scotopic ERG recorded at flash intensity of 3000 mcds/m^2 and photopic ERG recorded at 25 cds/m^2 in mice at 3 month of age (wt n = 10 and mut n = 7). Mutant mice show a mild reduction of the scotopic a-wave while the photopic response was not affected. (C) *Rpgr*$^{\Delta Ex4}$ BALB/c ERG data recorded equivalently as the *Rpgr*$^{\Delta Ex4}$ BL/6 data. Here, a

decline of the photopic b-wave as well as the scotopic a-wave was evident already at the age of 1 month. The decline of the photopic b-wave was progressive over time. The scotopic a-wave was diminished in both wild type and mutant animals from 6 month onwards during aging process. (D) The mean *Rpgr*$^{\Delta Ex4}$ BALB/c ERG curves recorded under the same scotopic and photopic conditions like in *Rpgr*$^{\Delta Ex4}$ BL/6 revealed that scotopic responses were mildly reduced while the photopic responses were severely diminished at three month of age (wt n = 5 and mut n = 7).

Retinal morphology

In order to determine morphologic changes accompanying the retinal dysfunction as indicated by ERG examinations, the same five time points of ERG measurements were chosen for histological analyses of the retina (1, 3, 6, 9 and 12 months). In both lines, retinal morphology was properly organized in mice at the age of 1 month, indicating normal retinal development (Figure 3A and B). In both lines (*Rpgr*$^{\Delta Ex4}$ BL/6 and *Rpgr*$^{\Delta Ex4}$ BALB/c) no obvious differences in retinal architecture were identified between wild type and mutant animals. The age-related retinal degeneration naturally occurring in BALB/c mice was again evident from 6 months onwards.

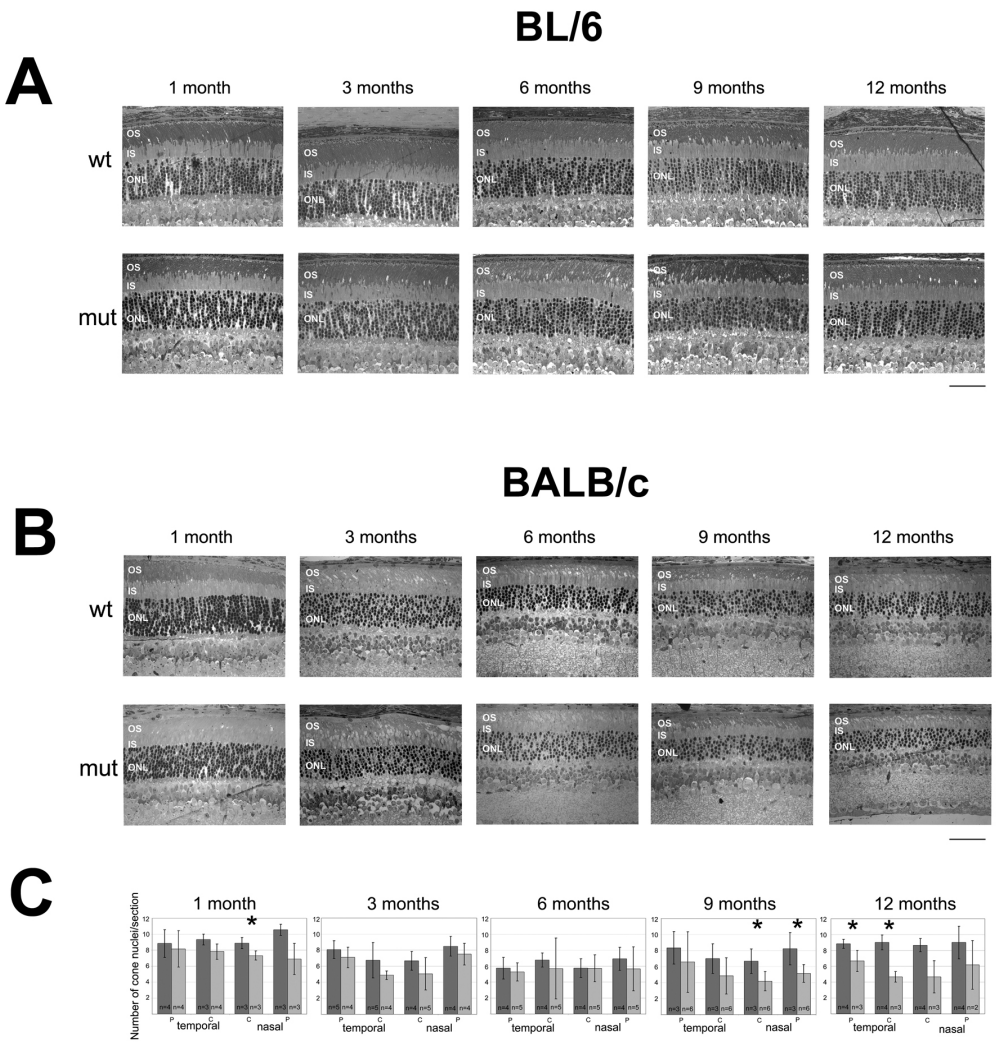

Figure 3: Histological analysis of *Rpgr*$^{\Delta Ex4}$ BL/6 and *Rpgr*$^{\Delta Ex4}$ BALB/c retinae

(A) Morphology was examined in semi-thin plastic sections at 1, 3, 6, 9 and 12 months. In *Rpgr*$^{\Delta Ex4}$ BL/6 no obvious differences between wild type and mutant animals were detected. (B) Histological sections of *Rpgr*$^{\Delta Ex4}$ BALB/c animals showed similar morphology in wild type and mutant animals. In aging BALB/c mice of 6 months and older natural occurring retinal degeneration was found in both genotypes. (C) Quantification of cone nuclei in *Rpgr*$^{\Delta Ex4}$ BALB/c mice based on their morphological appearance. Mutant animals displayed a loss of cone cells. Scale bar = 50 µm

For detection of subtle changes within the retina that might reflect the reduction in the rod and cone responses in the ERG, a detailed morphometric analysis was performed. In *Rpgr*$^{\Delta Ex4}$ BL/6 animals, a tendency towards reduction of the thickness of the outer nuclear layer (ONL), outer and inner segments (OS and IS) was found in mice aged 6 month or older (Supplemental Figure 1). Overall, these subtle changes in retinal morphology fit well with the observed mild decrease in the photoreceptor response upon ERG. In the *Rpgr*$^{\Delta Ex4}$ BALB/c line no differences between wild type

and mutant mice were apparent up to 3 months. We can not exclude mutation-specific effects at later stages, which might be masked by the age-related retinal degeneration.

The defect in the cone system in *Rpgr*$^{\Delta Ex4}$ BALB/c identified by ERG prompted us to test whether this defect is caused by the loss of cone photoreceptor cells. Cones can be discriminated from rods by the morphological appearance of their cell nuclei in semithin plastic sections [34]. We counted the number of cone cells in wild type and mutant animals at the five time points examined before and found that the numbers were slightly reduced in mutants as early as one month of age (Figure 2C). In older animals of 9 and 12 months, cones were significantly reduced. Cone numbers of wild type animals of 1 and 12 months were comparable indicating that cones are not prone to age-related degeneration like the rods are (Figure 3B and Supplemental Figure 1B). These observations are consistent with the cone dysfunction identified in ERG measurements and further emphasize the effect of the *Rpgr*$^{\Delta Ex4}$ mutation on cones in BALB/c mice

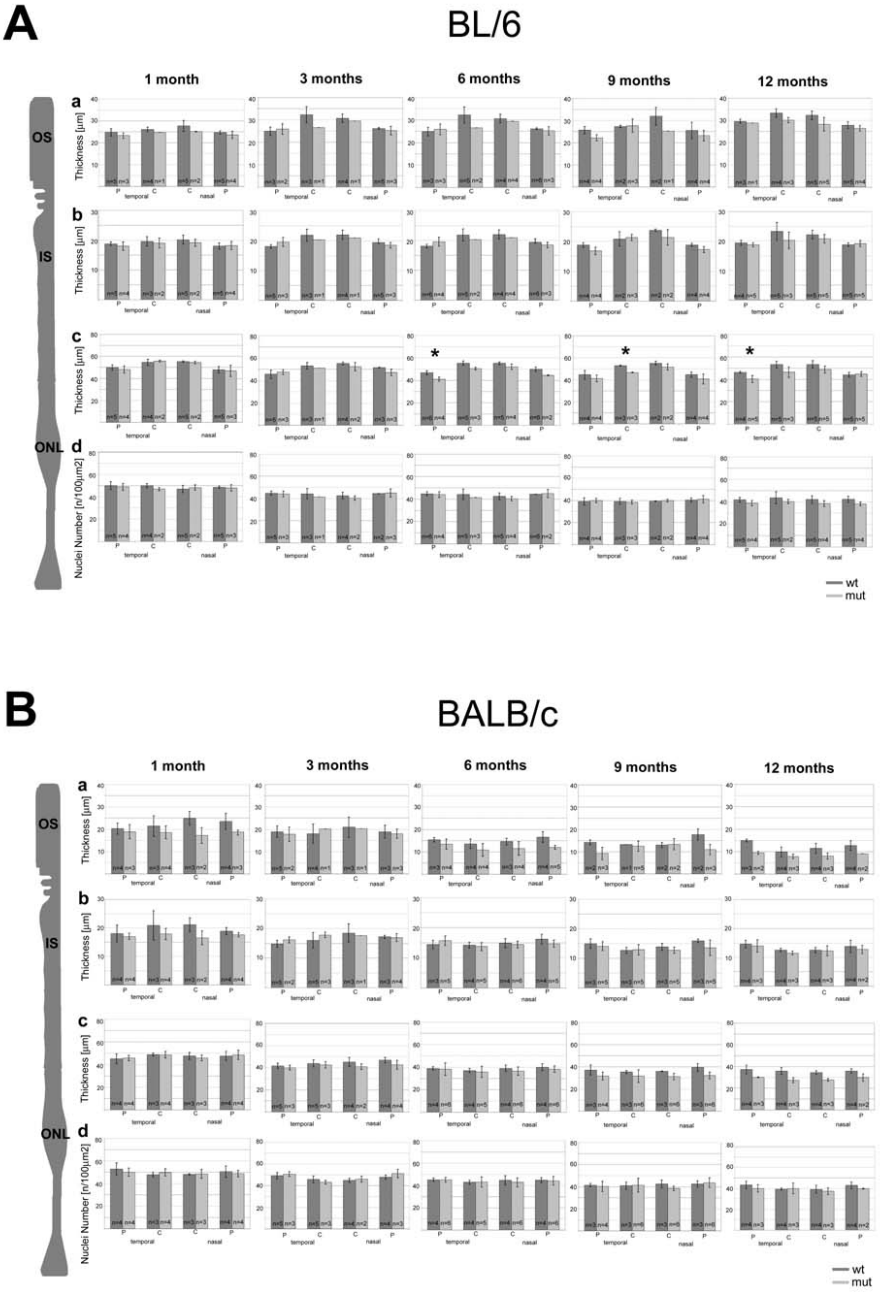

Supplemental Figure 1: Morphometric analysis of the retina of *Rpgr*$^{\Delta Ex4}$ BL/6 and *Rpgr*$^{\Delta Ex4}$ BALB/c

Morphometric analysis was performed by determining the thickness of the outer segments (OS) (a), the inner segments (IS) (b) and the outer nuclear layer (ONL) (c). The density of photoreceptor nuclei (mainly rods) was determined by counting an area of 100µm^2 (d). (A) In *Rpgr*$^{\Delta Ex4}$ BL/6 mice a slight trend towards a thickness reduction of the ONL was detected ($2 \geq n \geq 5$ per genotype). The OS and IS as well as the overall density of nuclei was not altered. (B) In the *Rpgr*$^{\Delta Ex4}$ BALB/c line, no differences between the genotypes could be detected ($2 \geq n \geq 5$ per genotype). However, the reduction of the thickness of OS, IS and ONL due to an age-related retinal degeneration in this strain was observed.

Localization of RPGR-ORF15, interacting proteins and ciliary markers

We next investigated the localization of wild type and mutant protein in the retina. A set of antibodies against RPGR, its interaction partners, as well as ciliary and other photoreceptor-specific proteins was applied on retinal sections. The RPGR antibody was directed against the ORF15 isoform (AbC2.1) and produced strong and specific signals. Specificity was shown by blocking with the cognate peptide in Western Blots (Figure 1D). An intense punctuate staining pattern was observed in the area of the connecting cilium with AbC2.1 (Figure 4A-D). This localization of RPGR-ORF15 has been described in mouse using a different set of antibodies [15]. Furthermore, Western blot experiments detected an immunoreactive band corresponding to the RPGR-ORF15 variant (Figure 1D). Comparison of the staining between wild type and mutant revealed the same pattern. Thus, the mutation had no influence on localization of the protein. The staining pattern observed with this antibody closely resembled γ-tubulin, a marker for the basal body, indicating that the ORF15 isoform specifically localizes there (Figure 4I-J). Additionally, we investigated the localization of RPGRIP1. As expected, RPGRIP1 was found along the ciliary axoneme in wild type and mutant retinas similar to acetylated α-tubulin (Figure4E-H and 4M-P).

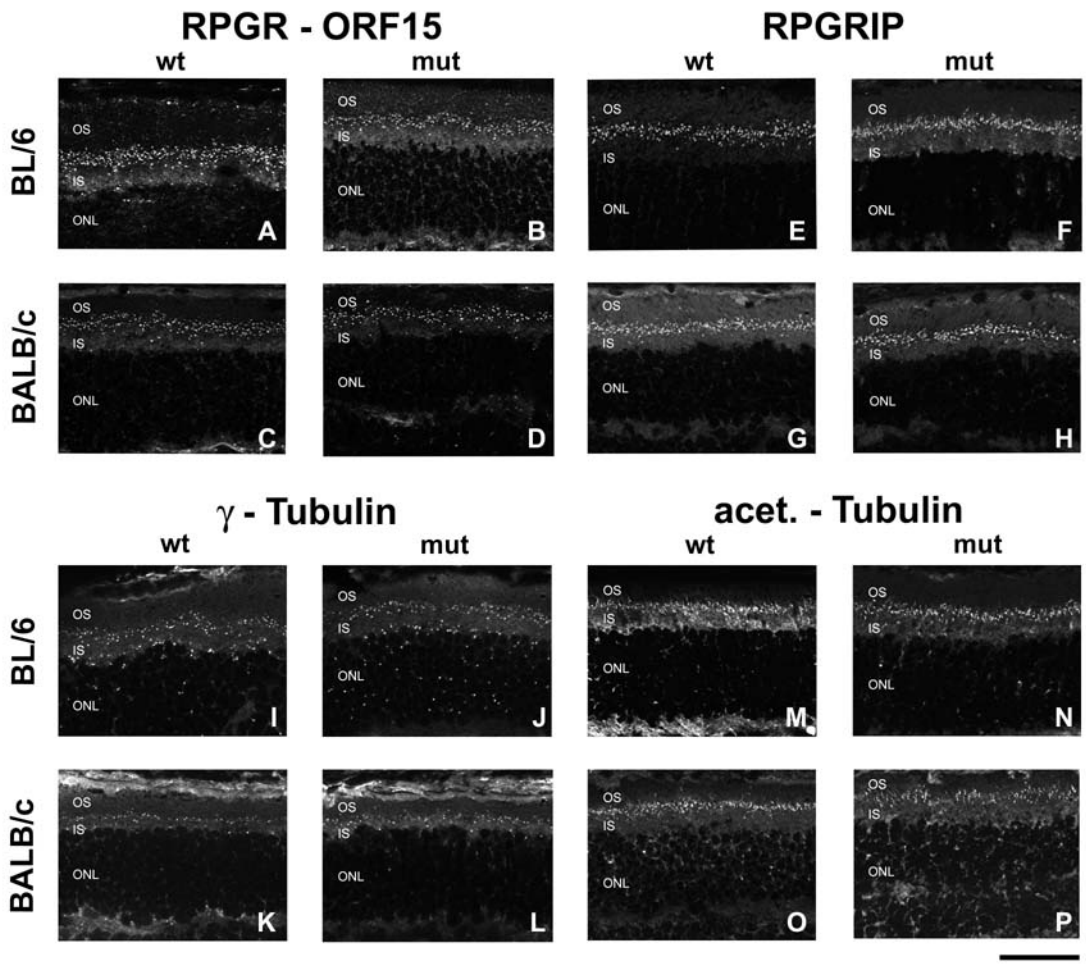

Figure 4: Localization of different ciliary proteins

(A-D) The RPGR-ORF15 isoform was localized with the AbC2.1 in frozen sections in wild type and mutant animals (n=2 per genotype) of both backgrounds at 6 months of age. A speckled fluorescent pattern reminiscent of basal body localization was observed (see γ-tubulin as a marker for basal bodies). No obvious differences between the genotypes or the strains were found. (E-F) Localization of RPGRIP1 (Ab#38, gift of R,Roepman) revealed staining of the ciliary axoneme (see acet. α-tubulin as a marker of the ciliary axoneme). Again, the same pattern was found in wild type and mutant animals of the *Rpgr*$^{\Delta Ex4}$ BL/6 and *Rpgr*$^{\Delta Ex4}$ BALB/c lines. (I-L) The basal body marker γ-tubulin confirmed the staining pattern of RPGR-ORF15. (M-P) Likewise, acet. α-tubulin, a marker for the ciliary axoneme, revealed a staining similar to RPGRIP1. The two markers of the basal body and the axoneme suggested that the cilium in the mutants in both backgrounds was preserved. Of note, staining of RPGR, RPGRIP1 and the ciliary markers were performed in consecutive sections. Scale bar = 50 μm.

An antibody against PDE6δ/PrBPδ, which was the first known interaction partner of RPGR, stained the inner segments of rods and cones in both mouse lines, as described by others before (Supplemental Figure 2)[35].

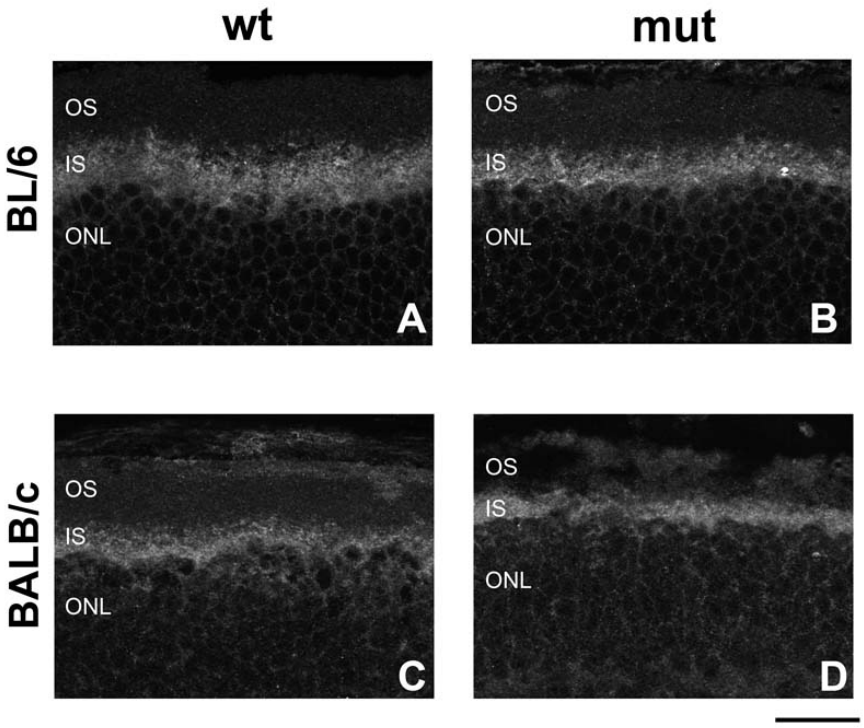

Supplemental Figure 2: Localization of PDE6δ/PrBP6δ

Immunohistochemical labelling of PDE6δ/PrBPδ on frozen retinal sections (A, B) PDE6δ/PrBPδ was localized to the inner segments (IS) of rods and cones in the wild type and mutant *Rpgr*$^{\Delta Ex4}$ BL/6 animals (n = 2 per genotype) (C, D) as well as in wild type and mutant *Rpgr*$^{\Delta Ex4}$ BALB/c animals (n = 2 per genotype). Scale bar = 50μm.

The integrity of the ciliary structures and components was not disturbed in mutant photoreceptors as suggested by staining with the ciliary markers γ-tubulin and acetylated α-tubulin. Thus, mislocalization of RPGR or gross disarrangement of connecting cilia is not the cause of retinal dysfunction and degeneration in these two mouse lines.

Mislocalization of visual pigments in Rpgr mutant mice

Several mouse models with defects in known or putative proteins of ciliary transport pathways show aberrant localization of components of the phototransduction cascade like rhodopsin, cone opsin, arrestin and transducin [18,36-38]. For RPGR, several lines of evidence exist that it also might be involved in ciliary transport. In addition, in a knock-out mouse model for *Rpgr* and in a canine XlPRA2 model, alterations in the localization of visual pigments were described [39,40]. We stained retinas with antibodies against rhodopsin and cone opsin and analyzed mice at one

month of age in order to elucidate primary defects before or simultaneous with the occurrence of functional impairments. These experiments revealed mislocalization of cone opsin in both mutant mouse strains (Fig 5B and D). Beside the localization in cone outer segments (COS), it was found in the outer nuclear layer and the cone synapses (Figure 5B and D, arrow). Similarly, rhodopsin was partially mislocalized in the perinuclear region of rod photoreceptor cells from mutant male mice of both lines (*Rpgr*$^{\Delta Ex4}$ BL/6 as well as *Rpgr*$^{\Delta Ex4}$ BALB/c, Figure 5F and H).

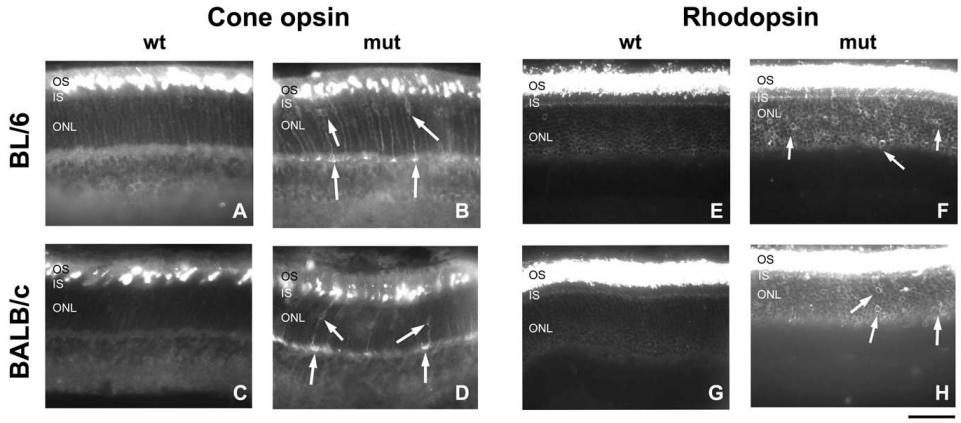

Figure 5: Localization of rhodopsin and MWL cone opsin

Immunohistochemistry on frozen sections of wild type and mutant mice of the BL/6 (n=4 per genotype) and BALB/c (n=2 per genotype) background at the age of 1 month. (A–D) Staining with an antibody against cone opsin (MWL cone opsin, kindly provided by C.Grimm) revealed mislocalization in the perinuclear region and the cone pedicles (arrows). This defect was detected in 3 out of 4 *Rpgr*$^{\Delta Ex4}$ BL/6 as well as all *Rpgr*$^{\Delta Ex4}$ BALB/c mutant mice. (E – H) Rhodopsin staining identified a localization defect in mutant animals of both genetic backgrounds. Fluorescent signals were not only found in the outer segments but also in the perinuclear region of photoreceptor nuclei (arrows). Scale bar = 50µm.

To test whether or not other proteins might be affected by a localization defect, we additionally stained dark adapted retinae for arrestin and transducin. These proteins were shown to localize in the IS and OS in the dark, respectively [41]. In contrast to cone opsin and rhodopsin, these proteins showed no aberrant localization in mutant mice (Supplemental Figure 3).

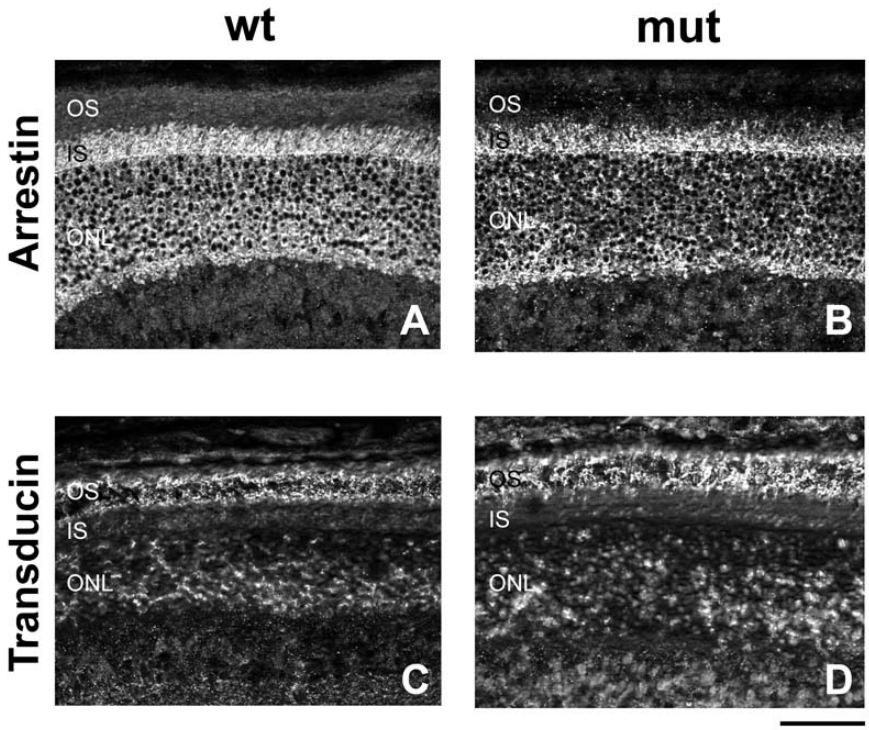

Supplemental Figure 3: Localization of arrestin and transducin in *Rpgr*$^{\Delta Ex4}$ BL/6

Detection of arrestin and transducin in dark-adapted BL/6 wild type and mutant retinae at 6 month of age (n=2 per genotype). (A) Arrestin was localized to the rod inner segments (IS), the outer nuclear layer (ONL) and the outer plexiform layer (OPL) in the wild type. (B) Accordingly, the staining pattern was distributed in mutant animals. (C) Transducin was found mainly in the outer segment (OS) in wild type animals. (D) The distribution of transducin was comparable in mutant animals. Scale = 50µm.

Evaluation of Rpe65 as modifier gene

Based on the different phenotypes occurring in BL/6 and BALB/c mice, both carrying the same *Rpgr*$^{\Delta Ex4}$ mutation, we assumed that a strain-specific modifier must exist. In order to test whether or not the RPE65 polymorphism at position 450 of the amino acid sequence has an effect on the phenotype in the BALB/c line, we designed a breeding scheme to obtain BALB/c mice carrying the BL/6 (methionine) variant at position 450. Wild type and mutant male mice at the age of 5-6 weeks were phenotyped by ERG. We still observed a cone-rod phenotype in mutant animals carrying the BL/6 variant (methionine) of RPE65 in an otherwise highly homogenous BALB/c background (<0.5 % BL/6 after 8 generations) (data not shown). Therefore, RPE65 alone is not responsible for this modifying effect.

3.3.5 Discussion

In this study we showed that two mouse strains carrying the same *Rpgr*$^{\Delta Ex4}$ mutation display strain-independent but also strain-specific characteristics of disease manifestations. Our findings indicate an important role of the genetic background on the degeneration of rod and cone photoreceptor cells as well as RPGR function. Moreover, the BALB/c line provides the first model for cone-rod degeneration due to an *Rpgr* mutation in mice.

Influence of the genetic background on the disease phenotype

The most striking finding of our study was the manifestation of different phenotypes in the two mouse lines carrying the same *Rpgr* mutation. We observed that *Rpgr*$^{\Delta Ex4}$ BL/6 mice presented with a mild rod phenotype while the *Rpgr*$^{\Delta Ex4}$ BALB/c strain developed an early-onset cone-rod phenotype. This result indicates that genetic modifiers act on the physiological homeostasis of rod and especially cone photoreceptors in addition to the *Rpgr*$^{\Delta Ex4}$ mutation. Variability in clinical manifestations was found in carrier females with the same mutation in exon 8 and also dizygotic twins with an RPGR-ORF15 mutation [26,42]. One sibling had RP while the other showed a cone-rod dystrophy. This situation is reminiscent to the phenotypic variability of our *Rpgr*$^{\Delta Ex4}$ mutant mice. To the best of our knowledge, we for the first time describe an impact on the primarily affected photoreceptor cell type, i.e. rods versus cones, as it was also observed in human patients. One previously identified modifier gene for retinal degeneration in mice is *Rpe65*. The variant with a leucine at position 450 of this protein renders BALB/c mice more susceptible to light-induced retinal degeneration by altering rhodopsin regeneration kinetics compared to mice carrying methionine at this position (e.g. BL/6) [43]. Introducing the methionine at position 450 (Met450) into the BALB/c background allowed us to elucidate the influence of this polymorphism on the phenotype of *Rpgr*$^{\Delta Ex4}$ mice. Based on this experiment, we found that the BL/6 variant of *Rpe65* alone has no significant effect on the cone phenotype of *Rpgr* mutant mice of the BALB/c line. Another potentially protective factor in BL/6 retinae might be the pigment. However, since we did not observe a difference in the two lines regarding the impairment of the rod system but only for cones, we consider this explanation rather unlikely. Additional genetic analyses, as for example QTL mapping, are necessary in order to map and identify

the respective modifiers. Identification of such genes might help to better understand the distinct molecular characteristics of rod and cone photoreceptors.

Disease course of retinal degeneration due to RPGR mutations

In humans, mutations in *RPGR* lead to XlRP, a severe early-onset rod degeneration, in some cases followed by cone degeneration. To date, 3 different splice site mutations in intron 4 were reported in patients with XLRP [28,44,45]. All of them occurred at the splice donor site (positions +1 and +3) and are supposed to lead to omission of exon 4 in the respective transcripts. Indeed, exon skipping was demonstrated for the mutation at position +3 [28]. Exon 4 is part of the coding region of the RCC-1 like domain (RLD) [5]. The amino acid residues are 100% identical in man and mouse and a significant portion of mutations are located in the RLD. In addition, it was shown to bind several interaction partners like RPGRIP1 [13], SMC1 and SMC3 [15], and PDE6δ [14]. Of importance, it has been shown that missense mutations within the RLD abolished its binding to RPGRIP1 isoforms[13].

Patients with cone-dominated phenotypes and *RPGR* mutations were also described, illustrating the clinical heterogeneity of *RPGR*-related retinopathies. Likewise, two natural occurring canine models develop a mild late-onset or very severe early-onset disease depending on the mutation[46]. Nevertheless, in both models rods were affected primarily with later involvement of cones. These models thus reflect the classical pathogenesis of RP as rod degeneration precedes cell death of cones.

In addition, two *Rpgr* mouse lines were described before. An *Rpgr* knock-out mouse line exhibits mild retinal degeneration involving both rods and cones. The ERG was taken at a single time point (6.5 months), thus no discrimination of rod and cone photoreceptors can be made over time. Still, the cone phenotype was more pronounced. Of note, the mouse is on a mixed BL/6J1 background. Thus, either the lack of the RPGR default variant leads to affection of both rod and cone photoreceptors, or the mixed genetic background has an impact on the additional involvement of cones that was not present in our $Rpgr^{\Delta Ex4}$ BL/6 mice. Transgenic mice with expression of a truncated RPGR-ORF15 protein revealed rapid photoreceptor degeneration in contrast to the slow degeneration in the knock-out line. ERG measurements displayed a decrease of the scotopic a- and b- waves at about 1.5 months of age (P40). Cone responses also declined however, this effect was not quantified. Compared to the canine and murine models, the $Rpgr^{\Delta Ex4}$ BALB/c

line represents a model for cone-rod degeneration. Our mouse lines expressing a protein with a deletion of 21 amino acids in the RLD can be regarded as a model for disease associated human mutations (in-frame deletions and insertions as well as missense mutations) leading to altered RPGR proteins in patients, which account for approximately 48% of all mutations described (http://rpgr.hgu.mrc.ac.uk).

Defect of ciliary transport but not ciliary structure

We showed that RPGR and RPGRIP1 are correctly localized in mutants and that the ciliary structure is not obviously compromised. Thus, retinal disease might rather be explained by an altered protein function due to different disease-associated mutations. This is supported by the observed mislocalization of rhodopsin and cone opsin early in disease. Mislocalization preceded the decline in the scotopic but not the photopic ERG amplitudes in *Rpgr*$^{\Delta Ex4}$ BL/6 animals but occurred simultaneously to amplitude reduction in *Rpgr*$^{\Delta Ex4}$ BALB/c. Thus, partial mislocalization of visual pigments might not be sufficient to trigger impairments in the phototransduction cascade or signal transmission that is sensitive to ERG. Mislocalization of visual pigments is a common phenotype in patients and animals with *RPGR* mutations as well as in mouse models with mutations in proteins of ciliary transport pathways [36,39,40,47,48]. Based on these results and the findings in our *Rpgr* overexpressing[49] and knock-in mouse lines we hypothesize that quantitative or qualitative alterations of RPGR lead to changes in the composition of a large ciliary protein complex. Consequently, these alterations may result in functional defects of ciliary transport mechanisms leading to disease.

In conclusion, we have generated two mutant mouse lines carrying the same in-frame mutation (*Rpgr*$^{\Delta Ex4}$) on two different genetic backgrounds. A strain-specific impact mainly on the cone photoreceptors in the BALB/c line was observed. Therefore, this mouse line represents the first model for a cone-rod phenotype caused by a mutation in an RP-associated gene. This is similarly to a subset of human patients and therefore this mouse line provides the basis to improve our understanding of the observed differences in clinical outcomes of *RPGR*-related retinal degenerations. Furthermore, it allows to further investigate the function of *RPGR* in rods and also in cones.

3.3.6 Acknowledgements

We are grateful to Christian Grimm (University Hospital Zurich, Switzerland) for help with epon histology and for kindly providing cone opsin antibody, to Coni Imsand (University Hospital Zurich, Switzerland) for technical advice with epon histology, to Rick Cote (University of New Hampshire, U.S.) for providing anti-PDE6δ/PrBPδ antibody, to Stephan Labs (University of Zurich, Switzerland) for help with digital images and to Barbara Kloeckener-Gruissem (University of Zurich, Switzerland) for valuable discussions.

3.3.7 References

1. Koenekoop RK, Loyer M, Hand CK, et al. Novel RPGR mutations with distinct retinitis pigmentosa phenotypes in French-Canadian families. *Am J Ophthalmol*. 2003;136:678-687.

2. Aguirre GD, Yashar BM, John SK, et al. Retinal histopathology of an XLRP carrier with a mutation in the RPGR exon ORF15. *Exp Eye Res*. 2002;75:431-443.

3. Vervoort R, Lennon A, Bird AC, et al. Mutational hot spot within a new RPGR exon in X-linked retinitis pigmentosa. *Nat Genet*. 2000;25:462-466.

4. Schwahn U, Lenzner S, Dong J, et al. Positional cloning of the gene for X-linked retinitis pigmentosa 2. *Nat Genet*. 1998;19:327-332.

5. Kirschner R, Rosenberg T, Schultz-Heienbrok R, et al. RPGR transcription studies in mouse and human tissues reveal a retina-specific isoform that is disrupted in a patient with X-linked retinitis pigmentosa. *Hum Mol Genet*. 1999;8:1571-1578.

6. Yan D, Swain PK, Breuer D, et al. Biochemical characterization and subcellular localization of the mouse retinitis pigmentosa GTPase regulator (mRpgr). *J Biol Chem*. 1998;273:19656-19663.

7. Roepman R, van Duijnhoven G, Rosenberg T, et al. Positional cloning of the gene for X-linked retinitis pigmentosa 3: homology with the guanine-nucleotide-exchange factor RCC1. *Hum Mol Genet*. 1996;5:1035-1041.

8. Mavlyutov TA, Zhao H, Ferreira PA. Species-specific subcellular localization of RPGR and RPGRIP1 isoforms: implications for the phenotypic variability of congenital retinopathies among species. *Hum Mol Genet*. 2002;11:1899-1907.

9. Neidhardt J, Glaus E, Barthelmes D, Zeitz C, Fleischhauer J, Berger W. Identification and characterization of a novel RPGR isoform in human retina. *Hum Mutat*. 2007;28:797-807.

10. Meindl A, Dry K, Herrmann K, et al. A gene (RPGR) with homology to the RCC1 guanine nucleotide exchange factor is mutated in X-linked retinitis pigmentosa (RP3). *Nat Genet*. 1996;13:35-42.

11. Ralf F, Ponstingl H. Catalysis of guanine nucleotide exchange on Ran by the mitotic regulator RCC1. *Nature*. 1991;354:80-82.

12. Riddick G, Macara IG. A systems analysis of importin-{alpha}-{beta} mediated nuclear protein import. *J Cell Biol*. 2005;168:1027-1038.

13. Roepman R, Bernoud-Hubac N, Schick DE, et al. The retinitis pigmentosa GTPase regulator (RPGR) interacts with novel transport-like proteins in the outer segments of rod photoreceptors. *Hum Mol Genet*. 2000;9:2095-2105.

14. Linari M, Ueffing M, Manson F, Wright A, Meitinger T, Becker J. The retinitis pigmentosa GTPase regulator, RPGR, interacts with the delta subunit of rod cyclic GMP phosphodiesterase. *Proc Natl Acad Sci U S A*. 1999;96:1315-1320.

15. Khanna H, Hurd TW, Lillo C, et al. RPGR-ORF15, Which Is Mutated in Retinitis Pigmentosa, Associates with SMC1, SMC3, and Microtubule Transport Proteins. *J Biol Chem*. 2005;280:33580-33587.

16. Otto EA, Loeys B, Khanna H, et al. Nephrocystin-5, a ciliary IQ domain protein, is mutated in Senior-Loken syndrome and interacts with RPGR and calmodulin. *Nat Genet*. 2005;37:282-288.

17. Shu X, Fry AM, Tulloch B, et al. RPGR ORF15 isoform co-localizes with RPGRIP1 at centrioles and basal bodies and interacts with nucleophosmin. *Hum Mol Genet*. 2005;14:1183-1197.

18. Chang B, Khanna H, Hawes N, et al. An in-frame deletion in a novel centrosomal/ciliary protein CEP290/NPHP6 perturbs its interaction with RPGR and results in early-onset retinal degeneration in the rd16 mouse. *Hum Mol Genet*. 2006.

19. He S, Parapuram SK, Hurd TW, et al. Retinitis Pigmentosa GTPase Regulator (RPGR) protein isoforms in mammalian retina: Insights into X-linked Retinitis Pigmentosa and associated ciliopathies. *Vision Research*. 2008;48:366-376.

20. Ebenezer ND, Michaelides M, Jenkins SA, et al. Identification of novel RPGR ORF15 mutations in X-linked progressive cone-rod dystrophy (XLCORD) families. *Invest Ophthalmol Vis Sci*. 2005;46:1891-1898.

21. Yang Z, Peachey NS, Moshfeghi DM, et al. Mutations in the RPGR gene cause X-linked cone dystrophy. *Hum Mol Genet*. 2002;11:605-611.

22. Ayyagari R, Demirci FY, Liu J, et al. X-linked recessive atrophic macular degeneration from RPGR mutation. *Genomics*. 2002;80:166-171.

23. Iannaccone A, Breuer DK, Wang XF, et al. Clinical and immunohistochemical evidence for an X linked retinitis pigmentosa syndrome with recurrent infections and hearing loss in association with an RPGR mutation. *J Med Genet*. 2003;40:e118.

24. Zito I, Downes SM, Patel RJ, et al. RPGR mutation associated with retinitis pigmentosa, impaired hearing, and sinorespiratory infections. *J Med Genet*. 2003;40:609-615.

25. Moore A, Escudier E, Roger G, et al. RPGR is mutated in patients with a complex X-linked phenotype combining primary ciliary dyskinesia and retinitis pigmentosa. *J Med Genet*. 2005:jmg.

26. Walia S, Fishman GA, Swaroop A, et al. Discordant phenotypes in fraternal twins having an identical mutation in exon ORF15 of the RPGR gene. *Arch Ophthalmol*. 2008;126:379-384.

27. Sharon D, Bruns GA, McGee TL, Sandberg MA, Berson EL, Dryja TP. X-linked retinitis pigmentosa: mutation spectrum of the RPGR and RP2 genes and correlation with visual function. *Invest Ophthalmol Vis Sci*. 2000;41:2712-2721.

28. Buraczynska M, Wu W, Fujita R, et al. Spectrum of mutations in the RPGR gene that are identified in 20% of families with X-linked retinitis pigmentosa. *Am J Hum Genet*. 1997;61:1287-1292.

29. Knobeloch KP, Wright MD, Ochsenbein AF, et al. Targeted inactivation of the tetraspanin CD37 impairs T-cell-dependent B-cell response under suboptimal costimulatory conditions. *Mol Cell Biol*. 2000;20:5363-5369.

30. Ruether K, van de Pol D, Jaissle G, Berger W, Tornow RP, Zrenner E. Retinoschisislike alterations in the mouse eye caused by gene targeting of the Norrie disease gene. *Invest Ophthalmol Vis Sci*. 1997;38:710-718.

31. Danciger M, Matthes MT, Yasamura D, et al. A QTL on distal chromosome 3 that influences the severity of light-induced damage to mouse photoreceptors. *Mamm Genome*. 2000;11:422-427.

32. Danciger M, Lyon J, Worrill D, LaVail MM, Yang H. A Strong and Highly Significant QTL on Chromosome 6 that Protects the Mouse from Age-Related Retinal Degeneration. *Invest Ophthalmol Vis Sci*. 2003;44:2442-2449.

33. Gresh J, Goletz PW, Crouch RK, Rohrer B. Structure-function analysis of rods and cones in juvenile, adult, and aged C57bl/6 and Balb/c mice. *Vis Neurosci*. 2003;20:211-220.

34. Carter-Dawson LD, LaVail MM. Rods and cones in the mouse retina. I. Structural analysis using light and electron microscopy. *J Comp Neurol*. 1979;188:245-262.

35. Norton AW, Hosier S, Terew JM, et al. Evaluation of the 17-kDa prenyl-binding protein as a regulatory protein for phototransduction in retinal photoreceptors. *J Biol Chem*. 2005;280:1248-1256.

36. Marszalek JR, Liu X, Roberts EA, et al. Genetic evidence for selective transport of opsin and arrestin by kinesin-II in mammalian photoreceptors. *Cell*. 2000;102:175-187.

37. Nishimura DY, Fath M, Mullins RF, et al. Bbs2-null mice have neurosensory deficits, a defect in social dominance, and retinopathy associated with mislocalization of rhodopsin. *Proc Natl Acad Sci U S A*. 2004;101:16588-16593.

38. Abd-El-Barr MM, Sykoudis K, Andrabi S, et al. Impaired photoreceptor protein transport and synaptic transmission in a mouse model of Bardet-Biedl syndrome. *Vision Research*. 2007;47:3394-3407.

39. Hong DH, Pawlyk BS, Shang J, Sandberg MA, Berson EL, Li T. A retinitis pigmentosa GTPase regulator (RPGR)-deficient mouse model for X-linked retinitis pigmentosa (RP3). *Proc Natl Acad Sci U S A*. 2000;97:3649-3654.

40. Beltran WA, Hammond P, Acland GM, Aguirre GD. A frameshift mutation in RPGR exon ORF15 causes photoreceptor degeneration and inner retina remodeling in a model of X-linked retinitis pigmentosa. *Invest Ophthalmol Vis Sci*. 2006;47:1669-1681.

41. Elias RV, Sezate SS, Cao W, McGinnis JF. Temporal kinetics of the light/dark translocation and compartmentation of arrestin and alpha-transducin in mouse photoreceptor cells. *Mol Vis*. 2004;10:672-681.

42. Banin E, Mizrahi-Meissonnier L, Neis R, et al. A non-ancestral RPGR missense mutation in families with either recessive or semi-dominant X-linked retinitis pigmentosa. *Am J Med Genet A*. 2007;143A:1150-1158.

43. Wenzel A, Reme CE, Williams TP, Hafezi F, Grimm C. The Rpe65 Leu450Met variation increases retinal resistance against light-induced degeneration by slowing rhodopsin regeneration. *J Neurosci*. 2001;21:53-58.

44. Sharon D, Sandberg MA, Rabe VW, Stillberger M, Dryja TP, Berson EL. RP2 and RPGR mutations and clinical correlations in patients with X-linked retinitis pigmentosa. *Am J Hum Genet*. 2003;73:1131-1146.

45. Breuer DK, Yashar BM, Filippova E, et al. A comprehensive mutation analysis of RP2 and RPGR in a North American cohort of families with X-linked retinitis pigmentosa. *Am J Hum Genet*. 2002;70:1545-1554.

46. Zhang Q, Acland GM, Wu WX, et al. Different RPGR exon ORF15 mutations in Canids provide insights into photoreceptor cell degeneration. *Hum Mol Genet*. 2002;11:993-1003.

47. Adamian M, Pawlyk BS, Hong DH, Berson EL. Rod and cone opsin mislocalization in an autopsy eye from a carrier of X-linked retinitis pigmentosa with a Gly436Asp mutation in the RPGR gene. *Am J Ophthalmol*. 2006;142:515-518.

48. Pazour GJ, Baker SA, Deane JA, et al. The intraflagellar transport protein, IFT88, is essential for vertebrate photoreceptor assembly and maintenance. *J Cell Biol*. 2002;157:103-113.

49. Brunner S, Colman D, Travis AJ, et al. Overexpression of RPGR Leads to Male Infertility in Mice Due to Defects in Flagellar Assembly. *Biol Reprod*. 2008.

3.3.8 Appendix: ERG measurements of BALB/c mice homozygous for either the leucine or methionine variant of *Rpe65*

Introduction

Phenotypic characterization of *Rpgr*$^{\Delta Ex4}$ mice on the BL/6 and the BALB/c background revealed differences in the retinal disease manifestations. In the BL/6 mice a mild rod-dominated phenotype was observed while in BALB/c mice a more severe cone-rod phenotype was identified. These data indicate that modifier genes influence the effect of the *Rpgr*$^{\Delta Ex4}$ mutation in a strain-specific manner. One known modifier of retinal degeneration is a polymorphism in the *RPE65* gene (p.L450M) [1]. In order to evaluate *RPE65* as a potential modifier of the observed phenotypes, the methionine (Met) variant was crossed into BALB/c mice and compared with the natural leucine (Leu) variant. Retinal function of wild type and mutant (*Rpgr*$^{\Delta Ex4}$) male mice of both genotypes (homozygous Leu and homozygous Met) were assessed by ERG.

Materials and Methods

Breeding of BALB/c homozygous methionine variant was accomplished by crossbreeding BALB/c mice from the F8 generation. Males and females were both heterozygous for the RPE65 polymorphism and hemi-/heterozygous for the *Rpgr* mutation, respectively. Accordingly, the resulting male offspring had either the wild type or mutant allele for *Rpgr* and some were homozygous for either the methionine or the leucine variant. Genotyping and ERG measurements were performed as described in the main manuscript.

Results

Male offspring from an intercross of the F8 generation of the BALB/c line were genotyped for *Rpgr* and *Rpe65.* From those animals, 9 wild type and 6 mutant *Rpgr* mice were available for ERG studies. In the *Rpgr* wild type pool, 4 mice were homozygous for leucine at position 450 of RPE65 (homo Leu) and 5 were homozygous for methionine (homo Met). The *Rpgr* mutant animals were all homozygous for the methionine variant. In order to have ERG data for *Rpgr* mutant animals homozygous for leucine at position 450 of RPE65 for comparison, ERG data from former measurements had to be used. Therefore, the data obtained in ERG

measurements of *Rpgr* wild type BALB/c mice from the F7 generation were compared to the data from *Rpgr* wild type BALB/c animals obtained in this ERG study. The results were highly consistent between the two measurements (data not shown). Hence, data for the calculations of Rpgr mutant animals with the leucine variant of RPE65 were taken for this particular group from former ERG studies.

The selected male mice were examined by ERG at the age of approximately 1.5 months (P47-P55). At this time point, a severe cone and mild rod dysfunction has developed in $Rpgr^{\Delta Ex4}$ BALB/c (naturally L450)[2]animals while in $Rpgr^{\Delta Ex4}$ BL/6 (naturally M450)[2] animals no retinal dysfunction of either rods or cones was detectable.

First, the obtained ERG data were analyzed by comparing *Rpgr* wild type and $Rpgr^{\Delta Ex4}$ mice (Figure 1A). In the BALB/c line homozygous for leucine at position 450, a cone-rod dysfunction was observed as described in the preceding manuscript (Figure 1A, left panel) in $Rpgr^{\Delta Ex4}$ mice. Similarly, the BALB/c line homozygous for methionine also developed a cone-rod dominated phenotype; however, it was more pronounced than in homozygous leucine mice. (Figure 1A, right panel). Of note, the difference of the absolute photopic b-wave amplitudes between *Rpgr* wild type and mutant animals was bigger in animals homozygous for methionine than in animals homozygous for leucine. Strikingly, this effect on the cone responses became more evident when the data were compared for the RPE65 polymorphism (Figure 1B). In *Rpgr* wild type animals, the RPE65 polymorphism had no effect on the rod responses. Surprisingly, it had a strong influence on the cone response. Animals genotyped homozygous methionine performed significantly better regarding cone b-wave amplitudes than homozygous leucine animals (Figure 1B, left panel). In *Rpgr* mutant mice, homozygous methionine mice had slightly but significantly higher rod and cone b-wave amplitudes compared to homozygous leucine littermates (Figure 1B, right panel). The effect of the homozygous methionine variant on the cone amplitudes could be confirmed in mice at 3 months of age although the difference was less pronounced (Figure 1C).

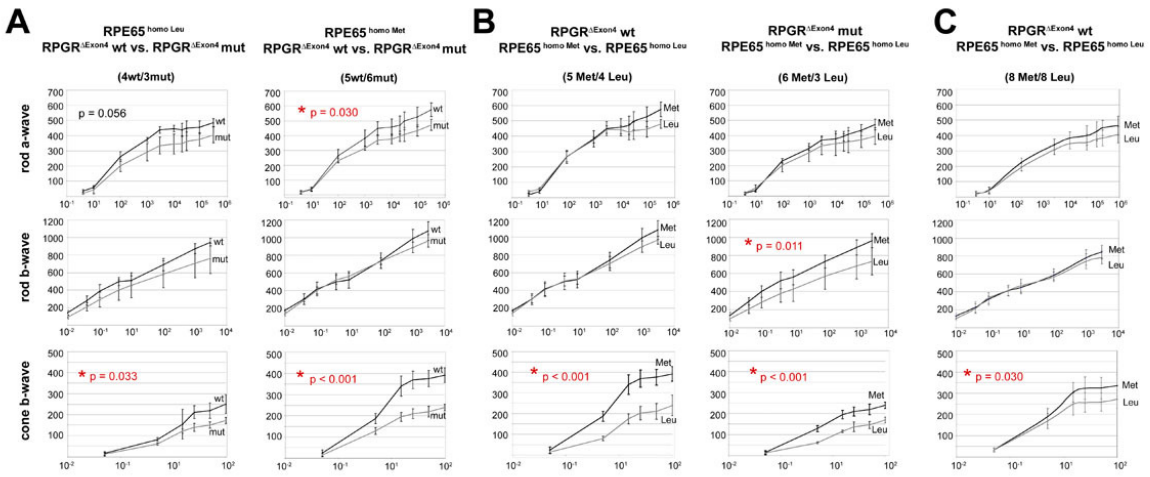

Figure 1: Scotopic and photopic ERG responses of the *Rpgr*$^{\Delta Ex4}$ BALB/c mice homozygous for either methionine at position 450 of RPE65 or leucine

ERG measurements were performed in male mice at 1.5 and 3 months of age under scotopic and photopic conditions. (A) Comparison of the *Rpgr* genotypes sorted by RPE65 variants. In homozygous leucine animals, the formerly identified cone-dominated phenotype in *Rpgr* mutant animals could be observed (left panel). Similarly, in homozygous methionine animals the cone dysfunction was more pronounced than the rod dysfunction (right panel). (B) Comparison of RPE65 variants sorted by *Rpgr* genotypes. In wild type animals the homozygous methionine mice displayed a "supernormal" cone response while the rod system was not influenced. In mutant animals, the homozygous methionine mice performed significantly better in both rod and cone b-wave responses than homozygous leucine mice. (C) Comparison of the effect of the RPE65 variants in *Rpgr* wt mice of 3 months. The cone amplitudes are significantly higher in homozygous methionine animals. Statistical analyses were done using ANOVA setting $p \leq 0.05$.

Hence, the RPE65 polymorphism has an influence on the amplitude of the cone b-wave, which is thought to be mainly generated by the rod ON-bipolar cells. In other words, wild type mice homozygous for methionine display a "supernormal" ERG in comparison to mice homozygous for leucine (Figure 2). The absolute amplitude of the photopic b-wave in animals homozygous methionine was found to be approximately twice as high as in homozygous leucine animals. It is worth mentioning, that the cone b-wave amplitude maximum in wild type BL/6 animals was in the range of wild type BALB/c mice (main manuscript, Figure 2).

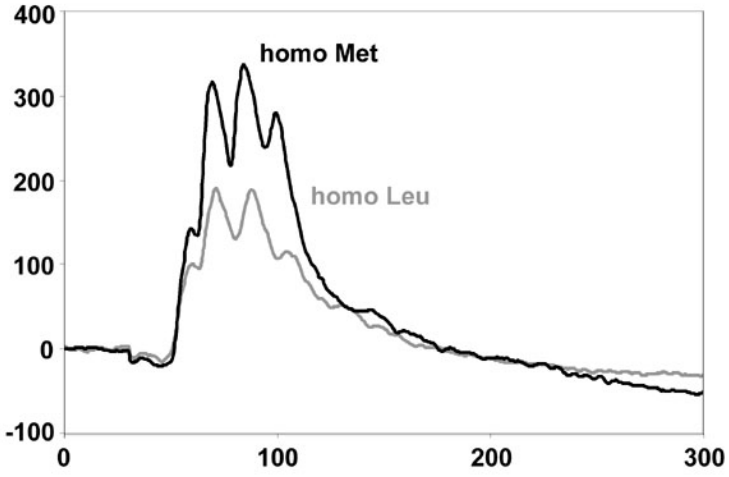

Figure 2: Photopic ERG of RPE65 homo Met and RPE65 homo Leu mice

ERG profile of a photopic response at 25 cds/m^2 flash intensity. BALB/c mice homozygous for methionine at position 450 of RPE65 show a "supernormal" cone response in comparison to homozygous leucine mice.

Discussion

The intention behind these experiments was to assess the influence of the RPE65 polymorphism on the observed differences in *Rpgr*$^{\Delta Ex4}$ BL/6 and BALB/c mouse lines. The hypothesis that the L450 variant in BALB/c might have an influence on the susceptibility of the cones to the *Rpgr*$^{\Delta Ex4}$ mutation and that the M450 variant in BL/6 might act protective was not confirmed. This finding implies that the methionine variant alone is not sufficient as the cone-dominated phenotype was still present in *Rpgr* mutant BALB/c mice. Surprisingly, this single polymorphism seems to have an impact on the general performance of the cone system. The BALB/c leucine and methionine line are supposed to be coisogenic lines, as the statistical part of BL/6 background should be reduced to < 0.5% after 8 generations crossing to BALB/c. One known differences between the two mouse lines is the single nucleotide change in the *Rpe65* gene. Practically, regions of low recombination might still harbour significant genomic regions with BL/6 origin that might have modifying influence on the retinal phenotype.

Possible explanations for this unexpected finding are very speculative. RPE65 is expressed only in RPE cells and was identified to be the key enzyme in the visual cycle by isomerising all-trans retinal to 11-cis retinal, which is the chromophore for opsin [3]. Furthermore, it is known that the RPE65 polymorphism has an effect on the rhodopsin regeneration kinetics [2]. Animals with the L450 variant (e.g. BALB/c) regenerate rhodopsin after bleach faster than animals with the M450 variant (BL/6). As a consequence, BALB/c animals are more susceptible to light damage than BL/6 animals are [2]. However, the effect that was found in this study exclusively concerns

the performance/amplitude of the cones. The function of RPE65 in cones is still controversial discussed. Neither the presence of the gene and its product nor the pathway of the cones that is used for chromophore regeneration is known, although several studies concerning these topics exist [4-9]. Therefore, it is mandatory to further investigate the effect on the cone system. The BALB/c mouse homozygous for methionine in RPE65 is a promising tool to further evaluate the role and function of RPE65 in cones.

References

1. Samardzija M, Wenzel A, Naash M, Reme CE, Grimm C. Rpe65 as a modifier gene for inherited retinal degeneration. *Eur J Neurosci*. 2006;23:1028-1034.

2. Wenzel A, Reme CE, Williams TP, Hafezi F, Grimm C. The Rpe65 Leu450Met variation increases retinal resistance against light-induced degeneration by slowing rhodopsin regeneration. *J Neurosci*. 2001;21:53-58.

3. Jin M, Li S, Moghrabi WN, Sun H, Travis GH. Rpe65 Is the Retinoid Isomerase in Bovine Retinal Pigment Epithelium. *Cell*. 2005;122:449-459.

4. Hemati N, Feathers KL, Chrispell JD, Reed DM, Carlson TJ, Thompson DA. RPE65 surface epitopes, protein interactions, and expression in rod- and cone-dominant species. *Mol Vis*. 2005;11:1151-1165.

5. Ma J, Xu L, Othersen DK, Redmond TM, Crouch RK. Cloning and localization of RPE65 mRNA in salamander cone photoreceptor cells1. *Biochim Biophys Acta*. 1998;1443:255-261.

6. Schonthaler HB, Lampert JM, Isken A, et al. Evidence for RPE65-independent vision in the cone-dominated zebrafish retina. *Eur J Neurosci*. 2007;26:1940-1949.

7. Wenzel A, von Lintig J, Oberhauser V, Tanimoto N, Grimm C, Seeliger MW. RPE65 is essential for the function of cone photoreceptors in NRL-deficient mice. *Invest Ophthalmol Vis Sci*. 2007;48:534-542.

8. Znoiko SL, Crouch RK, Moiseyev G, Ma Jx. Identification of the RPE65 Protein in Mammalian Cone Photoreceptors. *Invest Ophthalmol Vis Sci*. 2002;43:1604-1609.

9. Fleisch VC, Schonthaler HB, von Lintig J, Neuhauss SCF. Subfunctionalization of a Retinoid-Binding Protein Provides Evidence for Two Parallel Visual Cycles in the Cone-Dominant Zebrafish Retina. *J Neurosci*. 2008;28:8208-8216.

3.3.9 Contributions of authors to the manuscript “Cone versus rod disease in two mouse strains with a knock-in mutation in the retinitis pigmentosa GTPase regulator (*Rpgr) gene”*

S.B.: planning and administration of mouse breedings, preparation of animals, analysis of ERG data, epon histology, morphometric analyses, generation of antibodies, immunohistochemistry (IHC), Western blots (WB), interpretation of data, writing of the manuscript

S.S.: performance and planning of the phenotypical characterization by ERG measurements, breeding and keeping of the BALB/c line, preparation of animals

R.K.: cloning of the targeting construct, screening and selection of positively targeted ES cells, initial characterization of knock-in mice

K.P.K: Electroporation of ES cells, injection of ES cells, transfer of blastocysts

J.N.: assistance in analysis of IHC and WB results, interpretation of IHC of rhodopsin and cone opsin, conceptual input, editing of the manuscript

S.F.: technical assistance in antibody purification, WB, IHC and genotyping of mice

U.L.: participation (conceptual) in morphometric analysis and breeding of mice, editing of the manuscript

K.R.: (statistical) analyses and interpretation of ERG data, conceptual input

W.B.: P.I., conceptual planning, design and supervision of the entire study, interpretation of data, writing and editing of the manuscript

4. General Discussion

In this work two mouse models for *RPGR*-related diseases have been characterized. The insights gained by the observed phenotypic features of the overexpressing *Rpgr* mouse model and the mutant *Rpgr* mouse model with a knock-in mutation will help to further understand the function of RPGR in health and its role in pathogenesis.

4.1 Pathology of alterations in *Rpgr* quantity and quality

4.1.4 Aberrant sperm flagella due to overexpression of *Rpgr*

Transgenic animals are a powerful tool to study gene function. The widely used knock-out strategy is applied in order to examine the function of a gene by deleting it from the tissue or cell. However, the lack of a protein mimics only the situation of non-sense mutations in patients. Many mutations lead to alteration in the amino acid composition or in expression levels. Therefore, exogenous expression of the respective gene by introducing a transgene provides an additional method to study the function of a gene and its gene product. By using native regulatory and promoter sequences the transgene will be similarly expressed to the endogenous gene. Either the wild type gene or a mutated form can be transferred into the animal. Expression of wild type alleles allow to investigate expression and splicing patterns in different tissues, and putative pathogenic mechanisms based on overexpression. Several transgenic overexpressing mouse models were described to develop disease. One prominent model for retinal degeneration is a mouse line carrying a rhodopsin transgene [1]. In this mouse both the wild type and the mutant allele led to disease when overexpressed. To gain further insights into the expression and pathophysiology of RP based on aberrations in *RPGR* a transgenic mouse line was generated. The transgenic construct contains the entire genomic region of *Rpgr* including putative regulatory elements.

RPGR is known to lead to a variety of retinal degeneration phenotypes. Therefore, the transgenic mouse lines were examined for putative retinal manifestations. Based on electrophysiological, histological and molecular investigations no significant phenotype could be observed. Although transcript and protein levels were slightly elevated these alterations in expression had no effect on retinal function. This finding is in contrast to another overexpressing *Rpgr* mouse model in which retinal

degeneration was observed [2]. In this model a cDNA-based construct was ectopically expressed resulting in overexpression of the $RPGR_{1-19}$ isoform. The different pathogenic effects might be explained by tissue-specific expression patterns and alternative splicing of the *Rpgr* transgene based on genomic DNA. However, evaluation of the retinal phenotype in the overexpressing model described herein requires further examinations.

Surprisingly, the most prominent finding in the *Rpgr* overexpressing mouse line was infertility due to aberrant sperm flagella. The severity of the aberrations correlated with the number of *Rpgr* copies integrated into the genome of the respective mice. In histological studies on light and electron microscopic level animals with moderate number of *Rpgr* copies (i.e. 4-5 copies) disorganization of the periaxonemal structures was identified. The periaxonemal structures of the flagellum are the fibrous sheath, the outer dense fibres and the mitochondrial sheath and are accessory structures for stabilization of the axoneme (Chapter 3.2, Figure 4). In mice with high copy numbers of transgenic *Rpgr* (i.e. > 8 copies) a lack of the sperm flagellum was observed. Still, the initial flagellar development seems not to be disrupted as structures of the flagellar anlagen could be identified excluding a general failure in flagellar development. Therefore, the defects in the structural integrity of accessory structures of the sperm flagellum are very likely to emerge from a general defect in flagellar assembly.

Several other mouse models have been described exhibiting the same flagellar phenotype like the *Rpgr* overexpressing mice [3-7]. In those models, a lack of different *Bbs* genes (*Bbs2*, *Bbs4* and *Bbs6/Mkks*) and a novel ciliary gene *primary ciliary dyskinesia protein 1* (*Pcdp1)* led to a failure in the development of the flagellum although spermiogenesis proceeded as elongated spermatids were present. However, as the impaired sperm flagella of the *Rpgr* overexpressing mouse model results from an excess of protein, the molecular mechanisms might be different. Still, the striking similarity between the *Bbs,* the *Pcdp1* mouse models and the *Rpgr* overexpressing mouse line provides evidence that RPGR acts on similar molecular pathways like BBS and PCDP1 ciliary proteins. These observations provide valuable insights into the molecular function of *Rpgr* in flagella. Noteworthy, this is the first report of a phenotype in the flagellum due to alterations in protein quantity of *Rpgr.* It should be considered as putative novel candidate gene leading to isolated or syndromic male infertility also in humans.

4.1.2 Strain-specific retinal disease due to a knock-in mutation in *Rpgr*

The *Rpgr* knock-in mouse model carries an in-frame deletion of exon 4 and was designed in order to evaluate mutations occurring in patients that lead to altered protein that is still expressed (in-frame deletions, in-frame insertions and substitutions). The mutation mimics the effect of splice-site mutations found in RP patients that lead to the skipping of exon 4 [8,9]. Exon 4 consists of 63 bp and its lack results in the deletion of 21 amino acids without disrupting the reading frame. The deletion is located within the N-terminal RCC1-like domain (RLD) (see chapter 1 and [10,11]). Structurally, the RCC1-like domain (RLD) is assumed to resemble the seven-bladed propeller conformation that was shown for RCC1 and other homologous proteins [12]. According to this model, the deletion of exon 4 would lead to elimination of about half of blade 3. This could potentially have two major consequences. First, the hypothetical GTPase regulator function could be impaired as the β-wedge, which is involved in catalyzing nucleotide exchange, lies in close proximity to the site of deletion. However, a putative GTPase regulating function has never been proven so far. Second, interaction of RPGR with several proteins (PDE6δ/PrBPδ, RPGRIP1, SMC1 and SMC3) has been shown implicating that these might be impeded by the mutation. Therefore, localization of RPGR and its interaction partners was investigated. No obvious differences in the localization of RPGR-ORF15, RPGRIP1 and PDE6δ/PrBPδ were identified indicating that the mutation might not alter interaction in such a way that localization would be affected (Chapter 3.3, Figure 4). For SMC1 and SMC3 no definite conclusion of the localization can be drawn based on the staining that was performed. To further evaluate potential effects on the interaction of mutant RPGR to its direct interaction partners of the N-terminal RLD domain, co-immunoprecipitations and tandem-affinity-purification assays will be performed in future research. Those studies will provide further insights into the molecular pathophysiology of this particular mutation.

To further identify putative molecular defects, additional localization studies with a set of retinal proteins were performed. Those experiments revealed mislocalization of the visual pigments rhodopsin and cone opsin (Chapter 3.3, Figure 5). In contrast, no differences in the localization of two players of the phototransduction cascade (arrestin and transducin) were found. Therefore, the observed defect in the transport seems to be confined to specific proteins (i.e. opsins). Mislocalization of rhodopsin and cone opsin was also detected in *RPGR* mutant dogs, albeit cone opsin

mislocalization was transient and restored in older animals [13]. In the *Rpgr* knock-out mouse model, similar results were found for cone opsin, and probably rhodopsin is also mislocalized [14]. In addition, a female carrier with a Gly436Asp substitution in the RLD (exon 11) was also described to exhibit mislocalization of the two proteins [15]. These results suggest that RPGR might be involved in the transport of the two visual pigments. Therefore, the N-terminal protein domain (RLD) seems to play a crucial role for proper function as even a relative minor change (deletion of exon 4) results in a defect transport of visual pigment. The importance of this finding regarding the function of RPGR in ciliary transport pathways will be discussed later.

The two mutant mouse lines also revealed striking differences regarding their retinal phenotypes. BL/6 mice displayed a mild rod-dominated retinal disease while in contrast BALB/c mice revealed a more severe early-onset cone-rod phenotype (Chapter 3.3, Figure 2). Thus, as both mice carry the same *Rpgr*$^{\Delta Ex4}$ mutation genetic modifiers must be assumed acting on the primarily affected photoreceptor system. Several mouse models of retinal degeneration with variability in phenotypic expressivity have been described [16,17]. In a mouse carrying a mutant rhodopsin allele with three amino acid substitutions (V20G, P23H and P27L; VPP mouse), whereby P23H is the most frequent rhodopsin mutation in patients with dominant RP, the modifier was pinpointed to be a polymorphism in the *Rpe65* gene [17]. RPE65 is the key enzyme for regeneration of the chromophore for the visual pigment[18]. A polymorphism in the murine gene resulting in an amino acid substitution at position 450 (Met450Leu) slows kinetics of chromophore regeneration and consequently retinal photon catch capacity [19]. Therefore, mice carrying the methionine at position 450 (Met450) are less susceptible to light damage. All common inbred mouse strains (e.g. BALB/c) carry the leucine at position 450 (homo Leu) except Bl/6 mice which have the methionine (homo Met). However, the presence of RPE65 in cones and even more its direct involvement in the assumed cone visual cycle remains a matter of debate [20-23] . By introducing the methionine into the *Rpgr*$^{\Delta Ex4}$ BALB/c line the effect of this particular modifier on the cone phenotype could be evaluated. Strikingly, BALB/c mice with the Met450 variant still develop an early-onset cone dysfunction. Therefore, the *Rpe65* polymorphism alone is not the modifier of the cone-dominated phenotype in the BALB/c *Rpgr*$^{\Delta Ex4}$ mouse lines. However, it is worth mentioning that this single amino acid change seems to have an impact on the performance of the cones in general. Preliminary data suggest that amplitudes of the cone b-wave in

BALB/c mice homozygous for methionine are double as high as in wild type BALB/c animals with the leucine at position 450. Therefore, the BALB/c homo Met might provide a valuable model to study the function of RPE65 in cone photoreceptors. Furthermore, the results support that RPGR isoforms have an important function in cones in addition to its role in rods.

4.2 Diversity of RPGR protein isoforms

Little is known about the diversity of protein isoforms that theoretically could be produced by the abundance of transcript isoforms that have been described for *RPGR/Rpgr* [24-28]. In the last years, several studies described some protein variants mainly in the human, bovine and murine retina thereby giving an insight into the expected variety of protein isoforms [25,29,30]. In addition, phenotypic variability observed in patients might be explained by different function of different isoforms of RPGR. Despite the effort of producing unique sets of RPGR antibodies in several laboratories no definite correlation of protein to transcript isoforms could be established due to the high amount of isoforms described. Still, these studies and the present characterization of RPGR protein provided further evidence that more isoforms are synthesized in a tissue-specific manner than previously assumed. It is now becoming clear that the $RPGR_{1-19}$ isoform not only results in a protein calculated to migrate at 90 kDa but also of larger sizes (Chapter 3.1, Figure 4 and [30]). Similarly RPGR-ORF14/15 isoforms were detected at a broad molecular size range deviating from the calculated protein size based on the full-length transcript. Fractionation experiments further gave insights into the presence of distinct isoforms in defined cellular compartments thereby providing functional links of RPGR isoforms [30]. Recently, a cone-predominant isoform consisting of the N-terminal half of RPGR was reported [25]. Overall, these results indicate that the heterogeneous expression of *RPGR/Rpgr* on transcript level is reflected on protein level thereby suggesting that a significant portion of transcripts seem to be translated into protein.

Localization studies of RPGR that were performed in this study indicated that RPGR-ORF14/15 isoforms and presumably $RPGR_{1-19}$ as well reside in the connecting cilium area of mouse photoreceptor cells (Chapter 3.1, Figure 5). More specifically RPGR-ORF14/15 seems to localize at the basal bodies which is indicated by resembling the staining pattern of γ-tubulin, a known marker of centrosomes/basal bodies (Chapter

3.3, Figure 4). This is in accordance with previous findings [29,31]. In contrast, in localization studies with a different set of antibodies, $RPGR_{1-19}$ was reported to localize in the inner segments and the at the connecting cilium area of mouse photoreceptors [30]. Some further discrepancies on the exact cellular site within the photoreceptor in different species exist as well [32]. In cultured mammalian cells, the ORF15 isoform was detected to localize at the centrosomes at all stages of cell division [29]. Taken together, RPGR isoforms are found at several locations in photoreceptors within and across several species. Therefore, it is likely that RPGR isoforms rather execute distinct functions at distinct cellular sites than having only one defined cellular role. However, the most consistent finding in all studies that were performed was the localization at centrosomes/basal bodies and at the ciliary axoneme indicating that it has a similar function in these structures throughout the species.

4.3 The function of RPGR in cilia and flagella

At first glance, the two mouse models described herein developed very divergent phenotypes. However, at second glance those phenotypes seem to have a basic pathogenic mechanism in common. Both structures are cilia thereby sharing the same architecture (see chapter 1). Aberrations in RPGR protein quantity (overexpression) or quality (knock-in mutation) lead to a defect in flagellar assembly (transgenic mouse), and to retinal disease and impeded protein transport (knock-in mouse). Based on these findings it is very likely that *Rpgr* has an important function in cilia and flagella.

Patients harbouring mutations in RPGR reveal not only different types of retinal degenerations but also hearing problems, recurrent sinorespiratory infections and PCD [33-37]. These cases clearly indicate that not only the photoreceptors but also other ciliated tissues are affected by alterations in RPGR. The spectrum of phenotypes was extended in this study by showing that the sperm flagellum can also be affected by alterations in *Rpgr*, at least in mice. Translation of these insights to humans would imply to screen male infertility patients with unknown genetic defects for mutations in RPGR.

To date, two additional models and two natural occurring canine models for *RPGR*-related diseases exist. All of those developed mild to severe retinal degeneration

phenotypes depending on the mutation. The *Rpgr* knock-out mouse model and the XlPRA1 canine model with a mutation in exon ORF15 exhibited a relatively mild rod-cone dystrophy [14,38] while a transgenic mouse line with a truncated RPGR and the second canine model also with a mutation in exon ORF15 revealed a more severe rod-cone degeneration [38,39]. This finding further hints towards an important function in rod as well as cone photoreceptors. To date, no additional manifestations in other tissues of interest with regard to ciliopathies like the respiratory system, the kidney or testis have been reported. It would be of great interest to study these and our RPGR animal models for such possible phenotypes that are likely to exist but still remain undiscovered due to mild expressivity.

Further indications for a function of RPGR in cilia and flagella came from localization studies in cultured mammalian cells [29,31,40]. As mentioned, the RPGR-ORF15 isoform was consistently found at the centrosomes during cell division and at the basal bodies in post-mitotic cells. The centrosomes are the microtubule organizing center (MTOC) of dividing cells. Therefore, they have a crucial role in the organization of the spindle apparatus and regulation of the cell cycle. Basal bodies are the anchoring point for cilia and are assumed to act as a site for regulation of transport of proteins into the cilium [41]. In somatic cells the centrioles cycle between the centrosome and basal body state [42,43]. These processes have to be tightly regulated in a temporal and spatial manner. Two proteins of the IFT apparatus (IFT27 and IFT88) originally described as components of the basal body and the cilium have been found to localize at centrosomes during mitosis as well. Functional analyses indicated a dual role in IFT as well as cell cycle control [44,45]. In a very similar manner RPGR might have a dual function in centrosomes and cilia/flagella based on its dual localization depending on the cell cycle status.

4.4 An RPGR-containing ciliary protein complex

The characterization of the different phenotypes based on aberration in protein quantity and quality of RPGR and the evaluation of RPGR protein isoforms present mounting evidence that RPGR is part of a ciliary protein complex involved in transport, as it has been speculated before.

Rpgr knock-in mice displayed miss-localization of visual pigments (Chapter 3.3, Figure 5). Null mutations in *Kif3a*, *Ift88*, *Bbs2, Bbs4* and *Rpgr* also lead to

mislocalization of opsins in photoreceptor cells [3,14,46-48]. This common phenotype supports the idea that all proteins mentioned above are involved directly or indirectly in the transport of opsin. Principally, similar phenotypes in different mouse models strongly suggest related underlying molecular mechanisms. Internal membrane proteins like opsin are transported via intraflagellar transport (IFT) pathways along microtubules, although alternative pathways via actin filaments and an unconventional myosin (myosin7a) also seem to be used [49,50]. The localization site of RPGR at the basal body coincidences with the accumulation of IFT proteins at the basal bodies near the transition fibres [51]. These findings can be interpreted as that the basal body region and the transition fibres serve as a loading zone for the cargo (e.g. opsin) to the IFT particles and that RPGR might be involved in these processes.
In contrast, arrestin and transducin were properly localized in dark-adapted retinae of *Rpgr*$^{\Delta Ex4}$ mutant mice (Chapter 3.3, Supplemental Figure 3). In the *Bbs4*-/- mouse model localization of transducin in the dark and arrestin in the light was impaired. Likewise, in the rd16 mouse model, which has an in-frame deletion in the centrosomal protein CEP290, mislocalization of rhodopsin and arrestin was found [40]. Notably, interaction of CEP290 with RPGR-ORF15 was also shown. These findings suggest that RPGR might function on similar ciliary transport pathways like BBS4 and CEP290.
Consideration of the known complex partners of RPGR further aids to integrate the findings mentioned above. Some interaction partners are centrosomal/basal body proteins (i.e. RPGRIP1, RPGRIP1L, CEP290, Nephrcystin-5, 14-3-3-ε, nucleophosmin and γ-tubulin) and others are directly involved in microtubular transport pathways (i.e. KIF3A, KAP3, DIC, p150glued, p50-dynamitin and IFT88) (Chapter 1, Figure 13). Strikingly, mutations in several of the encoding genes of the proteins lead to ciliopathies with overlapping symptoms. Retinal degeneration is one symptom in patients with mutations in *RPGR*, *RPGRIP1*, *RPGRIP1*L, *CEP290/NPHP6* and *NPHP5* [52-56]. Likewise, retinal degeneration was identified in mice harbouring mutations in the *Rpgr*, *RPGRIP1*, *Cep290*, *Ift88* and *Kif3a* [14,40,46,48,57]. Renal dysfunctions are usually present in patients with mutations in *RPGRIP1L*, *CEP290/NPHP6* or *NPHP5* [54,56,58-60]. Similarly, renal phenotypes are observed in mice carrying mutations in *Ift88* and *Kif3a* [61,62]. These defects in the kidney are thought to arise from malfunction of the renal cilia like the retinal degeneration results from defects in the photoreceptor cilium. Abnormalities in

mouse sperm flagella, another ciliary structure within mammalians, have been observed presumably due to a defect in flagellar assembly due to overexpression of *Rpgr*. *Nphp1*-mutant mice revealed defects in late spermiogenesis [63]. Mutations in *Ift88* lead to the inability to assemble flagella. Accordingly, patients suffering from PCD and also some RP patients have been described to be infertile [64,65].

Bioinformatic, genomic and proteomic studies provided insights into the unique protein composition and mechanism that generate and assemble cilia/flagella [66-70]. The finding of the existence of a ciliary core protein complex – the ciliome – underlines the strong conservation of this organelle (http://www.ciliome.com and http://www.ciliaproteome.org). Further insights on a putative large ciliary protein complex were gained by the identification of three ciliary protein sub-complexes. Usher syndrome (USH), nephronophthisis (NPHP) and Bardet-Biedl syndrome (BBS) belong to the disease group of ciliopathies and are genetically very heterogeneous diseases as for each entity several genes are known to be mutated. Strikingly, for each disease group a protein network was identified linking the proteins of the underlying genes. Several USH proteins (USH2A, VLGR1, SANS, Myo7a, Cdh23 and Whirlin) were found to interact [71]. This complex was found at the junction between the inner segment and the connecting cilium of photoreceptors where it might be involved in the vesicular transport and handover of cargo for IFT. Likewise, several NPHP proteins (NPHP1, NPHP2, NPHP3, NPHP4) were found in a complex with NPHP1 as the key linking protein also in this case the proteins mainly reside at the base of the cilium [71]. NPHP5 and NPHP6 directly and NPHP4 indirectly interact with RPGR (via RPGRIP1). Just recently, genetic and physical interaction of NPHP5 and CEP290/NPHP6 has been shown [72]. The third ciliary complex is the BBS complex, also termed BBSome [73]. Seven of the known 14 BBS gene products form a complex which is thought to be involved in membrane trafficking of vesicles from the trans-Golgi network (TGN) loaded with cargo. It is tempting to speculate that these distinct protein complexes interact thereby explaining the phenotypic overlap of the different ciliopathies. Just recently, a study provided evidence that these complexes are molecularly linked by identifying a ciliary protein that interacts with USH2A, lebercilin (*LCA5*) and BBS6 [74]. BBS proteins in turn have been shown to be involved in IFT processes by coordinating the kinesin II motor proteins [75]. Overall, it is more and more becoming evident, that the key to understanding these phenotypes lies in the interplay of these proteins.

Based on these findings a model can be assumed where RPGR is located at the ciliary axoneme and ciliary base where it acts together with several other ciliary proteins (Figure 1). Membrane proteins (e.g. opsin) are packed in vesicles budding off from the trans-Golgi network (TGN). These might then be transported via the retrograde motor protein dynein 1a to the ciliary base. Docking and fusion of vesicles is assisted by the GTPase Rab8 which in turn is known to interact via Rabin8 with the BBSsome [73]. After fusion of the vesicles with the membrane the cargo is internalized into the ciliary membrane. The mechanism that takes over the transport of the cargo proteins through the cilium is intraflagellar transport (IFT). Based on a current model IFT can be subdivided into six phases [76]. Prior to transport components of the IFT machinery accumulate at the ciliary base at the transition fibres (phase 1). At this point RPGR might come into play. The disturbance in the IFT assembly and/or cargo loading process might be an explanation for defects in opsin protein transport. This is in accordance with the finding that opsin transport is similarly impeded by aberrations in BBS2, BBS4, ITF88 and CEP290 expression. However, taking the different results for arrestin and transducin into account, RPGR might only be involved in the transport of integral proteins of the ciliary membrane while Bbs4 and Cep290 might act on both routes. Unlike rhodopsin, arrestin and transducin are soluble and transiently membrane-bound proteins, respectively. The transportation route for soluble proteins still remains unknown. They might also be transported via IFT by direct connection to the IFT complex or indirectly to integral membrane cargoes. With regard to the *Rpgr* transgenic mouse line this hypothesis would explain the disorganization of the flagellar accessory structures in animals with moderate copy numbers. In those mice a defect in IFT initiation processes at the ciliary base might lead to impaired cargo import into the flagellum and hence to disorganized assembly. The complete lack of the flagellum might reflect complete breakdown of the flagellar transport by an excess of RPGR and a severe functional impairment of the assumed ciliary protein complex. An alternative explanation would suggest that different isoforms of RPGR might participate in different transport routes. However, this would imply that transport in the photoreceptor connecting cilium is selective for certain proteins but that in sperm flagella a general problem in transport occurs due to aberrations in RPGR. Of note, RPGR was also found to reside within the cilium along the ciliary axoneme. Potentially, the effect of alterations in RPGR quantity or quality could cause impairments in the ciliary shaft during flagellar transport of opsin or

sperm flagellum components. This hypothesis is also consistent with the flagellar and ciliary phenotype in *Bbs* knock-out mice. Based on the observed phenotypic indications the two possible ciliary sites of RPGR action can not be further discriminated. Still, the two mouse models provide novel significant insights to RPGR in health and disease and importantly in cilia and flagella in several tissues.

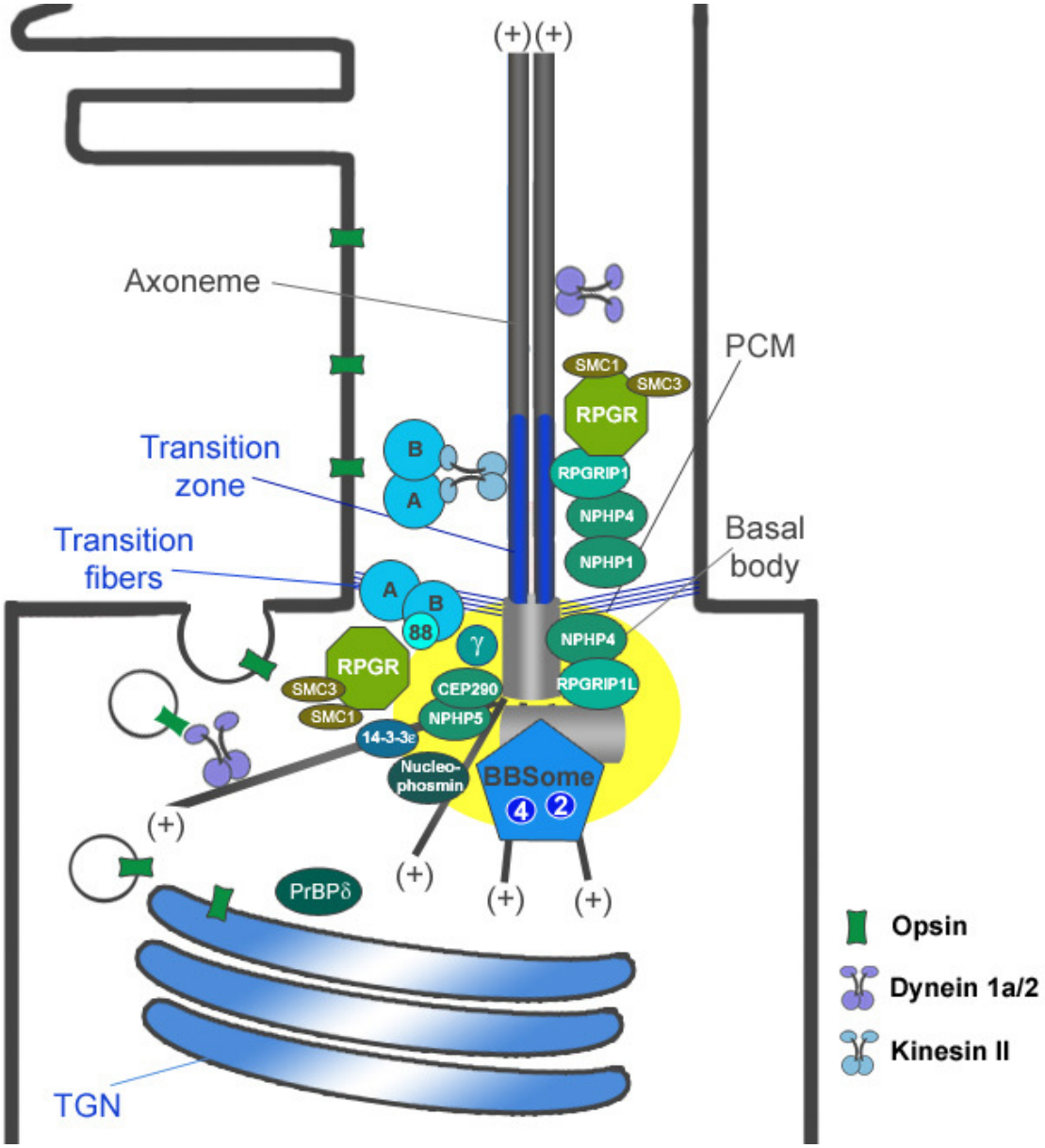

Figure 1: Model of the RPGR-containing ciliary protein complex

According to the current knowledge of RPGR, its interaction partners and their resulting disease phenotypes a model of a ciliary protein complex can be established. RPGR isoforms are known to reside at the basal body region in several species and in the ciliary shaft. Most of the reported direct interaction partners of RPGR (γ-tubulin, CEP290, Nephrocystin-5, Nucleophosmin, 14-3-3e, IFT88, SMC1 and SMC3) can be found at the ciliary base as well. Other direct and secondary molecular

partners were reported to localize within the cilium (RPGRIP1, Nephrocystin-4, Nephrocystin-1, SMC1, SMC3 and kinesin-II and dynein-2 motor protein subunits). For the BBSome including BBS2 and BBS4 no direct interaction with RPGR has been reported; however the localization at the basal body and the phenotypical similarities argue for a direct or indirect molecular crosstalk. Although interaction with PrBPδ has been reported, localization of is different from that of RPGR. However, the trans-Golgi network (TGN) expands close to the basal body region therefore making transient interaction possible. Transmembrane proteins like opsin are transported in vesicles from the TGN to the ciliary membrane. This presumably occurs via cytoplasmic dynein-1a motor proteins. The vesicles fuse with the periciliary membrane and are then thought to be transported via IFT. The RPGR-containing protein complex at the ciliary base might assist in this transport mechanism, therefore leading to the observed defects in protein transport.

Overall, good evidence based on the common phenotypic findings in ciliopathy disease phenotypes and the findings regarding the molecular interconnections of the ciliopathy underlying genes and their gene products exist, that RPGR is a part of this complex. Future key experiments should focus on putative interactions of RPGR wild type and mutant isoforms within the ciliary protein complex. It is very likely that further novel proteins and additional molecular links will be identified that might be disturbed due to mutations. They will help to understand the exact function of RPGR and the molecular basis leading to ciliopathies that might finally improve the diagnosis, counselling and therapy of patients.

4.5 References of General Discussion

1. Olsson JE, Gordon JW, Pawlyk BS, et al. Transgenic mice with a rhodopsin mutation (Pro23His): A mouse model of autosomal dominant retinitis pigmentosa. *Neuron*. 1992;9:815-830.

2. Hong D, Wright R. Overexpression of RPGR Default Variant Leads to Retinal Degeneration. *ARVO Meeting Abstracts*. 2008;49:2201.

3. Nishimura DY, Fath M, Mullins RF, et al. Bbs2-null mice have neurosensory deficits, a defect in social dominance, and retinopathy associated with mislocalization of rhodopsin. *Proc Natl Acad Sci U S A*. 2004;101:16588-16593.

4. Mykytyn K, Mullins RF, Andrews M, et al. Bardet-Biedl syndrome type 4 (BBS4)-null mice implicate Bbs4 in flagella formation but not global cilia assembly. *Proc Natl Acad Sci U S A*. 2004;101:8664-8669.

5. Fath MA, Mullins RF, Searby C, et al. Mkks-null mice have a phenotype resembling Bardet-Biedl syndrome. *Hum Mol Genet*. 2005;14:1109-1118.

6. Davis RE, Swiderski RE, Rahmouni K, et al. A knockin mouse model of the Bardet-Biedl syndrome 1 M390R mutation has cilia defects, ventriculomegaly, retinopathy, and obesity. *Proc Natl Acad Sci U S A*. 2007;104:19422-19427.

7. Lee L, Campagna DR, Pinkus JL, et al. Primary ciliary dyskinesia in mice lacking the novel ciliary protein Pcdp1. *Mol Cell Biol*. 2008;28:949-957.

8. Buraczynska M, Wu W, Fujita R, et al. Spectrum of mutations in the RPGR gene that are identified in 20% of families with X-linked retinitis pigmentosa. *Am J Hum Genet*. 1997;61:1287-1292.

9. Sharon D, Bruns GA, McGee TL, Sandberg MA, Berson EL, Dryja TP. X-linked retinitis pigmentosa: mutation spectrum of the RPGR and RP2 genes and correlation with visual function. *Invest Ophthalmol Vis Sci*. 2000;41:2712-2721.

10. Roepman R, Letteboer SJ, Arts HH, et al. Interaction of nephrocystin-4 and RPGRIP1 is disrupted by nephronophthisis or Leber congenital amaurosis-associated mutations. *Proc Natl Acad Sci U S A*. 2005;102:18520-18525.

11. Meindl A, Dry K, Herrmann K, et al. A gene (RPGR) with homology to the RCC1 guanine nucleotide exchange factor is mutated in X-linked retinitis pigmentosa (RP3). *Nat Genet*. 1996;13:35-42.

12. Hadjebi O, Casas-Terradellas E, Garcia-Gonzalo FR, Rosa JL. The RCC1 superfamily: From genes, to function, to disease. *Biochim Biophys Acta*. 2008;1783:1467-1479.

13. Beltran WA, Hammond P, Acland GM, Aguirre GD. A frameshift mutation in RPGR exon ORF15 causes photoreceptor degeneration and inner retina remodeling in a model of X-linked retinitis pigmentosa. *Invest Ophthalmol Vis Sci*. 2006;47:1669-1681.

14. Hong DH, Pawlyk BS, Shang J, Sandberg MA, Berson EL, Li T. A retinitis pigmentosa GTPase regulator (RPGR)-deficient mouse model for X-linked retinitis pigmentosa (RP3). *Proc Natl Acad Sci U S A*. 2000;97:3649-3654.

15. Adamian M, Pawlyk BS, Hong DH, Berson EL. Rod and cone opsin mislocalization in an autopsy eye from a carrier of X-linked retinitis pigmentosa with a Gly436Asp mutation in the RPGR gene. *Am J Ophthalmol*. 2006;142:515-518.

16. Ikeda A, Naggert JK, Nishina PM. Genetic modification of retinal degeneration in tubby mice. *Exp Eye Res*. 2002;74:455-461.

17. Samardzija M, Wenzel A, Naash M, Reme CE, Grimm C. Rpe65 as a modifier gene for inherited retinal degeneration. *Eur J Neurosci*. 2006;23:1028-1034.

18. Jin M, Li S, Moghrabi WN, Sun H, Travis GH. Rpe65 Is the Retinoid Isomerase in Bovine Retinal Pigment Epithelium. *Cell*. 2005;122:449-459.

19. Wenzel A, Reme CE, Williams TP, Hafezi F, Grimm C. The Rpe65 Leu450Met variation increases retinal resistance against light-induced degeneration by slowing rhodopsin regeneration. *J Neurosci*. 2001;21:53-58.

20. Znoiko SL, Crouch RK, Moiseyev G, Ma Jx. Identification of the RPE65 Protein in Mammalian Cone Photoreceptors. *Invest Ophthalmol Vis Sci*. 2002;43:1604-1609.

21. Wenzel A, von Lintig J, Oberhauser V, Tanimoto N, Grimm C, Seeliger MW. RPE65 is essential for the function of cone photoreceptors in NRL-deficient mice. *Invest Ophthalmol Vis Sci*. 2007;48:534-542.

22. Hemati N, Feathers KL, Chrispell JD, Reed DM, Carlson TJ, Thompson DA. RPE65 surface epitopes, protein interactions, and expression in rod- and cone-dominant species. *Mol Vis*. 2005;11:1151-1165.

23. Schonthaler HB, Lampert JM, Isken A, et al. Evidence for RPE65-independent vision in the cone-dominated zebrafish retina. *Eur J Neurosci*. 2007;26:1940-1949.

24. Kirschner R, Rosenberg T, Schultz-Heienbrok R, et al. RPGR transcription studies in mouse and human tissues reveal a retina-specific isoform that is disrupted in a patient with X-linked retinitis pigmentosa. *Hum Mol Genet*. 1999;8:1571-1578.

25. Neidhardt J, Glaus E, Barthelmes D, Zeitz C, Fleischhauer J, Berger W. Identification and characterization of a novel RPGR isoform in human retina. *Hum Mutat*. 2007;28:797-807.

26. Vervoort R, Lennon A, Bird AC, et al. Mutational hot spot within a new RPGR exon in X-linked retinitis pigmentosa. *Nat Genet*. 2000;25:462-466.

27. Kirschner R, Erturk D, Zeitz C, et al. DNA sequence comparison of human and mouse retinitis pigmentosa GTPase regulator (RPGR) identifies tissue-specific exons and putative regulatory elements. *Hum Genet*. 2001;109:271-278.

28. Hong DH, Li T. Complex expression pattern of RPGR reveals a role for purine-rich exonic splicing enhancers. *Invest Ophthalmol Vis Sci*. 2002;43:3373-3382.

29. Shu X, Fry AM, Tulloch B, et al. RPGR ORF15 isoform co-localizes with RPGRIP1 at centrioles and basal bodies and interacts with nucleophosmin. *Hum Mol Genet*. 2005;14:1183-1197.

30. He S, Parapuram SK, Hurd TW, et al. Retinitis Pigmentosa GTPase Regulator (RPGR) protein isoforms in mammalian retina: Insights into X-linked Retinitis Pigmentosa and associated ciliopathies. *Vision Research*. 2008;48:366-376.

31. Khanna H, Hurd TW, Lillo C, et al. RPGR-ORF15, Which Is Mutated in Retinitis Pigmentosa, Associates with SMC1, SMC3, and Microtubule Transport Proteins. *J Biol Chem*. 2005;280:33580-33587.

32. Mavlyutov TA, Zhao H, Ferreira PA. Species-specific subcellular localization of RPGR and RPGRIP1 isoforms: implications for the phenotypic variability of congenital retinopathies among species. *Hum Mol Genet*. 2002;11:1899-1907.

33. Demirci FY, Rigatti BW, Wen G, et al. X-linked cone-rod dystrophy (locus COD1): identification of mutations in RPGR exon ORF15. *Am J Hum Genet*. 2002;70:1049-1053.

34. Demirci FY, Rigatti BW, Mah TS, Gorin MB. A Novel RPGR Exon ORF15 Mutation in a Family With X-linked Retinitis Pigmentosa and Coats'-like Exudative Vasculopathy. *American Journal of Ophthalmology*. 2006;141:208-210.

35. Moore A, Escudier E, Roger G, et al. RPGR is mutated in patients with a complex X-linked phenotype combining primary ciliary dyskinesia and retinitis pigmentosa. *J Med Genet*. 2005:jmg.

36. Sharon D, Sandberg MA, Rabe VW, Stillberger M, Dryja TP, Berson EL. RP2 and RPGR mutations and clinical correlations in patients with X-linked retinitis pigmentosa. *Am J Hum Genet*. 2003;73:1131-1146.

37. Zito I, Downes SM, Patel RJ, et al. RPGR mutation associated with retinitis pigmentosa, impaired hearing, and sinorespiratory infections. *J Med Genet*. 2003;40:609-615.

38. Zhang Q, Acland GM, Wu WX, et al. Different RPGR exon ORF15 mutations in Canids provide insights into photoreceptor cell degeneration. *Hum Mol Genet*. 2002;11:993-1003.

39. Hong DH, Pawlyk BS, Adamian M, Li T. Dominant, gain-of-function mutant produced by truncation of RPGR. *Invest Ophthalmol Vis Sci*. 2004;45:36-41.

40. Chang B, Khanna H, Hawes N, et al. An in-frame deletion in a novel centrosomal/ciliary protein CEP290/NPHP6 perturbs its interaction with RPGR and results in early-onset retinal degeneration in the rd16 mouse. *Hum Mol Genet*. 2006.

41. Fliegauf M, Benzing T, Omran H. When cilia go bad: cilia defects and ciliopathies. *Nat Rev Mol Cell Biol*. 2007;8:880-893.

42. Dawe HR, Farr H, Gull K. Centriole/basal body morphogenesis and migration during ciliogenesis in animal cells. *J Cell Sci*. 2007;120:7-15.

43. Pan J, Snell W. The Primary Cilium: Keeper of the Key to Cell Division. *Cell*. 2007;129:1255-1257.

44. Qin H, Wang Z, Diener D, Rosenbaum J. Intraflagellar Transport Protein 27 Is a Small G Protein Involved in Cell-Cycle Control. *Current Biology*. 2007;17:193-202.

45. Robert A, Margall-Ducos G, Guidotti JE, et al. The intraflagellar transport component IFT88/polaris is a centrosomal protein regulating G1-S transition in non-ciliated cells. *J Cell Sci*. 2007;120:628-637.

46. Marszalek JR, Liu X, Roberts EA, et al. Genetic evidence for selective transport of opsin and arrestin by kinesin-II in mammalian photoreceptors. *Cell*. 2000;102:175-187.

47. Abd-El-Barr MM, Sykoudis K, Andrabi S, et al. Impaired photoreceptor protein transport and synaptic transmission in a mouse model of Bardet-Biedl syndrome. *Vision Research*. 2007;47:3394-3407.

48. Pazour GJ, Baker SA, Deane JA, et al. The intraflagellar transport protein, IFT88, is essential for vertebrate photoreceptor assembly and maintenance. *J Cell Biol*. 2002;157:103-113.

49. Wolfrum U, Schmitt A. Rhodopsin transport in the membrane of the connecting cilium of mammalian photoreceptor cells. *Cell Motil Cytoskeleton*. 2000;46:95-107.

50. Insinna C, Besharse JC. Intraflagellar transport and the sensory outer segment of vertebrate photoreceptors. *Dev Dyn*. 2008;237:1982-1992.

51. Rosenbaum JL, Witman GB. Intraflagellar transport. *Nat Rev Mol Cell Biol*. 2002;3:813-825.

52. Roepman R, van Duijnhoven G, Rosenberg T, et al. Positional cloning of the gene for X-linked retinitis pigmentosa 3: homology with the guanine-nucleotide-exchange factor RCC1. *Hum Mol Genet*. 1996;5:1035-1041.

53. Gerber S, Perrault I, Hanein S, et al. Complete exon-intron structure of the RPGR-interacting protein (RPGRIP1) gene allows the identification of mutations underlying Leber congenital amaurosis. *Eur J Hum Genet*. 2001;9:561-571.

54. Valente EM, Silhavy JL, Brancati F, et al. Mutations in CEP290, which encodes a centrosomal protein, cause pleiotropic forms of Joubert syndrome. *Nat Genet*. 2006;38:623-625.

55. Arts HH, Doherty D, van Beersum SE, et al. Mutations in the gene encoding the basal body protein RPGRIP1L, a nephrocystin-4 interactor, cause Joubert syndrome. *Nat Genet*. 2007;39:882-888.

56. Otto EA, Loeys B, Khanna H, et al. Nephrocystin-5, a ciliary IQ domain protein, is mutated in Senior-Loken syndrome and interacts with RPGR and calmodulin. *Nat Genet*. 2005;advanced online publication.

57. Zhao Y, Hong DH, Pawlyk B, et al. The retinitis pigmentosa GTPase regulator (RPGR)- interacting protein: subserving RPGR function and participating in disk morphogenesis. *Proc Natl Acad Sci U S A*. 2003;100:3965-3970.

58. Devuyst O, Arnould VJ. Mutations in RPGRIP1L: extending the clinical spectrum of ciliopathies. *Nephrol Dial Transplant*. 2008:gfn033.

59. Frank V, den Hollander AI, Bruchle NO, et al. Mutations of the CEP290 gene encoding a centrosomal protein cause Meckel-Gruber syndrome. *Hum Mutat*. 2008;29:45-52.

60. Helou J, Otto EA, Attanasio M, et al. Mutation analysis of NPHP6/CEP290 in patients with Joubert syndrome and Senior Loken syndrome. *J Med Genet*. 2007;44:657-663.

61. Pazour GJ, Dickert BL, Vucica Y, et al. Chlamydomonas IFT88 and its mouse homologue, polycystic kidney disease gene tg737, are required for assembly of cilia and flagella. *J Cell Biol*. 2000;151:709-718.

62. Lin F, Hiesberger T, Cordes K, et al. Kidney-specific inactivation of the KIF3A subunit of kinesin-II inhibits renal ciliogenesis and produces polycystic kidney disease. *Proc Natl Acad Sci U S A*. 2003;100:5286-5291.

63. Jiang ST, Chiou YY, Wang E, et al. Targeted disruption of Nphp1 causes male infertility due to defects in the later steps of sperm morphogenesis in mice. *Hum Mol Genet*. 2008:ddn231.

64. Gravesande KS, Omran H. Primary ciliary dyskinesia: Clinical presentation, diagnosis and genetics. *Ann Med*. 2005;37:439-449.

65. Hunter DG, Fishman GA, Kretzer FL. Abnormal axonemes in X-linked retinitis pigmentosa. *Arch Ophthalmol*. 1988;106:362-368.

66. Ostrowski LE, Blackburn K, Radde KM, et al. A Proteomic Analysis of Human Cilia: Identification of Novel Components. *Mol Cell Proteomics*. 2002;1:451-465.

67. Li JB, Gerdes JM, Haycraft C, et al. Comparative Genomics Identifies a Flagellar and Basal Body Proteome that Includes the BBS5 Human Disease Gene. *Cell*. 2004;117:541-552.

68. Avidor-Reiss T, Maer AM, Koundakjian E, et al. Decoding Cilia Function: Defining Specialized Genes Required for Compartmentalized Cilia Biogenesis. *Cell*. 2004;117:527-539.

69. Blacque OE, Perens EA, Boroevich KA, et al. Functional Genomics of the Cilium, a Sensory Organelle. *Current Biology*. 2005;15:935-941.

70. Liu Q, Tan G, Levenkova N, et al. The proteome of the mouse photoreceptor sensory cilium complex. *Mol Cell Proteomics*. 2007.

71. Roepman R, Wolfrum U. Protein networks and complexes in photoreceptor cilia. *Subcell Biochem*. 2007;43:209-235.

72. Schafer T, Putz M, Lienkamp S, et al. Genetic and physical interaction between the NPHP5 and NPHP6 gene products. *Hum Mol Genet*. 2008:ddn260.

73. Nachury MV, Loktev AV, Zhang Q, et al. A Core Complex of BBS Proteins Cooperates with the GTPase Rab8 to Promote Ciliary Membrane Biogenesis. *Cell*. 2007;129:1201-1213.

74. van Wijk E, Kersten FFJ, Zaghloul N, et al. A Centrosomal Protein Molecularly Links Usher Syndrome to Leber Congenital Amaurosis and Bardet-Biedl Syndrome in the Retina. *Invest Ophthalmol Vis Sci*. 2008;49:4033.

75. Ou G, Koga M, Blacque OE, et al. Sensory ciliogenesis in Caenorhabditis elegans: assignment of IFT components into distinct modules based on transport and phenotypic profiles. *Mol Biol Cell*. 2007;18:1554-1569.

76. Blacque OE, Cevik S, Kaplan OI. Intraflagellar transport: from molecular characterisation to mechanism. *Front Biosci*. 2008;13:2633-52.:2633-2652.

5. Acknowledgements

The "rocky road" of writing a dissertation bears many educational benefits. It also requires support and guidance through all the up's and down's occuring during this process. Therefore, the present thesis would not exist in this form without the help of many people accompanying me through the last four years.

My most cordial thanks go to my supervisor and mentor Prof. Wolfgang Berger. His constant scientific support and enthusiasm for the project but especially his open-mindedness helped me maturing to a responsible scientist.

My warmest thanks goes to the members of the "*RPGR* research group" including John Neidhardt, Fabian Schmid, Gaby Tanner and Esther Glaus sharing the office with me. They have been fantastic office mates and we had stimulating discussions of results and ideas.

Many thanks to all collaboration partners for tossing ideas and discussions, some resulting in acutal publications. I explicitly like to name here Andreas Wenzel, Christian Grimm, Uwe Wolfrum, Alexander Travis, Klaus Rüther and Marius Ueffing for respecting me as a "growing" scientist

I would love to thank Lucas Mohn, Jurian Zürcher, Niko Schäfer, Fabian Schmid, Walther Hänseler, Istvan Magyar, Stephan Labs, Gaby Tanner, Ursi Forster, Barbara Kloeckener, Christina Zeitz, Ulrich Luhmann, John Neidhardt and all the members past and present I met and worked with during the four years in the Berger laboratory. We had awsome times discussing scientifc problems but also spending time together for fun and pleasure. I gained many precious friendships that will hopefully persist and continue to grow.

Last but not least I owe deep thanks to my friends in Switzerland but also in Germany and very especially to my family. They constantly supported me during good and bad times and helped me to reach my goal.

6. Curriculum vitae

Name:	Sandra Brunner
Address:	Brahmsstrasse 15, 8003 Zuerich
Date of birth:	September 5th 1978
Place of birth:	Wuerzburg, Germany
Nationality:	German

School Education

09/89 – 07/98	Abitur *Mozart Gymnasium* Wuerzburg, Germany final grade: 2.2

Academic Education

09/98 – 10/03	Diploma in Biology Biochemistry, Human Genetics, Developmental and Cell Biology University of Wuerzburg, Germany
09/01 – 03/02	Exchange student of International ERASMUS Program Institute of Biochemistry and Molecular Biology, University of Salamanca, Spain
08/04 – to date	PhD in Biology Medical Genetics and Neurobiology Institute of Medical Molecular Genetics, University of Zurich, Switzerland

Work experience

11/03 – 07/04	Scientific Research Assistant Laboratory of Molecular Ophthalmology and Oncology, Institute of Human Genetics, University of Wuerzburg, Germany

Publications

Brunner S., Colman D., Travis A.J., Luhman U.F.O, Shi W., Feil S., Imsand C., Nelson J., Grimm C., Ruelicke T., Fundele R., Neidhardt J., and Berger W. "Overexpression of RPGR Leads to Male Infertility in Mice Due to Defects in Flagellar Assembly", *Biology of Reproduction, 2008 Jun 25*., Epub ahead of print

Brunner S., Skosyrski S., Kirschner-Schwabe R., Knobeloch K.P., Neidhardt J., Feil S., Luhmann U.F.O., Rüther K., and Berger W. "Cone versus rod disease in two mouse strains with a knock-in mutation in the retinitis pigmentosa GTPase regulator (*Rpgr)* gene", *Investigative Ophthalmology and Vision Research, 2008*, submitted

Conferences/Scientific meetings

Brunner S., "Phenotypic variability of *Rpgr* mutant mice in different genetic backgrounds", *Swiss Retina Meeting, Brunnen, Switzerland, January 18th&19th, 2005*, presentation

Brunner S., Skosyrski S., Colman D., Luhmann U.F.O., Neidhardt J., Kirschner-Schwabe R., Knobeloch K.P., Rohde E., Horak I., Rüther K., and Berger W."Functional and morphological characterization of a mouse model for X-linked retinitis pigmentosa (RP)", *ProRetina Meeting Potsdam, Germany, April 8th&9th, 2005*, poster presentation

Brunner S., Skosyrski S., Colman D., Luhmann U.F.O., Neidhardt J., Giessl A., Kirschner-Schwabe R., Knobeloch K.P., Rohde E., Horak I., Wolfrum U., Rüther K., and Berger W."Functional and morphological characterization of a mouse model for X-*linked retinitis pigmentosa (RP)", ZNZ Symposium, Zurich, Switzerland, October 21th, 2005*, poster presentation

Brunner S., Skosyrski S., Colman D., Luhmann U.F.O., Neidhardt J., Giessl A., Kirschner-Schwabe R., Knobeloch K.P., Rohde E., Horak I., Wolfrum U., Rüther K., and Berger W. "Retinal degeneration in a mouse model for X – linked retinitis pigmentosa (RP)", *ProRetina Meeting Potsdam, Germany, April 7th&8th, 2006*, poster presentation

Brunner S., Skosyrski S., Colman D., Luhmann U.F.O., Neidhardt J., Giessl A., Kirschner-Schwabe R., Knobeloch K.P., Rohde E., Horak I., Wolfrum U., Rüther K., and Berger W.“ Influence of the genetic background on retinal degeneration”, *ZNZ Symposium, Zurich, Switzerland, October 20th, 2006,* poster and oral presentation

Brunner S., “Cone versus rod disease in a mouse model for X-linked retinitis pigmentosa”, *Swiss Retina Meeting, Brunnen, Switzerland, January 17th&18th, 2007*, presentation

Brunner S., Skosyrski S., Luhmann U.F.O., Neidhardt J., Kirschner-Schwabe R., Knobeloch K.P., Rohde E., Horak I., Rüther K., and Berger W. “Cone versus rod disease in a mouse model for X-linked retinitis pigmentosa”, *ProRetina Meeting Potsdam, Germany*, *March 30th&31th, 2007*, poster presentation

Brunner S., Skosyrski S., Kirschner-Schwabe R., Knobeloch K.P., Rohde E., Horak I., Rüther K., and Berger W. “Retinal degeneration in a mouse model for X-linked Retinitis Pigmentosa”, *ZNZ Symposium, Zurich, Switzerland, September 14th ,2007*, poster presentation

Brunner S., “Effect of the genetic background on retinal degeneration”, *Swiss Eye Research Meeting, Brunnen, Switzerland, February 14th&15th, 2008*, presentation

Brunner S., Skosyrski S., Neidhardt J., Kirschner-Schwabe R., Knobeloch K.P., Rohde E., Horak I., Rüther K., and Berger W. “Cone versus rod disease in a mouse model for X-linked retinitis pigmentosa”, *ProRetina Meeting Potsdam, Germany*, *March 28th&29th, 2008*, presentation

Brunner S., Skosyrski S., Neidhardt J., Kirschner-Schwabe R., Knobeloch K.P., Rohde E., Horak I., Rüther K., and Berger W. “Retinal degeneration in a mouse model for X-linked Retinitis Pigmentosa”, *Association for Research in Vision and Ophthalmology (ARVO), Annual Meeting, Fort Lauderdale, Florida, U.S., April 27th – may 2nd, 2008*, poster presentation